Improving 3D Printability and Functional Performance of Polyethylene across Visible and IR Spectrums through IR Transparent Pigmentation and Polyolefin Additives

by

Mehnab Ali

A thesis submitted in partial fulfilment of the requirements of the degree of

Master of science

Department of Mechanical Engineering

University of Alberta

Abstract

Polyolefin thermoplastics form a significant fraction of the world scale production of plastics and are of high interest due to their toughness, low cost, good chemical resistance and excellent IR properties. Two grades of PE: Linear Low-Density Polyethylene (LLDPE) and High-Density Polyethylene (HDPE). LLDPE and HDPE have a huge number of applications in a diverse range of areas such as radiative passive heating and cooling, infrared (IR) and visible camouflage, additive manufacturing, defense sector and many more. However, LLDPE faces the challenge of being visibly semi-transparent, while HDPE exhibits severe warpage during 3D printing. This dissertation aims to address these challenges and enhance the performance of PE for expanded applications in IR camouflage and radiative passive heating and cooling applications. Chapter one focuses on resolving the semi-transparency issue of LLDPE by pigmenting the material using a simple and easier compounding method while making sure to maintain its highly desirable IR transparency. A comprehensive FTIR, UV-VIS, mechanical testing, and IR analysis is implemented to confirm the successful achievement of a visibly opaque LLDPE material without compromising its exceptional IR transparency. This breakthrough enables the utilization of LLDPE in various applications, including radiative passive heating and cooling, IR and visible camouflage, and IR shielding applications. Chapter two addresses the warpage challenges experienced during the 3D printing of HDPE. Incorporation of 10 wt% LLDPE into HDPE helps reduce crystallinity and mitigate stresses during 3D printing, by optimizing printing parameters and exploring different print bed options. Through this approach, this research provides a successful solution to provide significant reduction in warpage for 3D printing of HDPE leading to its expansion of potential applications in additive manufacturing. Overall, this thesis dissertation highlights the excellence of PE as a material, the challenges it faces and addresses those challenges.

Through custom compounding of PE, we have successfully produced PE based metamaterials which have high visible opacity, are available in diverse range of colors and still maintain their high IR transparency properties. HDPE based grades of PE can be successfully 3D printed which pave the way for 3D printing functionality of these metamaterials which can further be drawn into fibers to make fabrics for civilian and military camouflage and radiative heating/cooling applications.

Key words: *Additive manufacturing, HDPE, LDPE, Fused filament fabrication, polyethylene printing, warpage, polymer blends, shrinkage, stresses, Pigmentation, Compounding LLDPE, polymer composites, FTIR, UV-VIS, IR analysis, IR transparency, IR reflectance, IR emittance, Mechanical characterization, Tensile strength, Young's modulus, Elongation at break.*

Preface

This master dissertation is an original work by Mehnab Ali. Chapters 2 and 3 have been presented in two conference proceedings.

Chapter 2 was presented as “Micro-structured and Visibly Pigmented Polyolefin Surfaces for Visibly Opaque and Thermally Scattering Materials for camouflage applications” at Beilstein Nanotechnology Symposium (May 9-11, 2023) at Limburg, Germany.

Chapter 3 was presented as “Adhesion and Warpage Improvements in HDPE 3D Printing” at 46th Adhesion Society Annual Meeting (February 19-22, 2023) at Orlando, USA.

This research endeavor is currently in the process of being translated into a successful product creation through the establishment of a startup venture, which has been initiated in collaboration with Dr. Dan Sameoto and Dr. Asad Asad. I am working as Chief Operating Officer of this startup called KryoZesto.

Furthermore, these chapters are being further revised, and are in the process for publication in relevant scientific journals afterwards.

Dedicated to my loving parents,

Maqbool Ahmad & Shaheen kausar

And my adored siblings,

Aftab Anjum, Mahtab Ul

Hassan & Nimra Maqbool

For their endless love and support through all times.

Acknowledgement

I would like to express my deepest respect to my supervisor Dr. Dan Sameoto, for his continuous support and help through this journey. I am very thankful to you. You trusted me to join your group and have always been there for me through tough times. I cannot express my gratitude enough. From the deepest spot in my heart, thank you for everything!

I would like to thank my thesis examiners Dr. Ahmad Jawad Qureshi and Dr. James Hogan for their support.

Special thanks to my colleague Dr. Asad Asad for his endless support and help.

Thanks to my colleagues: Xiaoruo Sun, Luka Morita, Zhaoqi Ma, Abolfazl Vaheb, Shima Jalali for their continuous support and nice memories.

Table of contents

Contents

List of Tables

List of Figures

Chapter 1

Introduction

1.1. Polyolefins

A polyolefin is a polymer produced from an olefin or alkene as a monomer. In organic chemistry, an alkene, olefin, or olefin is an unsaturated chemical molecule containing at least one carbon to carbon double bond [1]. Polyolefins include polyethylene - PE (low-density, high-density, and linear low-density polyethylene), polypropylene - PP , and polybutene - PB (polybutene-1 and polyisobutylene) in which PE and PP are the most commonly used commercially available polyolefins [2]. Radical polymerization and coordination catalysis are two major methods of polymerizing ethylene and propylene [3]–[5]. The worldwide market size of polyolefins was approximately USD 294 billion in 2022 and is expected to rise to USD 355 billion by 2026 [6], [7]. This high rise in demand is due to its various industry applications due to its easy ability to form desired shapes and easy molding and their low cost. It has become essential for applications such as packaging, construction, automotive and medical industries due to low cost, low density, good chemical resistance and excellent processability [8]–[11]. Out of the two major polyolefins, PE is an interesting polymer from point of the view of its molecular structure. Different grades of PE are available based on the degree of branching, such as high-density polyethylene (HDPE), low-density polyethylene (LDPE), and linear-low density polyethylene (LLDPE). LLDPE is a copolymer of ethylene with longer olefin, has short-chain branching (<100 per 1000 C-atoms) [12]. LDPE has a higher number of long-chain branching (8–40 per 1000 C-atoms), which leads to a loss of molecular symmetry and a lower degree of crystallinity (40–50%) [12]. HDPE has a low amount of short chain branching (5–10 per 1000 C-atoms) and a high degree of crystallinity (70–80%) [12]. Their schematic is shown in Figure 1. On the other hand, PP is popular for having lower density among commodity plastics. It is a nonpolar, and partially crystalline polymer with good strength, stiffness, and chemical resistance but poor UV stability [13]. It can be processed by

a variety of processing techniques, such as extrusion or injection molding [14], [15].

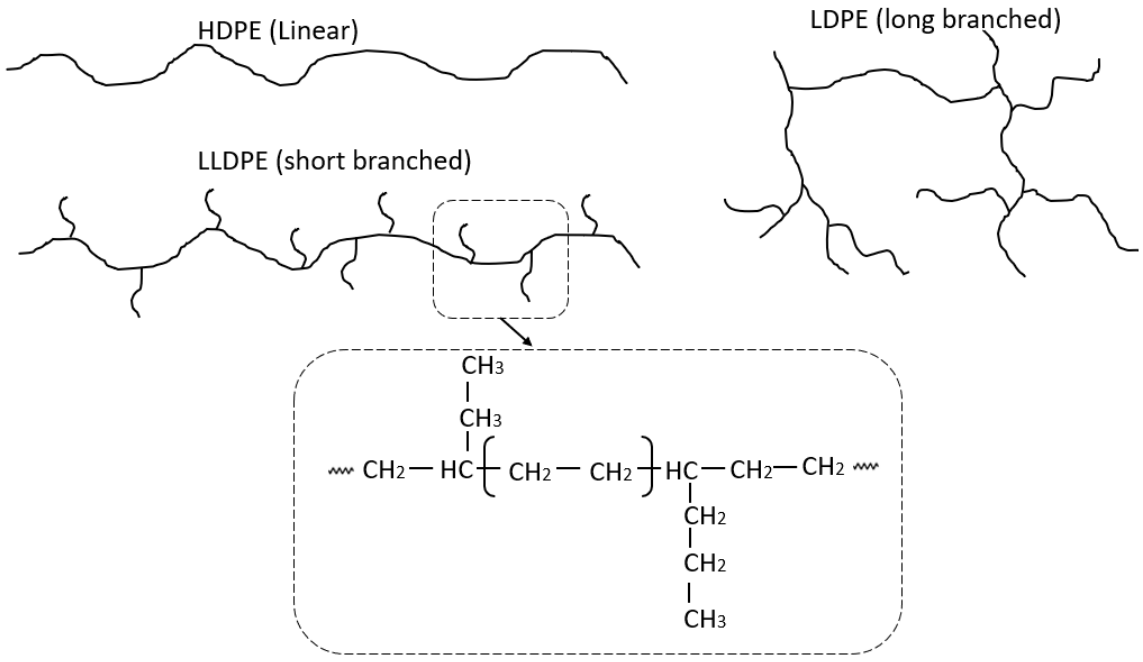

Figure 1: Grades of PE. High-density polyethylene (HDPE), low-density polyethylene (LDPE), and linear low-density polyethylene (LLDPE).

1.2. Additive manufacturing

Currently, there is a high demand for 3D printing technology due to its revolutionary impact on the manufacturing and design of ceramics, metals, concretes, polymers, and their composites [16]. Additive manufacturing, also known as 3D printing, constructs a 3D object using a computer-aided design (CAD) and a layer-by-layer approach, as opposed to the subtractive manufacturing process which involves removing material from a solid piece to create the desired shape [17]–[19]. Initially, 3D printing was primarily used for producing prototypes. However, it is now increasingly used in large-scale applications in various industries such as automotive, aerospace, construction, electronics, and medical industries, owing to its ability to mass customize [19]–[35]. There are many types of 3D printing processes available, such as selective laser sintering [36],

stereolithography [37], digital light processing [38], direct metal laser sintering [39], fused deposition modeling (FDM) [40], and electron beam melting [41]. FDM is the most versatile and commonly used method, among these techniques, used for polymeric materials, due to its low cost, easy processing, variation in build styles, and simple support removal [42], [43]. Compared to traditional processing techniques, FDM 3D printing is budget-friendly and scalable. It does not require a mold to produce a product, which saves the significant investment cost of creating product-specific molds. It is also easy to operate and can create complex 3D parts with ease [43]–[45]. However, the mechanical strength of printed objects is lower than that of a product made using conventional molding techniques. Furthermore, there is a limited availability of thermoplastics feedstock that can be used for FDM 3D printing due to its dependence on amorphous feedstocks [47]–[51].

1.3. Hight density polyethylene (HDPE)

High-density polyethylene (HDPE) is used in various applications such as plastic bottles, pipes, containers due to its high durability, toughness, and resistance to chemicals and UV radiation [52]. Its market was valued at 70.7 billion U.S. dollars in 2020. The HPDE market is expected to reach a value of almost 90 billion U.S. dollars by 2026 whereas global HDPE production is projected to reach 53.62 million metric tons by 2025 [53]. Application of different grades of polyethylene in FDM is very challenging due to their high melting temperature, low thermal conductivity, semi crystalline nature and low adhesion properties [54]. When semi crystalline polymers, like HDPE, are used in 3D printing, they tend to shrink and warp during cooling after being melted. This is because the molten polymer chains rearrange themselves in a more ordered manner as they cool, which can cause problems with bed adhesion and lead to failure in the printing process [55]–[58]. These issues can result in 3D objects that are distorted or do not meet design specifications.

Therefore, there is a need to improve 3D printing compatibility of HDPE with FDM in order to enhance the flexibility and capabilities of their use in diverse applications [59], [60] .

1.4. Linear Low-density polyethylene (LLDPE)

Linear low-density polyethylene (LLDPE) is produced by the copolymerization of ethylene with a small amount of a comonomer, typically an alpha-olefin such as 1-butene, 1-hexene, or 1-octene [61]–[63]. This results in a linear polymer structure with short side chains, which gives LLDPE its unique mechanical properties such as excellent tensile strength, impact resistance, and puncture resistance [64]–[67]. Due to its abundant supply, good chemical resistance, low cost, superior processability, low energy requirement for processing, and high specific modulus and strength it is extensively used in packaging applications such as films, bags, and pouches [68]–[71]. LLDPE is also compounded with various additives and agents to enhance its properties and expand its applications. Compounded LLDPE is widely used in various other applications such as agriculture, medical, electrical and construction industry [72]–[78]. Recently, LLDPE has found interesting usages in radiative passive cooling and heating applications due to its desirable and unique properties such as high transparency in infrared region. Its ability to absorb, transmit which is most important for us, and reflect IR radiation in different ranges makes it a versatile material for use in radiative cooling and heating applications [77], [79]–[82]. However, compounding of LLDPE can be very challenging due to its poor compatibility with fillers and additives due to its low surface energy, lack of polar groups, high melt viscosity, and degradation at higher temperatures. Some complex manufacturing and chemical process are listed in the literature which are used to achieve compounding conventionally [83]–[87]. Another challenge is that PE exists in a translucent or milky-white color in its natural state [88] and is difficult to dye, or paint due to its low surface energy [89]–[94]. Therefore, it is important to come up with simple fabrication methods for

compounding of LLDPE while maintaining its desirable visible, mechanical and IR properties.

1.5 Research motivation

Polyethylene (PE) is an exceptional material renowned for its remarkable properties and versatility, making it highly sought after across various industries. With its wide range of grades and formulations, PE offers unparalleled advantages for numerous applications, including radiative passive heating and cooling, infrared (IR) and visible camouflage, IR shielding, packaging, agriculture, medical and numerous other applications. It has diverse capabilities and significant contributions to industrial, military, and civilian sectors equally.

1.5.1 Visible and infrared camouflage applications

Traditionally, military textiles have been used to visibly camouflage and blend the soldiers and military equipment with their environment and background. Typical desired colors for visible camouflage, while may slightly based on the regions, are olive, green, khaki, brown and black [95]. These are mostly used in the manufacturing of soldier clothing, light flexible nets, garnishing and covers to provide visible camouflage and in doing so conceal them from enemy weaponry and visual detection equipment [96]. In modern warfare, while visible camouflage is still highly desired, with the addition of hyperspectral imaging technologies being more available, Infrared (IR) or thermal camouflage is an area of high interest by the defense sector around the world [97]. The integration of visibly and IR camouflage capabilities in the military textiles present several challenges. Comfort, maintaining garment functionality, resistance to laundering and switchability between high and low emitting surface are some of the crucial factors to keep in mind. Therefore, there is need to avoid complex-embedded electronics and powering devices while at the same time, it is desired to maintain compatibility, modularity and adherence to existing textile standards for intuitive use [98].

Three-dimensional (3D) printing, surface dyeing, embedded additives, low-emissivity coatings, metamaterials and microfluidics are some of the potential solutions for improved camouflage capabilities. 3D printing offers opportunities for fabricating complex fabric structures using metamaterials and microfluidics. Examples include 3D metamaterial absorber textiles for radar stealth, and hierarchical metamaterials for multispectral camouflage. The application of microfluidics in adaptive camouflage, through the manipulation of chromatophores and hyperplastic matrices, is also discussed in the literature [95], [99]–[102]. visible and IR camouflage solutions in designing low and high IR emitting surfaces using techniques such as kirigami, electrowetting, lenticular lens, micro-structuring and microfluidics etc. are of great interest in the literature [95], [99]–[102] . Kirigami, a variation of origami, with the concept of using one high emitting and one low emitting surface, can be utilized to create unique surface structures for achieving IR camouflage [103]. A highly reflective surface, such as aluminum, reflects the surrounding thermal temperature, which makes the object appear at the same temperature as its surroundings under IR or thermal imaging cameras providing excellent IR camouflage. However, reflective materials fail to provide visible camouflage. Therefore, thee kirigami solutions need to be covered under such metamaterials which are highly visibly opaque, and are available in typical military camouflage colors while still providing high IR transparency so that they don't affect the kirigami's IR capabilities. Thus, these solutions as a whole unit can provide camouflage under both visible and IR range without impacting on each other's performance. In this work, we will investigate, develop, test and characterize these metamaterials for effective visible and IR camouflage applications. Chapter 3 directly addresses to and is an integral part of this work.

1.5.2 Blackbody, Grey body Radiation, the Stefan–Boltzmann Law and IR transparency

A blackbody is an idealized object that absorbs all incident electromagnetic radiation and emits radiation over a wide range of frequencies, depending solely on its temperature. The radiation emitted by a blackbody is referred to as blackbody radiation [104]. One of the fundamental laws governing blackbody radiation is the Stefan–Boltzmann law, which states that the total energy radiated per unit surface area of a blackbody is directly proportional to the fourth power of its absolute temperature (T). Mathematically, this is expressed as [105]:

$$E = \sigma . T^4 \qquad (1)$$

E is the total radiant energy emitted per unit area.

σ is the Stefan–Boltzmann constant, approximately equal to $5.67\times10^{-8}\mathrm{W}m^{-2}K^{-4}$. This law is essential for understanding the relationship between the temperature of an object and the amount of IR radiation it emits. In the context of thermal imaging, IR cameras exploit this principle to detect temperature differences in their field of view.

Not all materials are blackbodies, meaning they do not absorb and emit radiation perfectly. Most real-world objects are grey bodies, which emit less radiation compared to a blackbody [106]. The emissivity (ε) of a material quantifies its ability to emit thermal radiation relative to a blackbody. Emissivity values range from 0 (perfect reflector, no radiation emission) to 1 (perfect blackbody) [107]. For our research, we are considering grey bodies as our point of interest for thermal camouflage applications. The heat source and surrounding environments for camouflage research motivation are treated as grey bodies with FLIR thermal camera, which is widely used for capturing thermal images and detecting IR radiation [108], set at 95% emissivity.

For materials like LLDPE, which are intended to be IR transparent for camouflage purposes, it is essential to for them to let most of IR radiation pass through depicting as IR transparent to fool thermal cameras. They allow IR radiation to pass through without significant absorption and emission, making them challenging to detect by IR cameras [109], [110]. We are interested in the

8 μm to 12 μm range of IR which ensures compatibility with FLIR thermal cameras, which are optimized for this wavelength region.

The motivation of the research is to investigate the IR properties of compounded LLDPE with an aim to thermally mimic the surroundings and making it less detectable by thermal imaging systems, allowing for effective camouflage. By matching the emissivity of the material to its background, it becomes exceedingly challenging for IR cameras to distinguish the material from its environment [111], [112]. This principle is instrumental in deceiving IR cameras, making objects or individuals appear as if they are part of their surroundings.

1.5.3 Radiative passive cooling and heating applications

The energy consumption in buildings contributes to over 30% of global final energy use and is responsible for 10% of global greenhouse gas emissions [113]. This has significant environmental and economic implications. Space heating and cooling account for approximately 48% of the total energy consumed in buildings [103], [104], . With the effects of climate change and population growth, it is projected that the demand for heating and cooling energy will increase by 79% and 83%, respectively, from 2010 to 2050 [114]–[116]. Specifically, in Alberta, about 89% of the power is generated by burning fossil fuels- approximately 36% from coal and 54% from natural gas. Fossil fuels emit greenhouse gasses which pollute the environment and are directly responsible for global warming and climate change. Alberta's total energy demand is the largest in Canada at 410 petajoules (PJ) in 2019 with commercial and residential being one of the largest consuming sectors. Space heating is the number one form of energy consumption in commercial and residential buildings, making up 63% of the total energy consumption [117]–[119].

To address these challenges and promote sustainability, there is a pressing need for innovative science and technology to achieve high energy efficiency in buildings while minimizing carbon

emissions. One such solution is radiative passive heating and cooling which can be implemented to our buildings to passively heat and cool them using advanced radiative surface materials. Some of the major challenges are the dynamic nature of weather conditions, which can compromise the effectiveness of passive solar heating or radiative cooling. These variations occur spatially and temporally, including seasonal fluctuations and variations across climate zones. Development of switchable thermal management systems utilizing the concepts of radiative passive heating and cooling are of great interest in this field [79], [120], [121]. In this regard, we have launched a new startup called Kryozesto under which we are developing a new inexpensive switchable radiative cooling (RC) and solar heating (SH) system for thermal management applications which uses outer space as a passive heat sink and harvests heat from the sun as a renewable energy source through switching the functionality of a variety of passive radiative systems [122]. This combination is achieved through deploying a multilayer thin-film composite system with a sliding mechanism to allow switching between two systems upon request at different times of the day/seasons of the year as per the need. For radiative passive cooling is achieved with a highly visible reflective surface combined with an efficient thermal emitter. When insulated from conduction and convection to the surroundings, these systems can in theory cool to many 10s of degrees Celsius below ambient temperatures. Efficient radiative heating requires the opposite, with a highly visibly absorbing and low IR emitting material. This solution promises the benefits of both with minimum manufacturing and actuation complexity. Use of PE is shown in the schematic diagram of the dual mode thermal management system is shown in Figure 2.

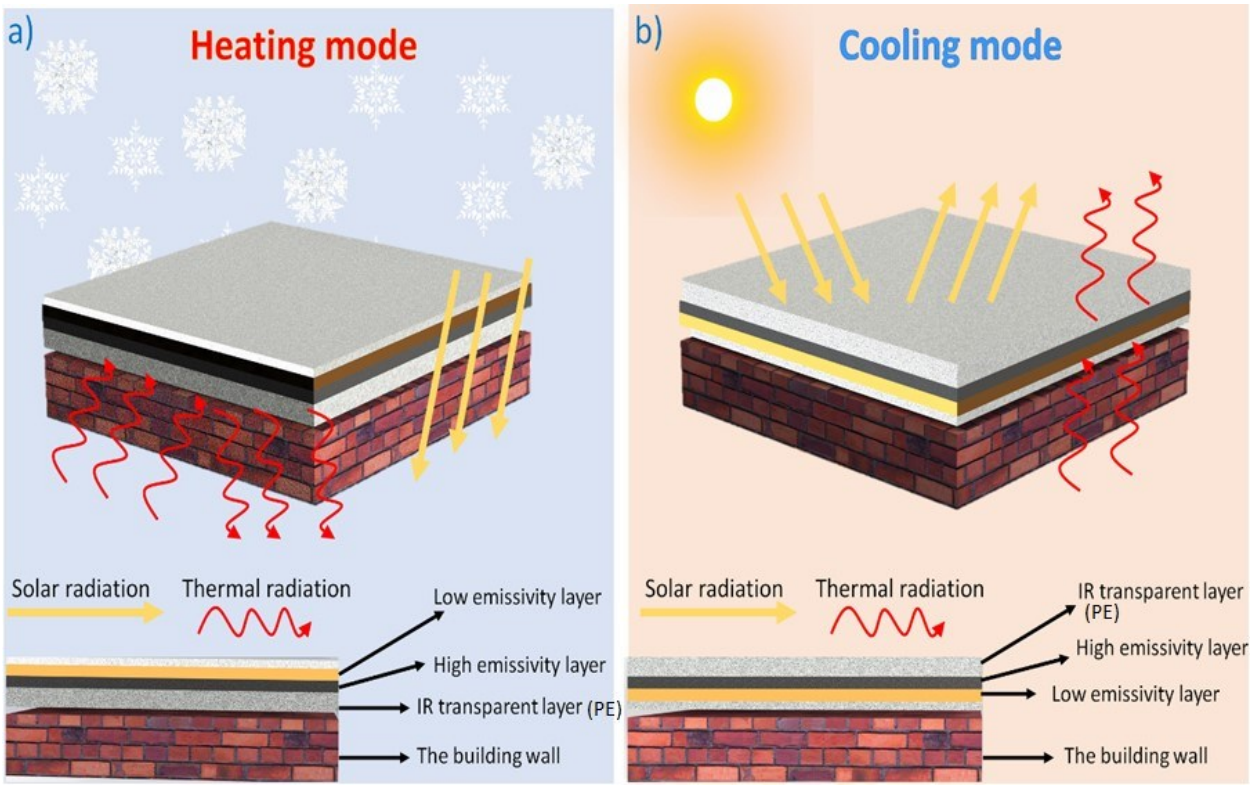

Figure 2: a) & b) represent two scenarios of radiative heating and cooling using radiative passive heating and cooling thermal management system being developed in our lab.

In this work, we are investigating, developing, testing and characterizing highly IR transparent, high IR scattering, surfaces which are to be used for heating and cooling applications. Chapter 3 directly addresses to and is an integral part of this project.

1.5.4 3D printing applications

As we know, 3D printing of plastics has widespread application in various industries and has the potential to revolutionize manufacturing processes [123]. It enables rapid prototyping, customization, and cost-effective production of complex geometries with high precision. Industries such as aerospace, automotive, healthcare, and consumer goods benefit from reduced lead times, increased design flexibility, and improved efficiency [124]. From lightweight

components in aircraft to medical implants and consumer products, 3D printing of plastics offers transformative possibilities in the manufacturing world. Even though 3D printing has made great progress and is available for a wide range of materials, there are still many challenges for printing with polyolefins. Polyolefin materials, especially such as polyethylene (PE), is very challenging to 3D print with due to its high crystalline nature and very little is available about it in the literature [125]. PE thermoplastics often cause severe warpage and delamination problems during 3D printing. Therefore, it is very important to solve this problem so that we can 3D print complex objects using highly desired PE materials and increase their applications across the board. In this regard, we will investigate, test and optimize 3D printing parameters, print bed materials and techniques to help solve this problem and making 3D printing of polyolefins more accessible. Chapter 4 directly addresses to and is an integral part of this work.

1.5.5 Thermal draw tower applications

The thermal draw tower is a versatile and widely utilized apparatus in various fields, ranging from materials science to fiber optics. The thermal draw tower operates on the principle of controlled heating and stretching of materials to achieve desired properties and structures [126]. The process involves the controlled melting of a starting material, followed by drawing it into a thin, elongated shape through controlled tension. The key elements of a typical thermal draw tower setup include a furnace or heating zone, a drawing mechanism, and a cooling section [127]. The furnace raises the material's temperature to its melting point, allowing for proper viscosity and flow. The drawing mechanism controls the tension and elongation rate during the drawing process, while the cooling section solidifies the material into its final form [128].

Micro structured thermoplastic filaments which are traditionally made via die extrusion, can be successfully drawn and manufactured using thermal draw tower [129], [130]. In conventional

methods, each shape requires a specially designed and fabricated die. Co-extruding multiple materials and hollow features requires highly specialized dies, and multiple compounder and extrusion stages. Therefore, 3D printing and thermal draw tower technique are used together to manufacture complex and tailorable geometry in micro structured fibers without the significant infrastructure required for conventional fabrication such as dies, molds, etc. 3D printed complex specimens of PE grades can be thermally drawn and used to make micro structured fibers for making smart textiles, specialized complex and functional fibers such as sensors, air-core waveguides, actuators, and energy storage devices by creating preforms of diverse range of shapes and materials [131]–[133]. Chapter 4 provides successful 3D printing of HDPE which is an integral step toward thermal drawing of PE and achieving nanoscale fibers.

1.6 Research Objective

While Polyethylene (PE) is undeniably an excellent material with a multitude of applications, it is not without its challenges. Two specific challenges have been identified: the semi-transparency of LLDPE and the severe warpage experienced during 3D printing with HDPE. However, this dissertation aims to address these challenges head-on by proposing innovative solutions. This work aims to improve visible, IR and 3D printing properties of PE. For this purpose, the research work has been divided into two chapters.

1. In the first chapter, the semi-transparency issue of LLDPE is resolved through pigmenting techniques, ensuring that its highly desirable infrared (IR) transparency remains unaffected. A simpler and easier method to compound LLDPE with different pigments is devised that offer desirable IR properties as well as bold coloration potential to obtain both camouflage and visually appealing colors/ surface finishes of compounded LLDPE. Extensive analyses and testing, including FTIR analysis, UV-VIS analysis, mechanical

testing, and IR analysis under a FLIR E75 camera are implemented to investigate the visible, IR and mechanical properties of compounded LLDPE, and a comparison is made with pure LLDPE.

2. In the second chapter, the warpage challenge of HDPE during 3D printing is addressed. Various blends of HDPE are investigated and their impact on warpage is tested for various concentrations. Analyzing the impact of various angles on shrinkage and warpage of printed part and examining different process parameters and print bed materials to improve 3D printability of HDPE is also part of the scope of this work.

Through these efforts, the aim is to overcome the limitations of PE and unlock its full potential for a wide range of industrial, military, and civilian applications.

1.7 Thesis structure

This is a paper-based master dissertation that contains four chapters. Chapter 2 and 3 are written on a theme of a journal paper. Both chapters will be submitted separately for journal publications.

Chapter 1 presents a brief overview of polymeric materials and their classifications as well as a brief introduction to the two most common types of polyethylene: HDPE and LLDPE. It includes a brief introduction to Additive manufacturing techniques in particular to FDM technique and the challenges faced in FDM printing of polyethylene, especially HDPE. It outlines challenges associated with compounding of LLDPE with pigments which offer visually appealing color potentials without impacting its desirable IR and mechanical properties. It also provides the research motivation and background into this research and explains the importance of this work and how this research work enhances the functionality of

PE for diverse applications.

Chapter 2 presents detailed steps of the fabrication process of custom compounding master batches of pigments with LLDPE in various concentrations. In this phase, compounded LLDPE blends are extruded. Microscale sheets are fabricated and analyze to investigate their visible, IR and mechanical properties. Mechanical characterization was achieved using tensile testing. Visible characterization was checked using UV-VIS analysis. IR spectroscopy was done using FTIR analysis, and IR transparency, reflectance and emission were also analyzed and characterized using a FLIR E75 thermal camera and a heat source.

Chapter 3 presents a detailed process of reducing warpage problem of HDPE in FDM 3D printing. In this phase, HDPE is blended with LLDPE in various concentrations, filaments were manufactured and used for 3D printing to investigate impact of each blend on warpage values. Warpage values were also examined at different angles of the print specimen. Print process parameters and build materials were also optimized to minimize warpage of HDPE. Mechanical characterization tests were also performed on each blend and comparison was made with pure HDPE.

Chapter 4 summarizes the major findings and conclusion of this thesis and suggests future directions for this research work.

Chapter 2

Enhancing optical properties and preserving IR transparency: pigmentation technique for visibly opaque yet highly IR transparent LLDPE

2.1 Introduction

Linear low-density polyethylene is a semi-crystalline polymer with short branches on its main molecular chains. This means that these linear molecules do not become entangled as easily as LDPE and HDPE. It is a low-density polymer having a density that ranges between 0.915 and 0.930 g/cm3 [134], [135]. LLDPE plastic is typically made from one of three different co-monomers classified as alpha-olefins: octene, hexene, butene. Due to its lower cost, butene is the most common co-monomer for commodity plastic applications[136], [137]. The butene co-monomer has the shortest branch chains. Various blends of the above-mentioned co-monomers are also used to adjust the properties of LLDPE plastic, the most common being a blend of butene and hexene [61]–[63], [138]. Linear low-density polyethylene is manufactured via the copolymerization of ethylene and an alpha-olefin. The catalyst (either Ziegler-Natta or metallocene) and ethylene are blown into a fluidized bed reactor where copolymerization occurs. The polymer then settles at the bottom and exits the reactor as a powder which is then pelletized [139], [140]. Linear low-density polyethylene has many advantages and is well suited for thin-film properties. Their excellent properties like puncture-resistance, good flexibility, resistant to oxidation, high impact strength, stress cracking resistance and UV resistance make them desirable for various applications in packaging, agriculture, medical and industrial applications [135], [141]–[146]. LLDPE is often compounded with different filler and additives to enhance and tailor its applications for various applications. In the packaging industry, LLDPE is widely compounded with additives such as antioxidants, slip agents and anti-block agents to improve its performance to make films, bags, and other packaging sheets [87], [147]. For instance, Dadbin et al. performed a study to replace polyethylene multi-layer films used in food packaging industry with single-layer

polyethylene nanocomposites films. They reported that addition of organoclay even at low level (below 5 phr) in LLDPE had a significant effect on barrier properties of the nanocomposites and decreased oxygen permeability by 50% by adding only 3 per hundred resin (phr) of nanoclay into the blend [148]. Panrong et al. added Green tea (GT) and thermoplastic starch (TPS) from native starch (NS) and acetylated starch (AS) with different degrees of substitution (DS) with linear low-density polyethylene (LLDPE) to developed TPS-GT LLDPE films. These films showed high efficacy as active eco-friendlier food packaging, with enhanced stability of meat and oil-based food products [149]. Similarly, LLDPE is compounded with UV stabilizers and other additives to improve its UV resistance and degradation [150]. This has its application in agriculture industry in which LLDPE is compounded to make films for greenhouse covers, silage bags and mulch films [151], [152]. Korol et al. investigated the recycling potential of LLDPE wastes originated from the agricultural films recycling line. They modified LLDPE them with 2.5 wt % of commercially available compatibilizers and presented their reusability [153]. Seven and others presented the preparation and biological assessment of an insecticide releasing plastic film by incorporation of deltamethrin loaded, nano-sized halloysite nanotubes into LLDPE polymeric films for agricultural covering purposes. They presented nanocomposites are observed to repel mature aphids and kill young aphids and thrips [150]. In the construction industry, LLDPE is compounded to be used as geomembrane material for lining landfills, reservoirs, and other water containment systems [154]–[156]. LLDPE is compounded with additives such as carbon black and antioxidants to improve its resistance to UV radiation, weathering and chemical degradation [157]–[161]. In the medical industry, LLDPE is compounded with biocompatible additives to products such as medical tubing, bags, antibacterial containers etc. [65], [162]–[164]. For instance Harun et al. investigated the actions of LLDPE/TiO_2/ZnO (1:3) nanocomposites in different weight% against two

representative MDR pathogens, namely, methicillin-resistant *Staphylococcus aureus* (MRSA) and *Klebsiella pneumonia* (*K.pneumoniae*). The study presented reduction in the bacterial adherence and biofilm formation and found that high ZnO weight ratio killed both types of pathogens [165]. Recently, LLDPE has found renewed interest in radiative passive cooling applications due to its high infrared transparency and tunable visible opacity [79], [80], [166]–[171]. However, it is challenging and many a times involves complex chemical steps to achieve desirable compounding of LLDPE. For instance, Peng et al. used paraffin oil as solvent to dissolve PE, continuously extruded it by industrial extruder machine to form fibers with microscale diameter. Upon cooling, solid-phase PE was separated from liquid-phase paraffin oil. Subsequently, methylene chloride was used to extract oil phase from PE fibers. Their study found resulting fibers, compared with commercial cotton fibers showed greater cooling power [172]. In this study, we aim to present a simpler, and easier method to custom compound LLDPE to achieve visually appealing LLDPE blends for diverse applications while retaining their desirable IR and mechanical properties. Compounded LLDPE will be extruded into filaments and formed into micro composite sheets to test their mechanical, visible and IR properties.

2.2 Materials and methodology

2.2.1 Materials

Linear low linear low-density polyethylene (LLDPE, MKCH0863; melt index 1.0 g/10 min (190 °C/2.16 Kg)) in the form of pellets was purchased from Sigma-Aldrich. Zinc oxide (ZnO, powder, UPS-2 grade, min. 99%, CAS no. 1314-13-2, Lot # H5C 486) and Titanium dioxide (TiO_2, powder, FCC grade, min. 99%, CAS no. 13463-67-7, Lot # C8C039) were bought from ChemicalStore.com. Zinc Sulfide (ZnS, powder, 10 μm, 99.99% trace metals basis, CAS no. 1314-98-3, MW: 97.46 g/mol, density: 4.1 g/mol at 25 °C, Lot #MKCM9532) was acquired from Sigma-

Aldrich. Iron oxide yellow (FeO, Yellow 930 dark, synthetic (> 3 nm), temperature resistance: 120°C, Lot# 48045), Iron oxide light brown (FeO, brown 610 light, synthetic (> 3 nm), temperature resistance: 120°C, Lot# 48300), Iron oxide dark brown (FeO, brown 686 dark, synthetic (> 3 nm), temperature resistance: 120°C, Lot# 48360) were purchased from Kremer Pigmente. Polyethylene powder (low melting point 105°C, CAS# 9002-88-4, Lot# L8C722 (EP51102373)) was purchased from Chemcialstore.com. Heat press machine (hydraulic, model: CR2042-1, serial: AP005-209) was bought from Amazon.ca to make micro-composite films. Wellzoom B desktop single screw extruder (extrusion rate capacity of 10"-26"/min, and a temperature of 180-190 ℃) was used for extrusion. [173].

2.2.2 Fabrication of master batches of pigments

In this study, we introduced a simpler and easier method to custom compound LLDPE with pigments. Pigmentation of LLDPE is achieved using custom compounding of master batches of six pigments chosen for their high IR transparency and bold coloration potential to obtain visually appealing colors/ surface finishes while not interfering with IR properties of LLDPE. The six IR transparent pigments are: ZnO, TiO_2, ZnS, FeO yellow, FeO light brown, FeO dark brown. Three different concentrations of compounded LLDPE were studied: 1 wt%, 3wt% and 5 wt%. The process of making master batch of pigments is same for the blend. Each particular pigment was mixed with polymer wax (polyethylene powder) in 1:1 ratio by weight. A master batch of 50g of (1:1) pigment-wax mixture was made for each pigment. These mixtures were then melted under heat press for three times at a temperature of 190℃ to achieve uniform melting. When cooled, they were crushed into smaller granules and stored as master batch for each pigment. Desired amounts of pigment-wax mixture were mixed with LLDPE pellets to achieve the required pigment concentration levels for each blend. For instance, 6 g of pigment-wax mixture (which contains 3 g

pigment and 3 g wax) was taken out of master batch and mixed with 94 g of LLDPE to achieve 3 wt% ZnS-LLDPE blend. Similarly, 10 g of pigment-wax mixture was taken out of FeO Yellow pigment master batch and added with 90 g of LLDPE to achieve 5 wt% FeO yellow-LLDPE blend. The detailed concentration levels of pigment, polymer wax and LLDPE in each blend are listed in Table 1. Polymer wax was used as a mixing agent that ensures uniform mixing of pigment with LLDPE. A complete schematic diagram showing step by step process of making of master batches and subsequent compounding and extrusion of LLDPE blends is shown in Figure 3. There are six pigments, each pigment is blended with LLDPE in three concentrations (1,3 and 5 wt%) so in total, there are 18 compounded LLDE blends.

Table 1:Concentrations of custom compounded LLDPE blends

Custom compounded LLDPE Blends	Concentration levels		
	Pigment	Polymer wax	LLDPE
Pure LLDPE	0 wt	0 wt	100 wt
1 wt% ZnS-LLDPE	1 wt	1 wt	98 wt
3 wt% ZnS-LLDPE	3 wt	3 wt	95 wt
5 wt% ZnS-LLDPE	5 wt	5 wt	90 wt
1 wt% TiO_2-LLDPE	1 wt	1 wt	98 wt
3 wt% TiO_2-LLDPE	3 wt	3 wt	95 wt
5 wt% TiO_2-LLDPE	5 wt	5 wt	90 wt
1 wt% ZnS-LLDPE	1 wt	1 wt	98 wt
3 wt% ZnS-LLDPE	3 wt	3 wt	95 wt
5 wt% ZnS-LLDPE	5 wt	5 wt	90 wt

1 wt% FeO yellow-LLDPE	1 wt	1 wt	98 wt
3 wt% FeO yellow -LLDPE	3 wt	3 wt	95 wt
5 wt% FeO yellow -LLDPE	5 wt	5 wt	90 wt
1 wt% FeO light brown -LLDPE	1 wt	1 wt	98 wt
3 wt% FeO light brown -LLDPE	3 wt	3 wt	95 wt
5 wt% FeO light brown -LLDPE	5 wt	5 wt	90 wt
1 wt% FeO dark brown -LLDPE	1 wt	1 wt	98 wt
3 wt% FeO dark brown -LLDPE	3 wt	3 wt	95 wt
5 wt% FeO dark brown -LLDPE	5 wt	5 wt	90 wt

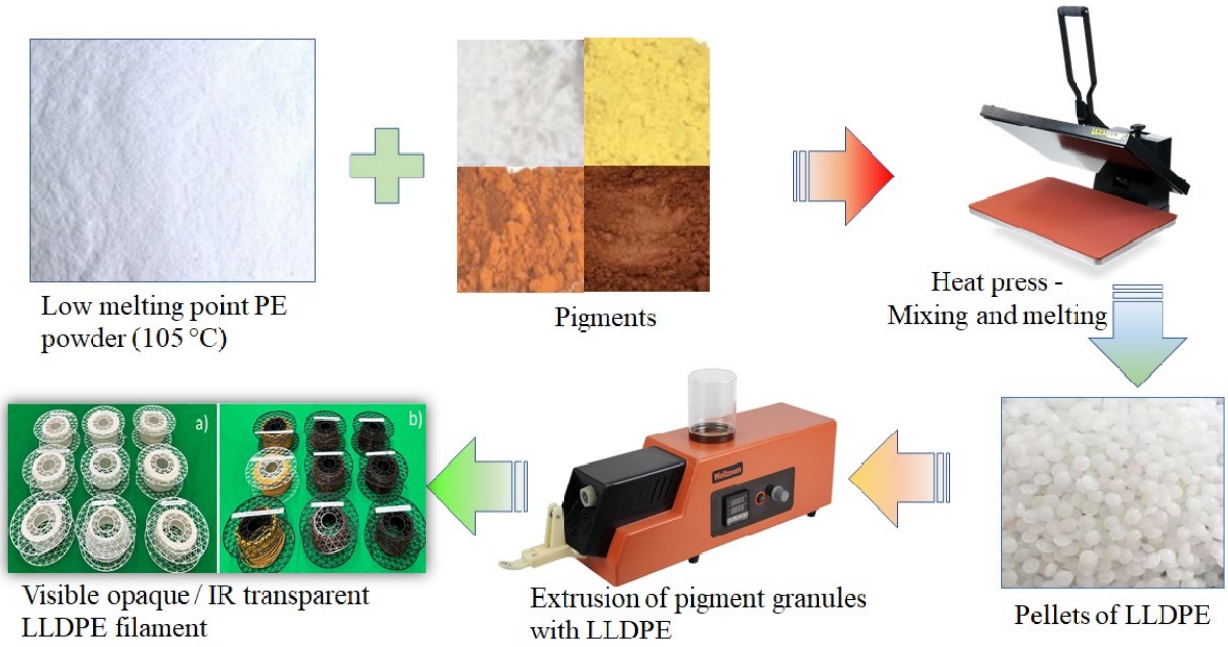

Figure 3: Schematic diagram of preparation of masterbatches of pigments and subsequent compounding and extrusion of LLDPE blends

2.2.3 Filament fabrication

After making the master batches of pigments, they were mixed with pellets of LLDPE in specified

concentration and extruded into filaments using Wellzoom desktop extruder. The extruded polymer strands were pulled off under a gravity fed pulling system, cooled at room temperature and then wound up on a spool [174]. The parameters used for filament extrusion are listed in Table 2. The filaments extruded for all the pigmented LLDPE concentrations are shown in Figure 4.

Table 2: Extrusion parameters for filament fabrication

Extrusion parameters	Value
Extrusion Temperature	190 °C
Speed of rotation	6 RPM
Ambient temperature	22 °C
Extrusion rate	14’’/min

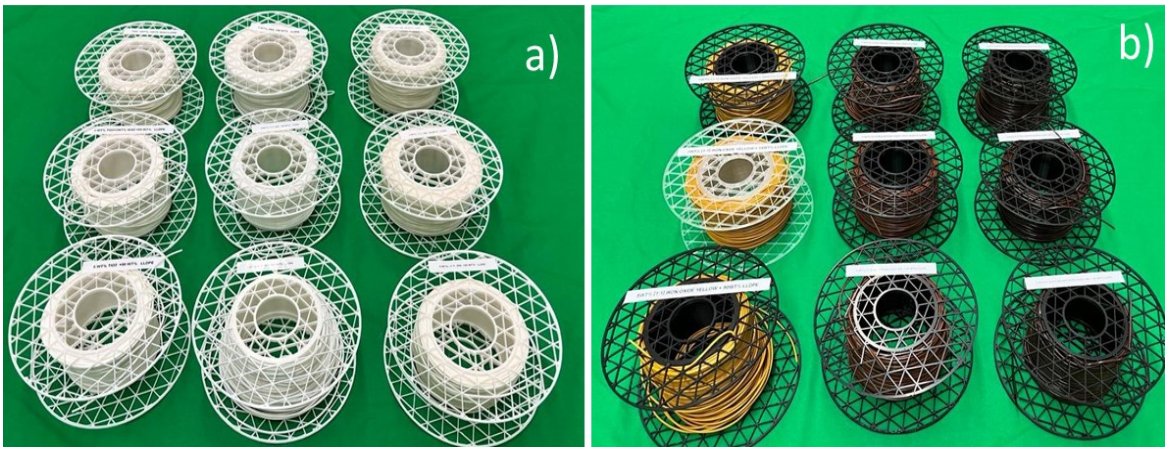

Figure 4: a) White filaments: ZnS, TiO_2, ZnO b) Colored pigments: FeO yellow, light brown, dark brown

2.2.4 Mechanical characterization

The tensile strength, also known as the ultimate tensile strength, is the load at failure divided by the original cross-sectional area where the ultimate tensile strength (U.T.S.). The equation is

$$\sigma_{max} = P_{max} / A_0 \qquad (1)$$

where P_{max} = maximum load, A_0 = original cross-sectional area. The actual area A at break is measured by measuring the diameter of fractured specimen and using the equation $A = \pi r^2$ where r is radius. The Young's modulus (E) is a property of the material that tells us how easily it can stretch and deform and is defined as the ratio of tensile stress (σ) to tensile strain (ε). The equation is

$$E = \frac{\sigma}{\varepsilon} \qquad (2)$$

where stress is the amount of force applied per unit area (σ = F/A) and strain is extension per unit length (ε = dl/l). Elongation at break, also known as fracture strain, is the ratio between changed length and initial length after breakage of the test specimen. The equation is

$$\varepsilon = (\Delta L/L) \times 100 \qquad (3)$$

Where ε is the elongation, ΔL is the final length, L is the initial length.

Mechanical characterization tests were performed on the extruded filaments. Sample filament of gauge length of 25 mm were cut for each of the 18 pigmented LLDPE blends. The samples were installed between two pneumatic clamps of Instron 5960 series machine. The Instron machine had a load cell with 50 N capacity. The filament specimens were elongated at a speed of 25 mm/min until break. Four samples were tested for each compounded LLDPE blend. Tensile strength, Young's modulus and elongation at break were investigated for each blend. Data was gathered, values were noted and relevant plots were drawn. Same tensile testing was also performed for pure LLDPE for comparison. The findings are presented in the results and discussion section. The

tensile testing setup is shown in Figure 5.

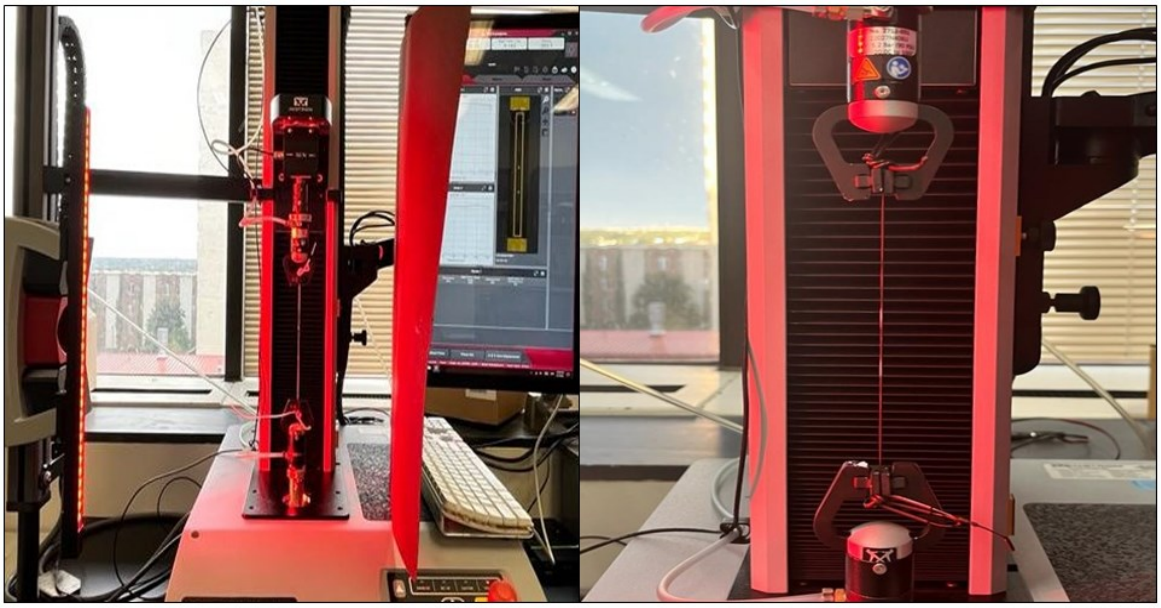

Figure 5: Instron tensile machine testing of pigmented LLDPE filaments

2.2.5 Fabrication of micro size pigmented LLDPE sheets

The extruded filaments of each blend of pigmented LLDPE were cut into small pieces. The pieces of filament were then melted in a heat press at 190°C and pressures of 2,4 and 6 bars to achieve sheets of 150, 100 and 50 µm thicknesses, respectively. The heat press process was repeated three times for each blend, each concentration and each thickness to achieve uniform thickness and coloration in the final sheets. Sheets of different thicknesses were prepared and cut into squares of 1x1 inch for each of the 18 blends. A set of two sheets for each thickness of each blend were prepared, so in total, there are 108 sheets of pigmented LLDPE blends. Along with this, sheets of different thickness (50,100,150 µm) were also prepared for pure LLDPE for comparison. The schematic process of micro sheet fabrication is shown in Figure 6.

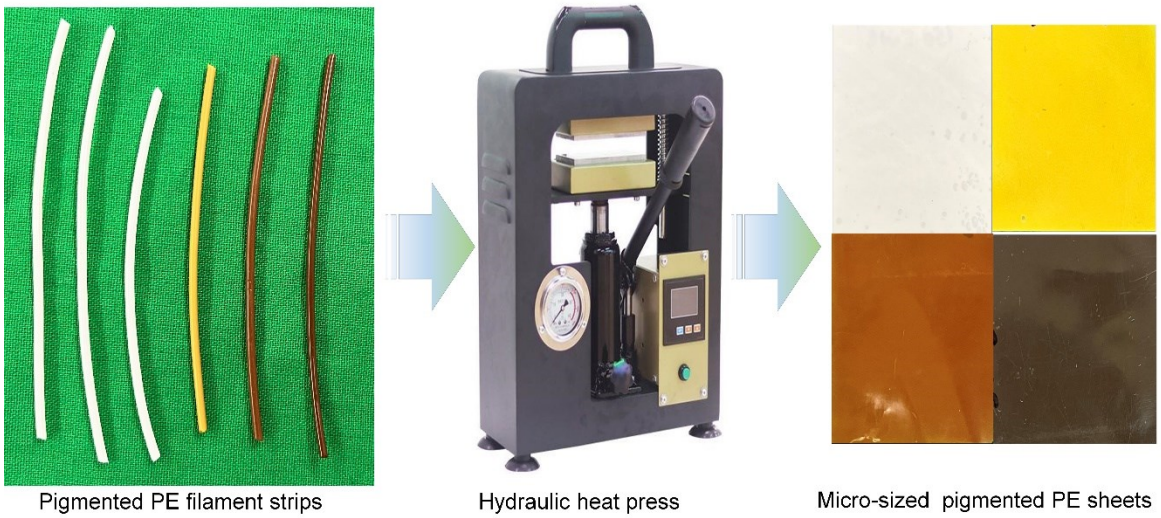

Figure 6: Pigmented PE sheet were hydraulically heat pressed in the thicknesses of 50, 100 and 150 μm for three different concentrations of 1, 3, 5 wt% for each pigment.

The pictures of pigmented sheets cut in 1x1 inch size are shown in Figure 7.

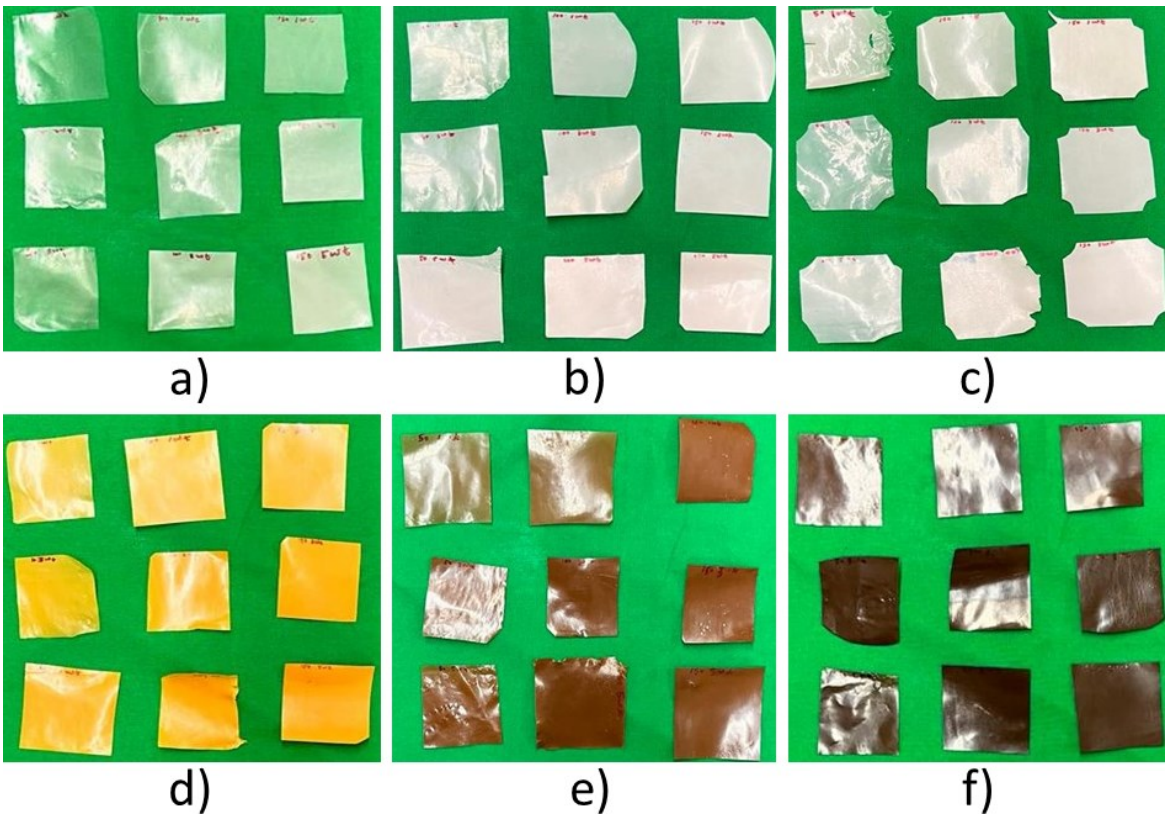

Figure 7: 50, 100, 150 µm thickness (vertical), 1, 3, 5 wt% concentrations (horizontal) for six pigments: a) ZnS, b) TiO_2, c) ZnO, d) FeO yellow, e) light brown, f) dark brown.

2.2.6 FTIR analysis

Fourier Transform Infrared Spectroscopy Technique (FTIR) is used for characterizing the pigmented blends of LLDPE. FTIR samples were cut from 150 µm thick sheets for each pigmented LLDPE blend. 50 and 100 µm thickness samples were neglected because FTIR is independent of the thickness of the sample sheets and only varies for each pigment concentration. Samples were cut in a 10x10 mm shape and were installed in the FTIR Spectrometer Spectrum. The data was collected from the absorption spectra ranges between 5 µm to 25 µm. Spectra of pure and pigmented blends of LLDPE film samples were acquired and normalized in order to identify characteristic absorbance peaks and quantify their relative absorbance values. Two different spots

on each film were selected to perform the measurement. The schematic of the FTIR setup is shown in Figure 8.

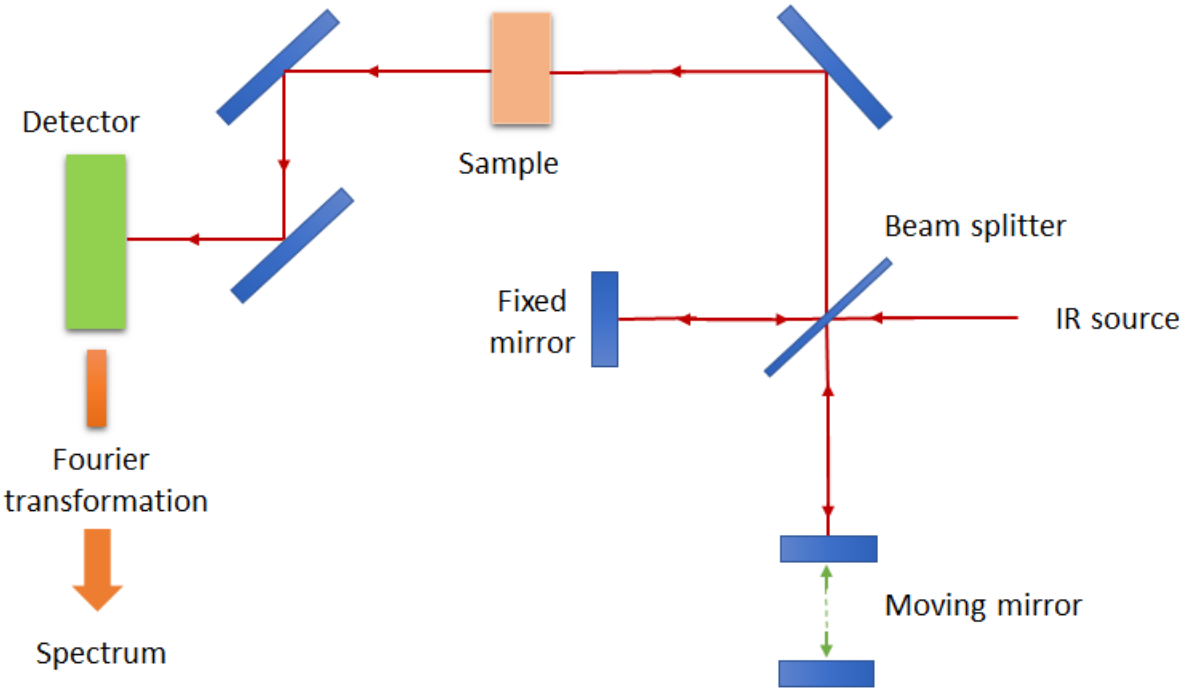

Figure 8: FTIR schematic diagram setup

2.2.7 UV-VIS analysis

The absorbance rate of the extruded blend films was measured by an ultraviolet-visible spectrometer. The diameters of the light source beam and the detector were approximately 3 mm. The distance between film and detector was 6 mm. The film samples were cut for each pigment, concentration, and thickness level. Through visual inspection, it was clearly seen that all of the colored pigmented LLDPE sheets are visibly opaque while it was harder to determine the opacity of white pigments through visual inspection. Therefore, UV-VIS was performed on the white pigments and compared with pure LLDPE. Two different spots on each film were selected to perform the measurement. The schematic of the UV-VIS spectroscopy setup is show in Figure 9. UV-VIS analysis was performed for sheets of pure LLDPE (50, 100, 150 µm thickness) and white

pigmented LLDPE blends (1,3, 5 wt% concentrations and 50, 100, 150 µm thickness) on the visible spectrometer. White pigments presented a range of opaqueness with some being highly opaque and some being semitransparent, therefor it was vital to rank their UV-VIS absorbance. Colored pigments, on the other hand, were highly and completely opaque under naked eye which is required for our applications, therefore they were not tested under UV-VIS. The visible spectrometer did not allow to extract data points therefore, pictures were taken, which were uploaded in ImageJ software and the data points were traced and extracted and gathered in excel using imageI software. The graphs were plot in the Origins software.

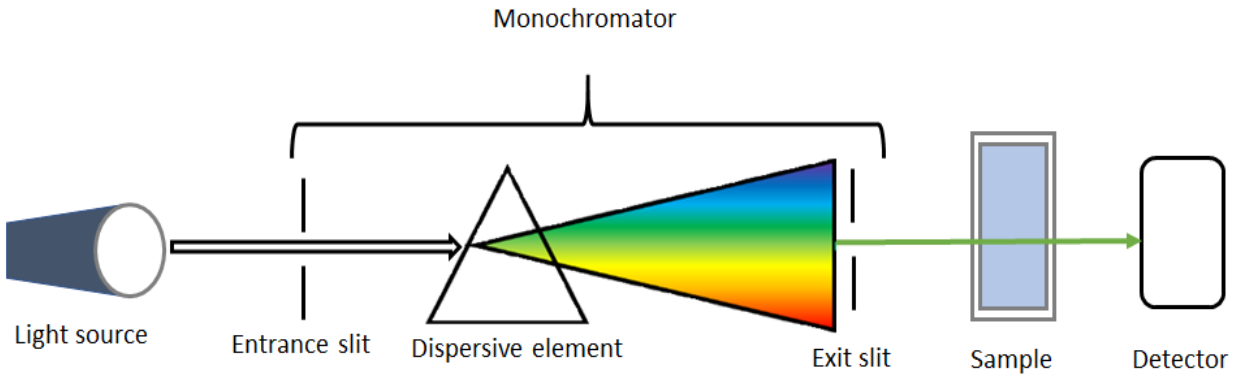

Figure 9: UV-VIS schematic diagram setup

2.2.8 IR analysis

To determine that all of the pigmented LLDPE blends still retained their desirable IR properties as close to that of pure LLDPE, a comprehensive IR analysis was performed. In this regard, three types of tests were performed and three types of IR properties - transparency, reflectance and emissivity - were tested. An experimental setup was designed for testing each property. An IR opaque fixture was designed and 3D printed to hold the 1x1 inch sheets of pigmented LLDPE. A FLIR E75 thermal camera was used to capture the data. For transparency testing: the 1x1 inch pigmented LLDPE sheets were installed in the fixture and placed directly in front of the heat source

at a distance of 1 inch. The heat source was set to 49°C for each test. The IR camera was placed on a tripod and pointed directly at the sheets at a distance of 2 feet. The IR radiation is emitted by the heat source, pass through the sheets and are detected by the IR camera to determine the IR transparency of each pigment, concentration and thickness level. The schematic of the setup is shown in Figure 10.

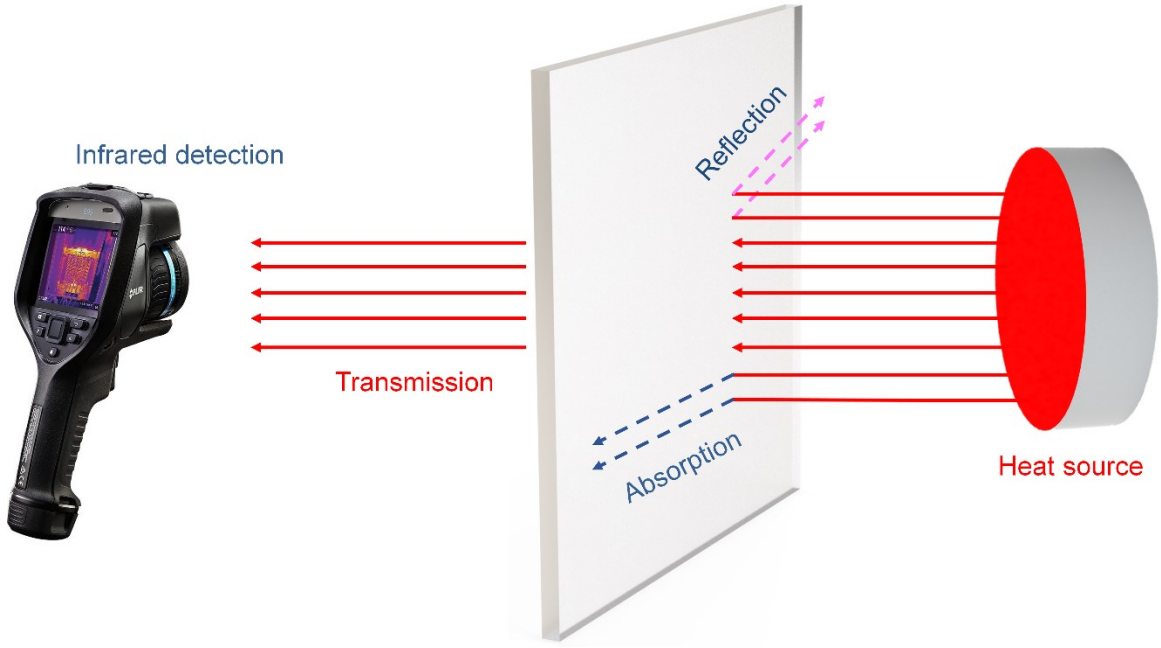

Figure 10: IR transmission testing setup - schematic diagram

For emittance tests, the pigmented LLDPE sheets were placed directly on top of the heat source. The readings were taken after five minutes to let the sheets temperature reach the heat source's temperature. Once the temperature was stable, the same process was repeated for testing the emittance radiation and the IR emission data was recorded using the IR camera pointed directly at the sheet at a standoff distance of 2 feet. The schematic of the setup is show in Figure 11.

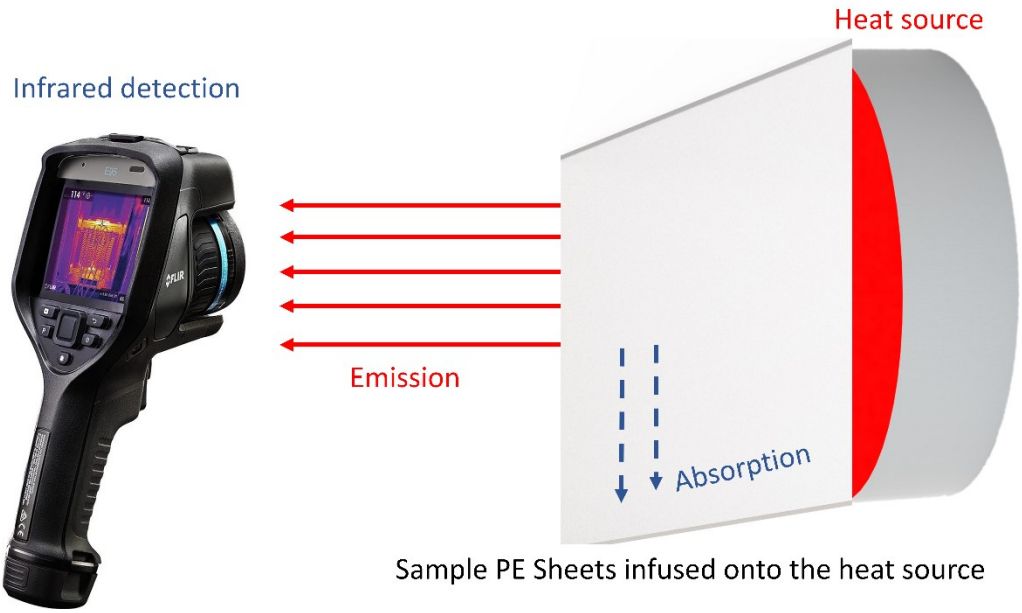

Figure 11: IR emission testing setup - schematic diagram

For reflectance testing, a 1.5x1.5-foot metalized mylar sheet was placed on top of a fixture which was used as a mirror to reflect IR radiation. The metalized mylar sheet was placed at a distance of 2 feet from the heat source at an angle of 45° and was adjusted until the heat source was completely reflected by the metalized mylar sheet as detected in the IR camera placed at a 45° angle. The pigmented LLDPE sheets were placed in front of the metalized mylar sheet at a distance of 1 inch and the IR radiation was collected through the IR camera. These results capture the transparency power of pigmented LLDPE sheets for IR radiations coming from a reflected heat source at an angle of 45°. The schematic of the setup is shown in Figure 12.

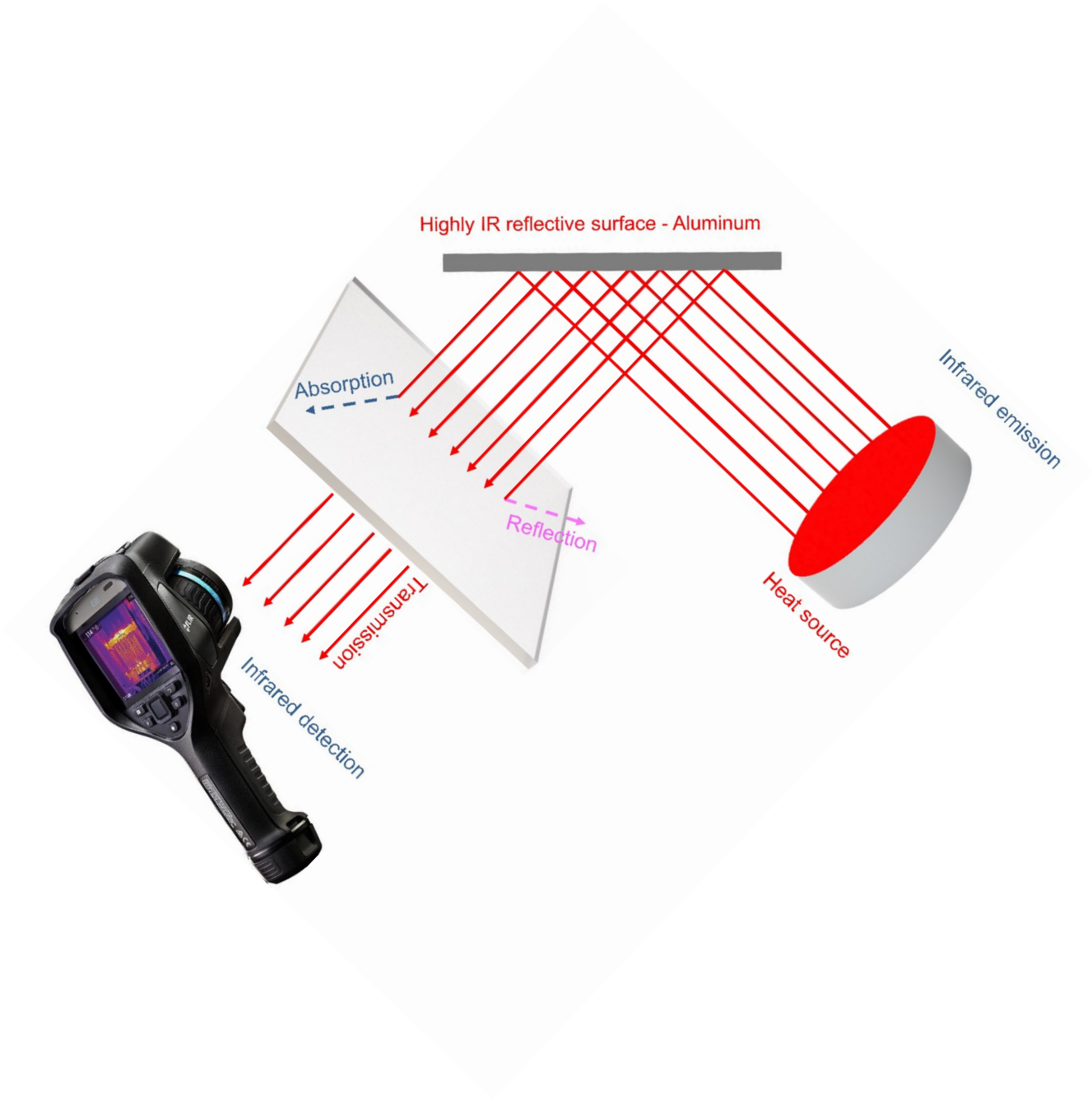

Figure 12: IR reflectance testing setup - schematic diagram

The IR camera was pointed at three points of each sheet and the tests were performed on two sets of sheets for testing each property and for each testing setup. The average was taken for each reading and noted as the temperature reading for that particular sheet. The actual pictures of these setups are shown in Figure 13.

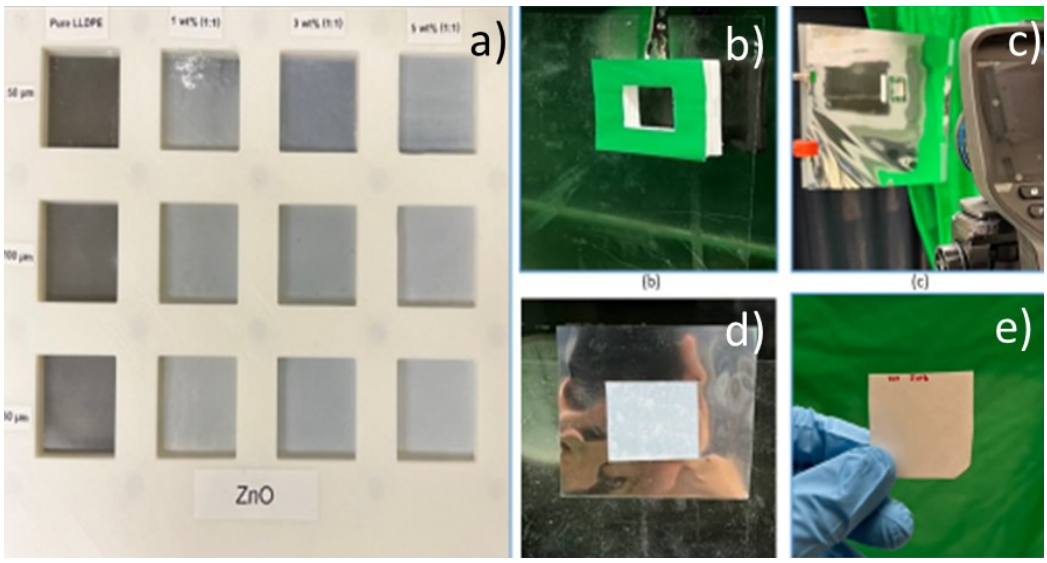

Figure 13: Setup of IR analysis. a) Fixture designed to hold pigmented sheets, b) Transparency setup c) Reflectance setup, d) Emissivity setup e) singular sheet of ZnO showing for reference.

2.3 Results and discussion

2.3.1 Mechanical characterization

The mechanical load capacity of pigmented LLDPE blends was investigated to determine what negative impacts on modulus and strength would occur with the addition of the pigments. In this regard, tensile strength, Young's modulus, and elongation at fracture were calculated for each blend and compared with the mechanical characterization values of pure LLDPE. Stress-strain curve is presented in Figure 14 which shows a trend similar to those of thermoplastics available in the literature [175]. The rest of the results are summarized in Table 3, Table 4, Table 5 and displayed in Figure 15, Figure 16, Figure 17. The results indicate that pure LLDPE exhibits the highest tensile strength value of 14 MPa while1 wt% pigmented blends also show similar tensile strength values. This is because the concentration level of the pigment/wax blend is so low that it does not affect the overall tensile strength of the blends. 3 wt% blends have tensile strength values

in the range of 13 MPa and 5 wt% blends have tensile strength in the range of 12 MPa which is lower than that of pure LLDPE. This reduction in tensile strength is due to presence of pigment and polymer wax which are not as strong as LLDPE. Overall, pigmented LLDPE filaments show a very small reduction in their tensile strength as compared to that of pure LLDPE unless added in higher quantities as it is suspected that most of the reduction comes mainly from the wax binder for the pigment due to its lower molecular weight.

A similar trend is observed with Young's modulus. The results indicate that pure LLDPE exhibits the highest modulus of 145 MPa. 1 wt% pigmented blends exhibit a similar value of Young's modulus in the range of 140 MPa. This is because the concentration level of the pigment is so low that it does not affect the overall Young's modulus of the blends. 3 wt% blends have Young's modulus in the range of 110-120 MPa which represent an approximate 20% reduction compared with pure LLDPE. This not significant reduction and does not affect overall mechanical strength properties of the blends. 5 wt% blends have Young's modulus in the range of 90 MPa. This reduction is observed due to the addition of wax and pigments which have lowered the overall Young's modulus of the compounded filaments.

Similar trend is also observed in elongation at break values. The results indicate that pure LLDPE filaments have elongation at break value of 1200%. 1 and 3 wt% pigmented blends exhibit a similar value of elongation at break in the range of 1150-1240%. This is very close to the elongation at break values of pure LLDPE which means addition of 1 and 3 wt% have almost negligible effect on the elongation at break of LLDPE blends. 5 wt% blends have elongation at break values in the range of 1040-1100% which represents a reduction of approximately 10.5% as compared to pure LLDPE. This reduction in overall elongation at break is still not significantly huge and does not impact the overall mechanical profile of blends. To sum up, the impact of mixing up to 3 wt% of

pigments LLDPE has shown very minimal impact on the overall mechanical strength whereas 5 wt% can show somewhat impactful reduction in the mechanical strength of filaments. Therefore, pigments concentration should be optimally limited up to 3 wt% in order to reduce any impact on mechanical strength of pigmented filaments.

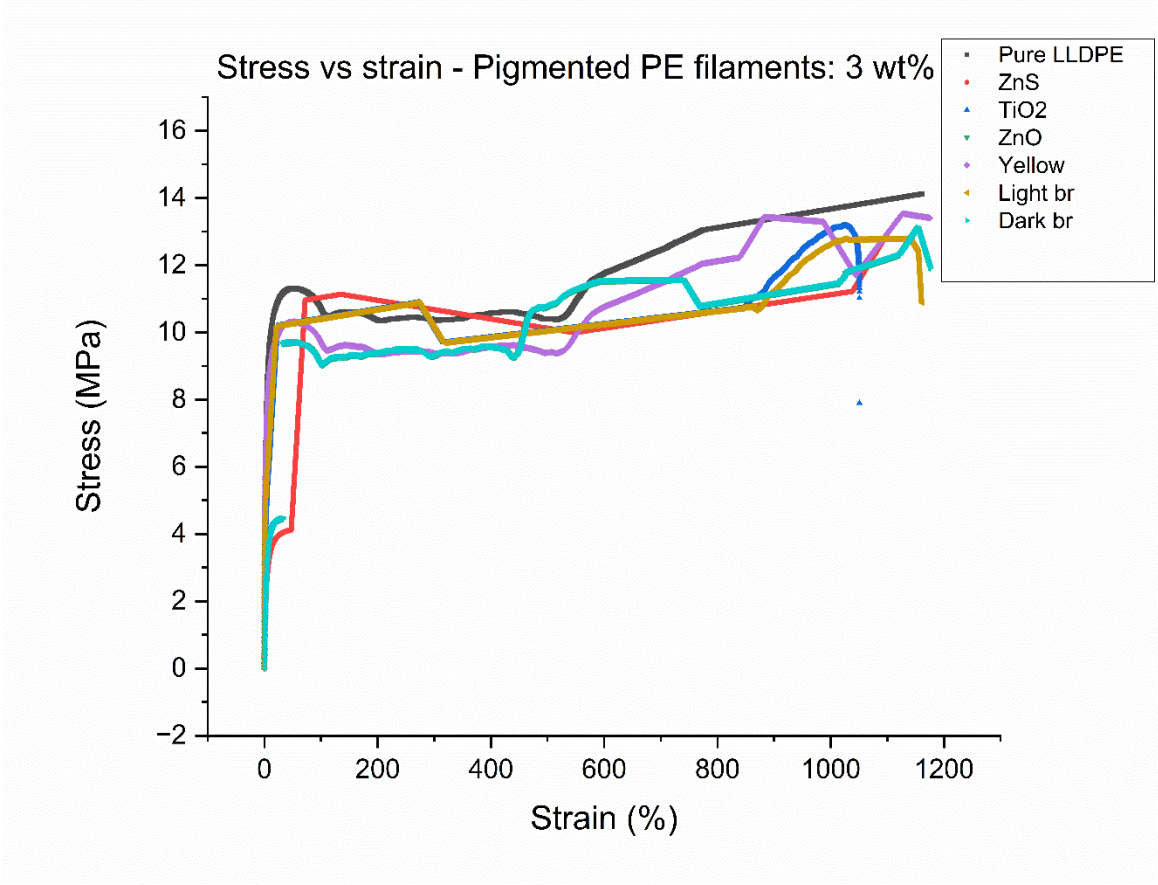

Figure 14: Stress vs strain curve for pigmented PE filaments at 3 wt%

Table 3: Mechanical properties (Young's modulus, tensile strength, elongation at break) of 1 wt% LLDPE blends

LLDPE filaments	**Young's modulus (MPa)**	**Tensile strength (MPa)**	**ε_{max} (%)**
Pure LLDPE	145 ± 30	14.0 ± 1.0	1200 ± 50

ZnS (1 wt%)	140 ± 40	14.0 ± 1.0	1240 ± 30
TiO_2 (1 wt%)	134 ± 25	13.8 ± 1.0	1225 ± 30
ZnO (1 wt%)	141 ± 40	14.5 ± 1.5	1220 ± 25
FeO yellow (1 wt%)	143 ± 25	15.0 ± 0.7	1230 ± 20
FeO light brown (1 wt%)	146 ± 15	14.3 ± 1.0	1165 ± 40
FeO dark brown (1 wt%)	147 ± 20	14.3 ± 1.0	1150 ± 50

Table 4: Mechanical properties (Young's modulus, tensile strength, elongation at break) of 3 wt% LLDPE blends

LLDPE filaments	**Young's modulus (MPa)**	**Tensile strength (MPa)**	**ε_{max} (%)**
Pure LLDPE	145 ± 40	14.0 ± 1.0	1200 ± 50
ZnS (3 wt%)	113 ± 30	13.0 ± 1.2	1175 ± 35
TiO_2 (3 wt%)	115 ± 25	13.2 ± 1.3	1155 ± 25
ZnO (3 wt%)	120 ± 20	13.0 ± 0.8	1170 ± 30
FeO yellow (3 wt%)	122 ± 25	13.4 ± 0.5	1160 ± 30
FeO light brown (3 wt%)	110 ± 20	12.9 ± 1.0	1175 ± 40
FeO dark brown (3 wt%)	110 ± 30	13.3 ± 1.0	1190 ± 35

Table 5: Mechanical properties (Young's modulus, tensile strength, elongation at break) of 5 wt% LLDPE blends

LLDPE filaments	**Young's modulus (MPa)**	**Tensile strength (MPa)**	**ε_{max} (%)**

Pure LLDPE	145 ± 40	14.0 ± 1.0	1200 ± 50
ZnS (5 wt%)	90 ± 40	12.5 ± 0.4	1055 ± 40
TiO_2 (5 wt%)	99 ± 25	12.0 ± 0.7	1100 ± 30
ZnO (5 wt%)	98.5 ± 30	12.2 ± 0.9	1080 ± 25
FeO yellow (5 wt%)	95 ± 15	12.1 ± 0.3	1070 ± 25
FeO light brown (5 wt%)	90 ± 25	12.3 ± 1.2	1040 ± 35
FeO dark brown (5 wt%)	92 ± 35	12.0 ± 1.1	1035 ± 30

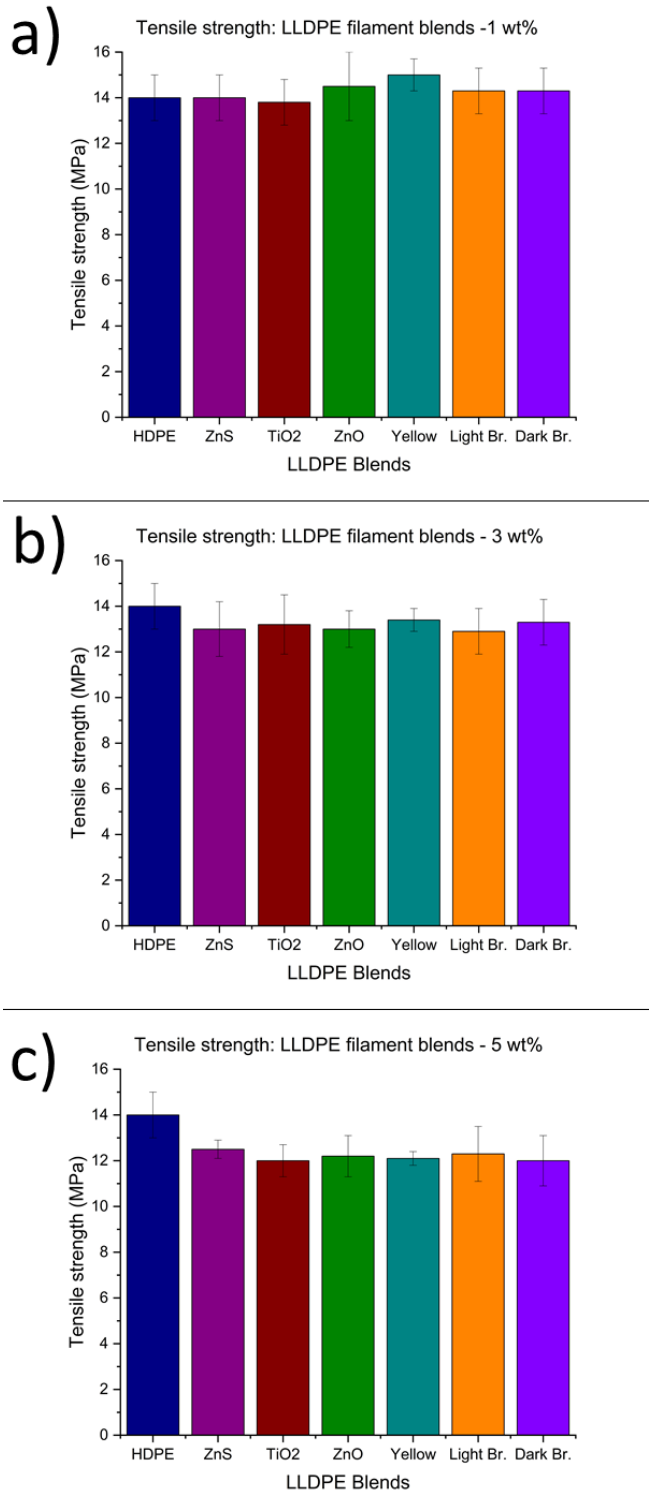

Figure 15: Tensile testing a) 1 wt% pigmented LLDPE blends b) 3 wt% pigmented blends c) 5 wt% pigmented blends

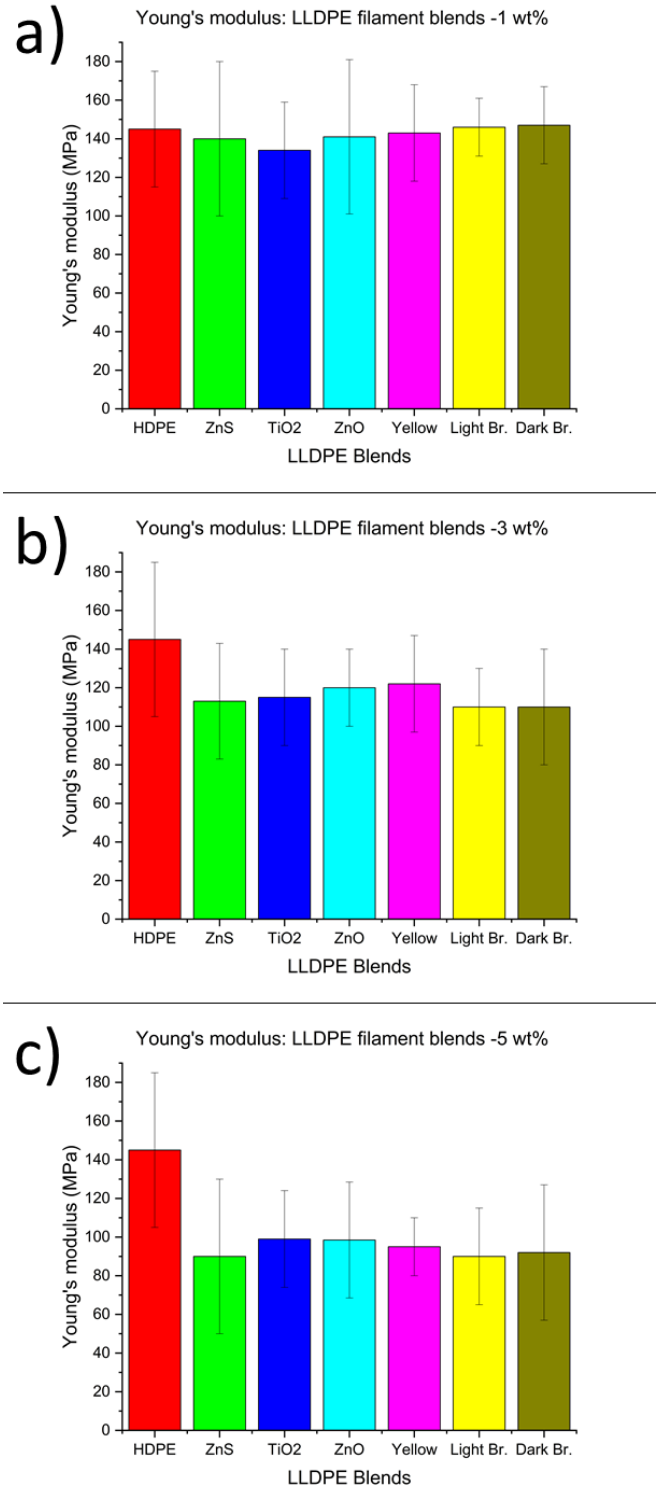

Figure 16: Young's modulus a) 1 wt% pigmented LLDPE blends b) 3 wt% pigmented blends c) 5 wt% pigmented blends

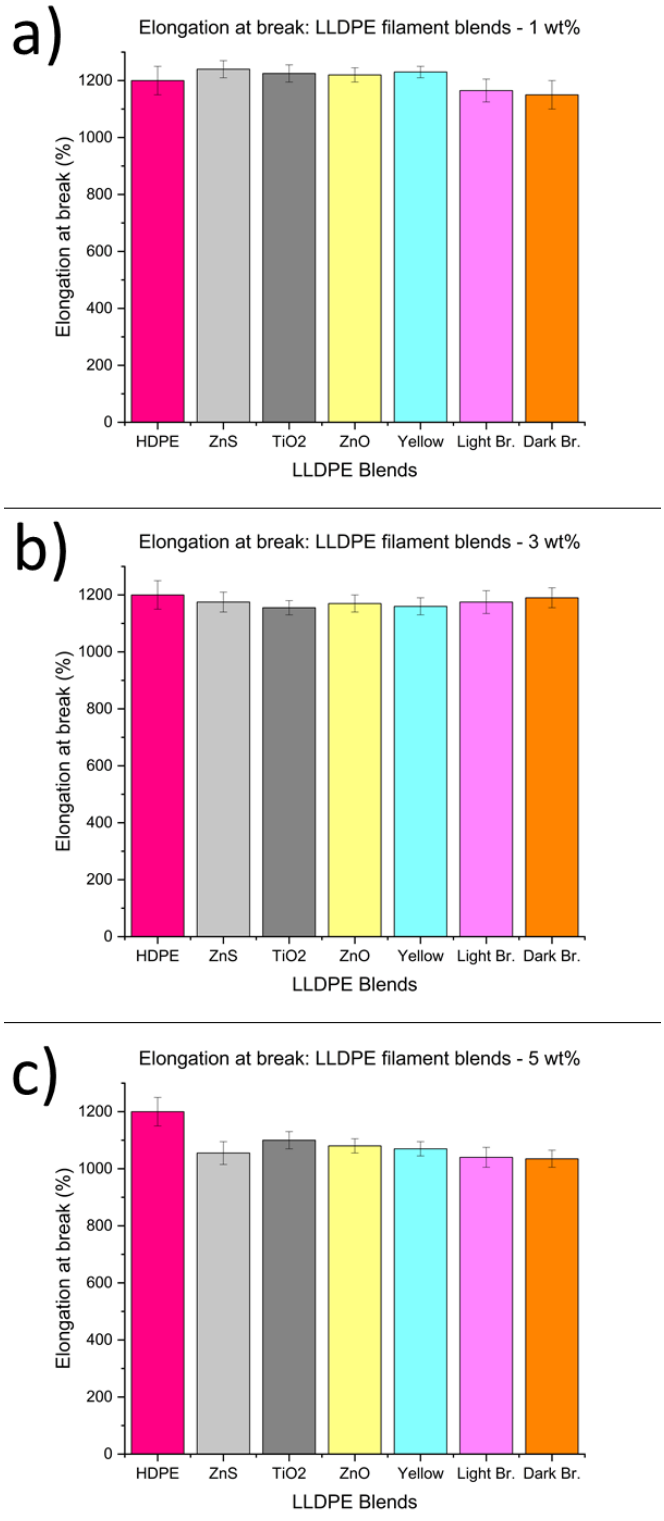

Figure 17: Elongation at break a) 1 wt% pigmented LLDPE blends b) 3 wt% pigmented blends c) 5 wt% pigmented blends

2.3.2 FTIR analysis

The FTIR analysis data was gathered, analyzed and plotted with wavenumber (in μm) along x-axis and peaks in percentage on y-axis. The FTIR graphs for white pigments were stacked along y-axis on one graph to make a comparison with pure LLDPE and each other. Similarly, FTIR graphs for colored pigments were stacked along y-axis on one graph to make a comparison with pure LLDPE and each other. The FTIR graphs for white pigmented blends (ZnS, TiO_2, ZnS with 1,3,5 wt% concentrations for each) are presented in Figure 18, whereas FTIR graphs for color pigmented blends (yellow, light brown, dark brown with 1,3,5 wt% concentrations for each) are presented in Figure 19.

For us, we are interested to know whether adding pigments in concentrations of 1,3,5 wt% in LLDPE have any impact on IR properties of LLDPE or not. Since IR wavelength spectrum for human body is around 10 μm range. By looking at Figure 18 and Figure 19, it is evident that there are no peaks at 8-12 μm wavelength range for LLDPE as well as for any of the white pigmented LLDPE blends, therefore, it means that white pigmented LLDPE blends exhibit a same IR behavior as pure LLDPE. This is because only those pigments were chosen specifically which have IR transparency properties similar to LLDPE at those wavelengths. Blends show a few smaller absorbance peaks at around 5 μm, 7 μm and 14.5 μm range which are due to presence of $C\text{-}CH_3$ and $C\text{-}CH_2$ groups and are in correspondence with the literature [176].

A similar trend was observed in FTIR plots of colored pigmented blends of LLDPE. By looking at the graphs, it is evident that there are no peaks at 10 μm wavelength range for LLDPE as well as for any of the colored pigmented LLDPE blends, therefore, it means that colored pigmented LLDPE blends exhibit a similar IR behavior as pure LLDPE at those wavelengths. This means that addition of colored pigments in concentrations of up to 5 wt% does not change the IR behavior of

LLDPE at wavelengths in the range of 8-12 µm. There are some a fewer absorbance peaks at around 5 µm, 7 µm, 14.5 µm range which are present due to the presence of methyl, ethyl groups as well as due to presence of pigments such as Fe_3O_4 group present in the colored pigments. Overall, the FTIR behavior shows us that pigmented LLDPE blends show a similar behavior in IR range in the 8-12 µm wavelength range which is very desirable for us for the camouflage and radiative passive heating and cooling applications.

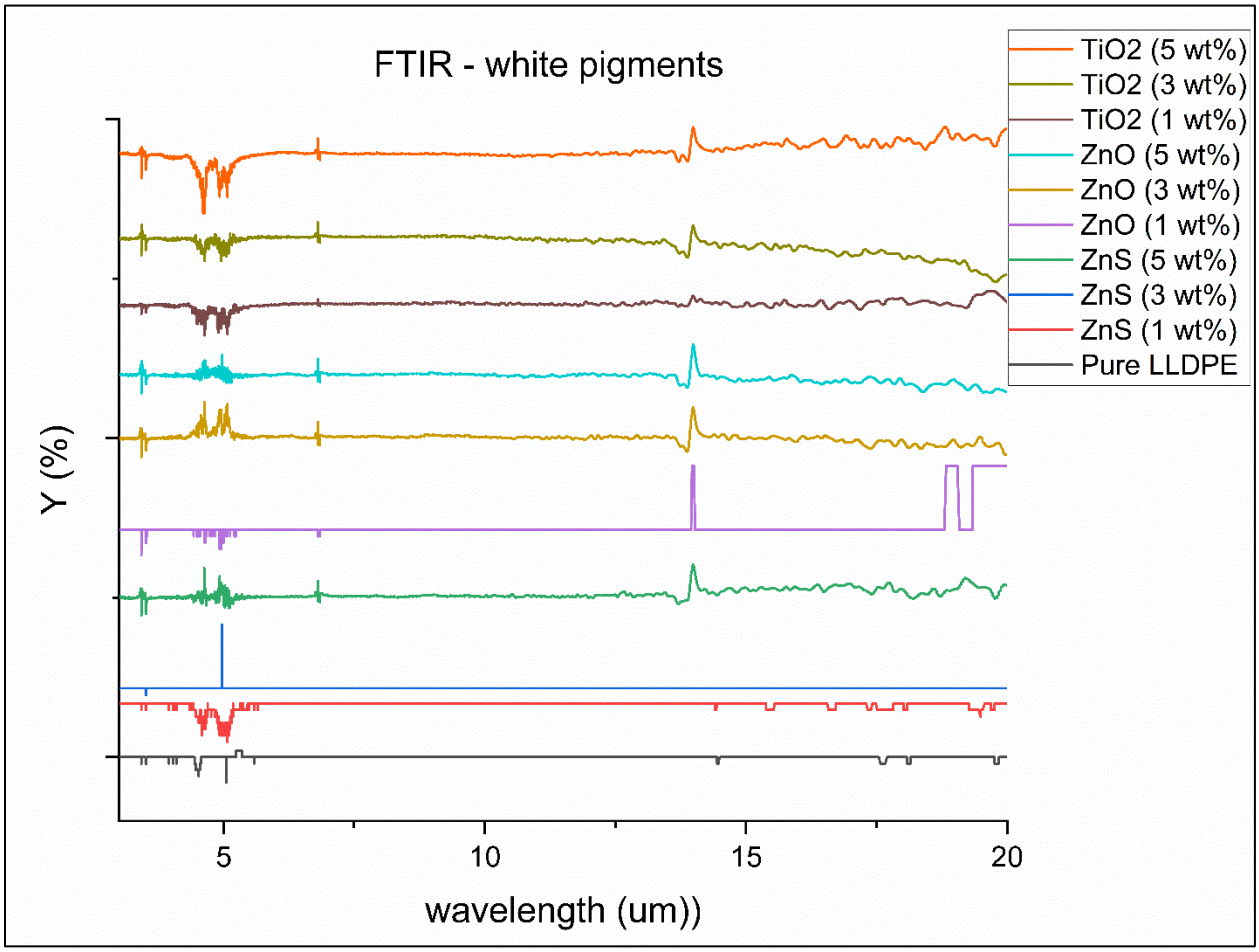

Figure 18: FTIR analysis - (1,3,5 wt%) white pigmented LLDPE blends

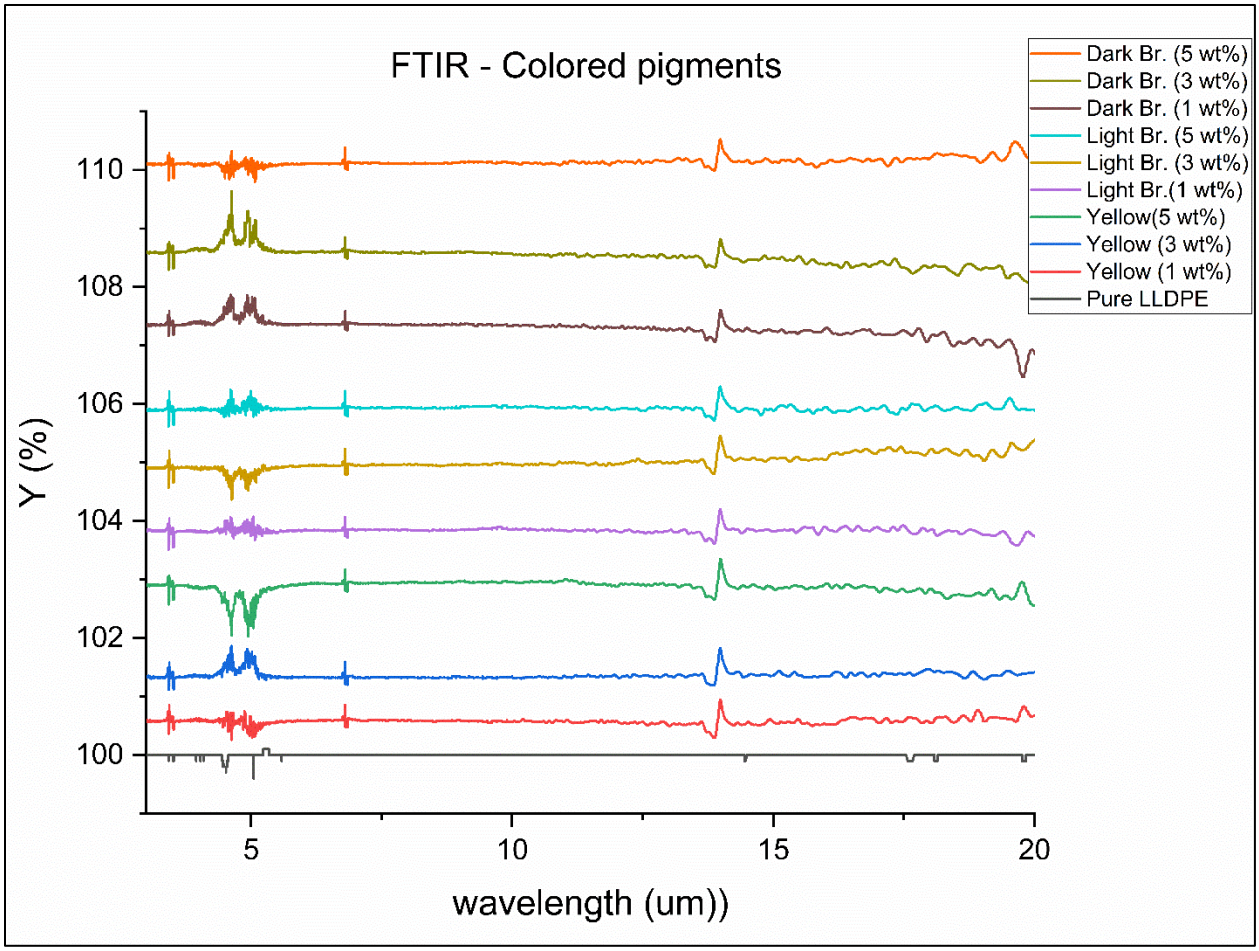

Figure 19: FTIR analysis - (1,3,5 wt%) colored pigmented LLDPE blends

2.3.3 UV-Vis analysis

The UV-Vis plots for 1 wt% (with 50, 100, 150 µm thickness), 3 wt% (with 50, 100, 150 µm thickness) and 5 wt% (with 50, 100, 150 µm thickness) are presented in Figure 20, Figure 21, Figure 22 respectively. The visible range (400-650) of the wavelength spectrum is plotted along x-axis and absorbance is plotted along y-axis since we are not interested in the UV range for our camouflage and radiative heating and cooling applications. Pure LLDPE has maximum absorbance value at around 0.1 for all the thicknesses. This is very close to zero meaning LLDPE is very transparent in the visible range. The graph shows that LLDPE has low absorbance. It tends to transmit a significant of visible light, particularly in the higher wavelength range. As a result, the

visible spectrum of LLDPE shows an almost flat or very little gradually decreasing baseline as the wavelength increases. LLDPE is known for its excellent transparency in the visible spectrum, allowing most visible light to pass through and that is what we saw in the graph as well which is in line with the literature. As we know that the visible spectrum for LLDPE can be influenced by various factors, such as the specific composition, additives, processing conditions, and thickness of the LLDPE sample [177], [178]. Therefore, the visible spectrum of LLDPE can exhibit some variations depending on these factors.

From the graphs, it is visible that white pigments absorb more visible light that LLDPE in the order of ZnS, TiO_2 and ZnO respectively with ZnO being the most absorbing. These trends align with our observations through naked eye under visible light. ZnO is more transparent as in closer in transparency to pure LLDPE followed by TiO_2 and ZnO which are opaquer. All the graphs show a gradually decreasing baseline as the wavelength increases which means that they absorb more at lower wavelengths. This trend is in coherence with that of pure LLDPE and the literature. Moreover, this trend is attributed to the presence of LLDPE since LLDPE holds at or more than 90 wt% concentration in the blends.

Apart from this, there are two main trends observed in the graphs. These trends are observed across all the pigments. One is that the blends absorb more at higher thicknesses i.e absorbance increases with increase in thickness. For instance, 1 wt% TiO_2 has approximate absorbance values of 0.6, 1.0 and 1.5 for 50 µm, 100 µm and 150 µm thicknesses respectively at 420 µm wavelengths. A similar trend is shown for the rest of the pigmented blends.

Number two is that the absorbance increases with increase in concentration of white pigments. For instance, at 100 µm, 1 wt%, 3 wt% and 5 wt% ZnO have an approximate absorbance value of 1.2, 1.45 and 1.8 respectively at 420 µm wavelengths. These trends are in line with our expectations

and visible qualitative observations because pigmentation makes LLDPE opaquer in the visible range.

To summarize, ZnS pigmented LLDPE blends are transparent and lie in the range of pure LLDPE. Then comes the TiO_2 which is somewhat transparent for 1 wt% pigmentation concentrations and lower thicknesses. However, becomes very opaque at higher thicknesses and concentrations especially at 5 wt%. ZnO is the opaquest of all when compared with pure LLDPE at all concentration and thickness levels. Therefore, for applications where LLDPE is required to be visibly opaque, pigmenting LLDPE with ZnO can be a great solution.

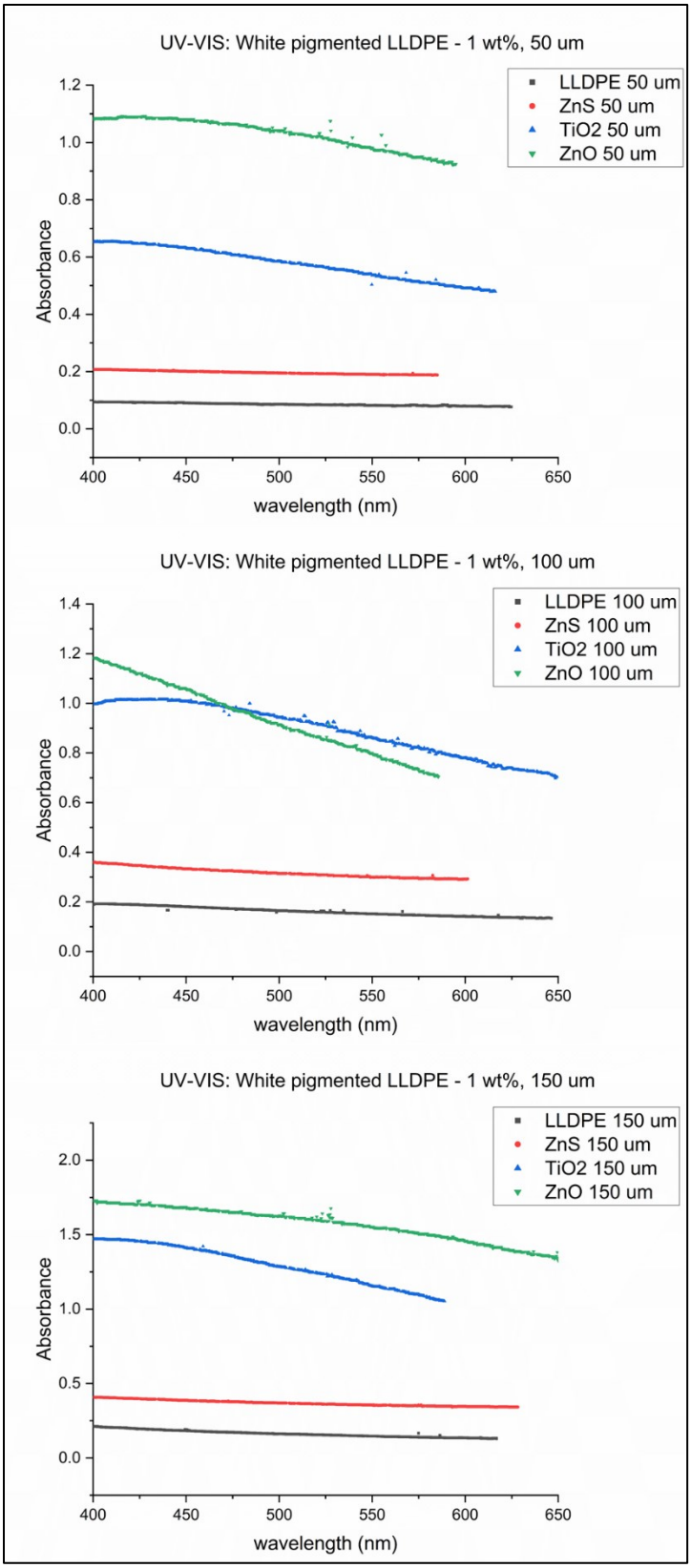

Figure 20: UV-VIS analysis - 1 wt% (50, 100, 150 µm) pigmented LLDPE blends

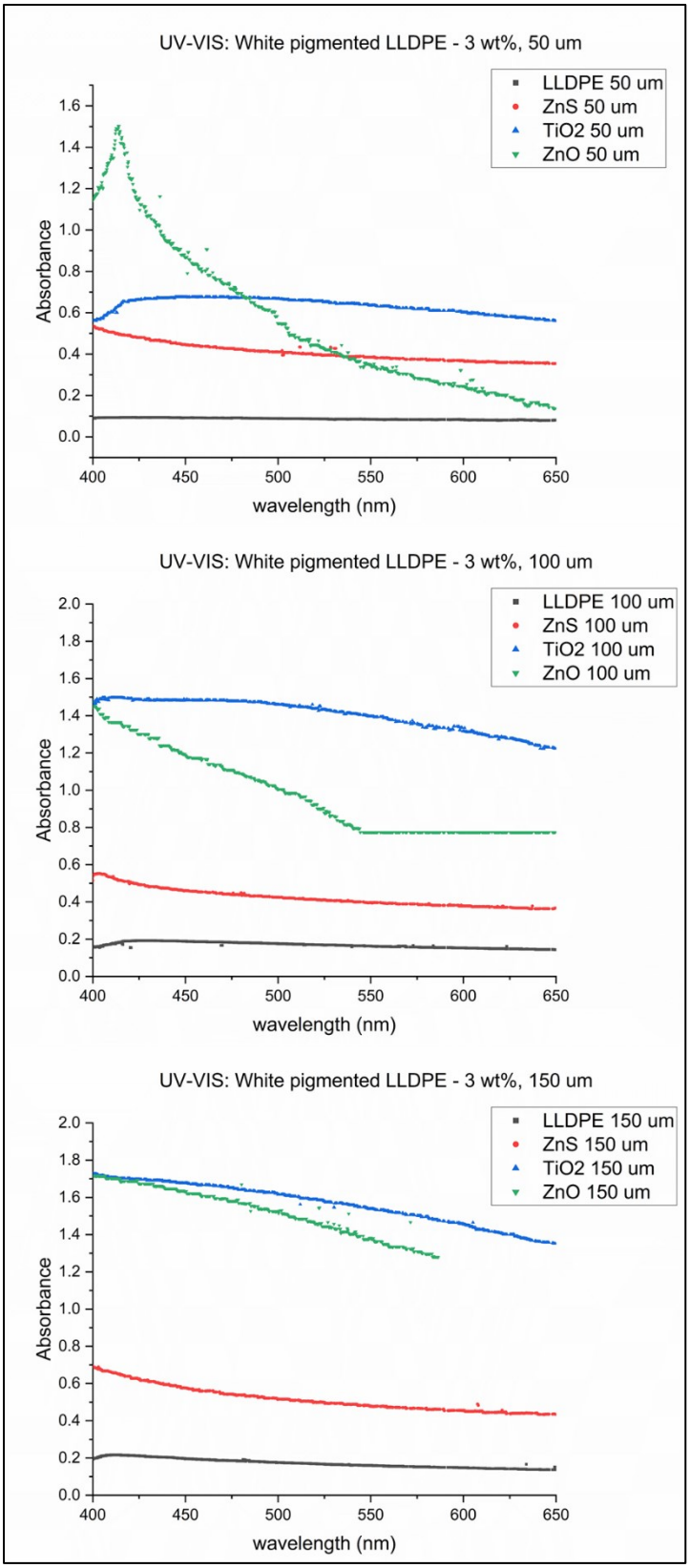

Figure 21: UV-VIS analysis - 3 wt% (50, 100, 150 µm) pigmented LLDPE blends

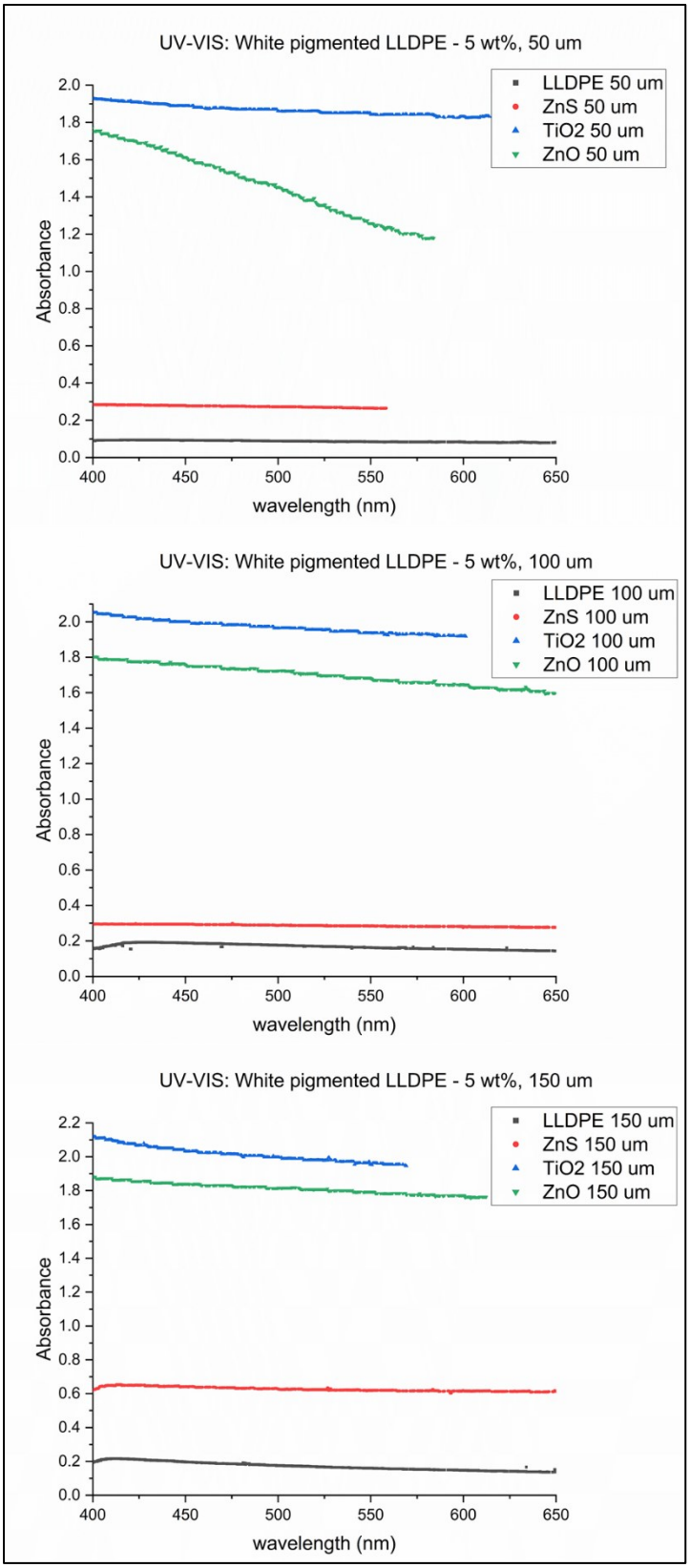

Figure 22: UV-VIS analysis - 5 wt% (50, 100, 150 µm) pigmented LLDPE blends

2.3.4 IR analysis

IR transparency, reflectance and emittance tests were performed, the data was collected by the IR camera for all pure LLDPE, all the pigments, concentrations and thicknesses along with IR picture taken by the camera. The pictures of the sheets along with their IR temperature reading were recorded, sorted and put together for each pigment and a comparison was made with pure LLDPE. This means that we have six pictures (one for each pigment) for transparency. Similarly, we have six pictures (one for each pigment) for reflectance and six pictures (one for each pigment) for emittance tests. Only the pictures for the most optimal pigments for each category will be presented. These pictures are presented in Figure 23, Figure 25, Figure 27. The rest of the data is shared and discussed in bar graphs so that we can compare them easily with one another. These graphs are presented in Figure 24, Figure 26, Figure 28.

2.3.4.1 IR Transparency

After recording the temperature reading for each sheet using FLIR E75 thermal camera and taking the average for all the readings, it is noted that under IR camera, pure LLDPE has temperature readings of 44.5° C, 43.5° C, 42.3° C for 50 μm, 100 μm and 150 μm thick sheets, whereas the source temperature reading is 49° C. This means that pure LLDPE lets approximately more than 85% of the IR radiations to pass through it. In other words, it is very highly transparent.

From the charts, it is clear that ZnO has the highest IR transparency among the white piments whereas yellow FeO has the highest IR transparency among colored pigments. Moreover, IR transparency decreases in the following order for the pigments: ZnO, ZnS, TiO_2, yellow, light brown and dark brown respectively with dark brown being the least IR transparent when compared with pure LLDPE. This is because, pigmented LLDPE samples exhibit increased light scattering due to imperfections, impurities, particle size and different absorbance spectra within the material.

Light scattering contributes to reduced transparency by redirecting and diffusing the incident IR radiation rather than transmitting it through the blended sheets.

ZnO is known for its relatively high IR transparency. It has a wide bandgap and exhibits minimal absorption in the IR region, allowing IR radiation to transmit through the material more readily. While ZnS has good transparency in the visible spectrum, it absorbs more in the IR region than ZnO. The particle size of ZnS used in pigmented LLDPE blends can vary, but it is usually larger than that of ZnO. The larger particle size contributes to some light scattering, reducing overall IR transparency compared to ZnO. TiO_2 exhibits lower IR transparency compared to ZnO and ZnS. The absorption spectra of TiO_2 typically show peaks in the IR range, indicating significant absorption of IR radiation.

FeO Yellow, FeO Light Brown, and FeO Dark Brown are iron oxide-based pigments which have Fe_3O_4 in them which has high IR absorbance properties. Iron oxide pigments exhibit absorption in both the visible and IR regions. The absorption spectra of iron oxide pigments show strong absorption bands in the visible range, which indicates that they are effective in providing coloration. However, this also implies that they absorb a significant portion of IR radiation, leading to reduced IR transparency. The particle size of iron oxide pigments used in pigmented LLDPE blends can also be responsible for affecting transparency, with larger particle sizes contributing to increased light scattering and decreased IR transparency.

Apart from this, there are two more trends visible from the charts. Number one is that IR transparency decreases very slightly with increase in the concentration of the pigments. For instance, for 150 µm sheets of TiO_2 at 1 wt%, 3 wt% and 5 wt%, the temperature reading under IR are 41.6° C, 41.2° C and 38.6° C respectively. This slight decrease, even though insignificant, is due to the higher concentration of pigment in LLDPE especially at 5 wt% . As the concentration

of the pigment increases, more pigment particles are present in the LLDPE material. These particles have absorption properties higher than LLDPE that can absorb and scatter IR. When IR radiation encounters pigment particles, they can scatter the light in various directions instead of transmitting it through the material. Moreover, with higher pigment concentrations, there is also a higher probability of particle aggregation or clustering within the LLDPE matrix. Aggregated pigment particles can create larger structures that effectively scatter and absorb more IR radiation. Therefore, as the concentration of the pigment increases, there is a higher absorption of IR radiation by the pigment particles, leading to a decrease in IR transparency of LLDPE blend.

The second trend is that IR transparency decreases slightly with increase in thickness of the sheets. This trend is observed across all the blends and is in line with our expectations and literature. For instance, 5 wt% light brown pigmented LLDPE sheet, under IR, shows a temperature reading of 43.1° C, 40.2° C, 37.4° C for 50 μm, 100 μm and 150 μm thicknesses. This is because LLDPE, like other polymers, has specific molecular vibrations and modes that can absorb IR radiation. In the mid-infrared region, these vibrations are associated with bending, stretching, and rotational motions of the polymer chains. When thin layers of LLDPE and its pigmented blends are encountered by IR radiation, the radiation can easily penetrate the material due to the relatively low probability of absorption by the limited number of polymer chains. However, as the thickness of the LLDPE increases, the probability of encountering absorbing groups and polymer chains also increases. Consequently, there is a greater chance of the IR radiation being absorbed by the polymer chains, resulting in reduced transparency.

To summarize, IR transparency tests of pigmented LLDPE sheets have presented excellent results with very high IR transparency values, very close to those of the pure LLDPE for corresponding thicknesses. Therefore, we can successfully pigment LLDPE to tune its visible properties without

significantly impacting its IR transparency which is desirable for our camouflage and radiative cooling and heating applications.

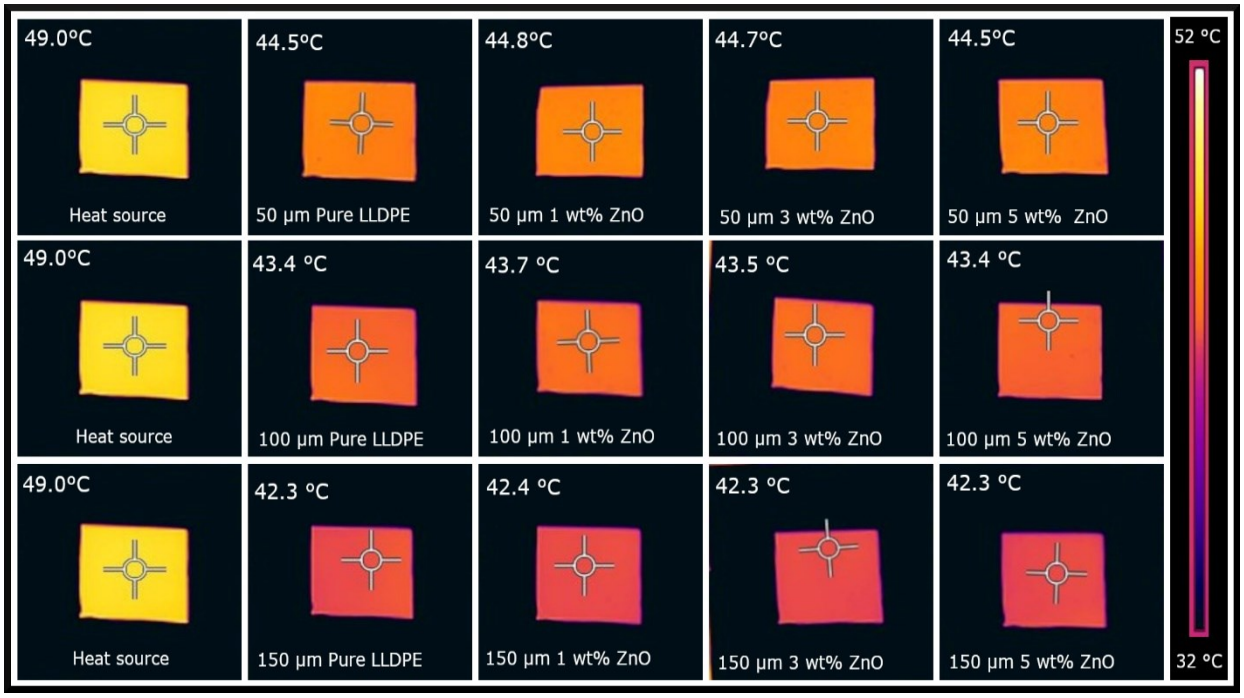

Figure 23: ZnO IR transparency. 1st column: Heat source, 2nd column (50,100,150um thickness downwards): pure LLDPE, 3rd column: 1 wt% ZnO, 4th column: 3 wt% ZnO, and 5th column: 5 wt% ZnO

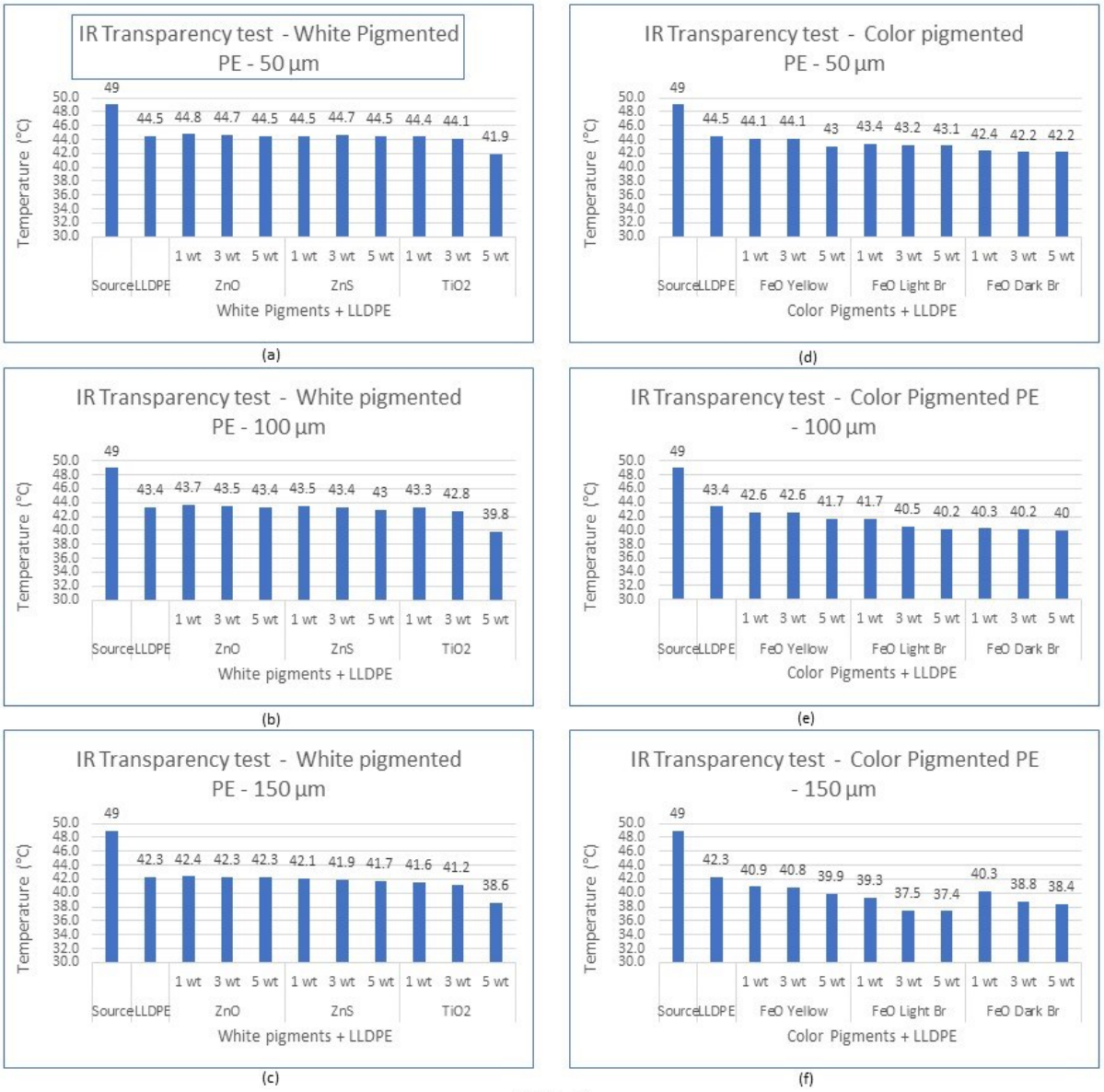

Figure - 1

Figure 24: IR transparency: a) White pigments (ZnO, ZnS, TiO_2) at 50 µm, b) white pigments at 100 µm, c) white pigments at 150 µm, d) colored pigments (FeO yellow, light brown, dark brown) at 50 µm, e) colored pigments at 100 µm, and f) colored pigments at 150 µm

2.3.4.2 IR Reflectance

After recording the temperature reading for each sheet using FLIR E75 thermal camera and taking

the average, it is noted that under IR camera, pure LLDPE, for reflectance, has temperature readings of 44.5° C, 43° C, 41.° C for 50 μm, 100 μm and 150 μm thick sheets, whereas the source temperature reading is 49° C. This means that pure LLDPE has high transmittance for reflected IR radiations.

When looked at the IR reflectance rates for pigmented LLDEP sheets, it is observed that ZnO has the highest IR reflectance among the white piments whereas yellow FeO has the highest IR reflectance among colored pigments. Moreover, IR transparency decreases in the following order for the pigments: ZnO, ZnS, TiO_2, yellow, light brown and dark brown respectively with dark brown showing the least IR reflectance when compared with pure LLDPE. The rest of the trends are also same as observed in IR transparency tests. That is IR reflectance decreases with increase in concentration of pigments as well as an increase in the thickness of sheets. The reasons are same as stated in the previous section. However, the IR reflectance values are overall lower than IR transparency values. This is because IR radiation that is reaching the sheets is itself being reflected through metalized mylar sheet which contributed to the its own absorption and scattering of IR before it reaches the sheets. That is why the trend is consistent across the board for all the sheets. Finally, it is seen that reflectance values of the pigmented LLDPE blends for lower thickness and concentrations are comparable with those of pure LLDPE. Therefore, it is concluded with confidence that LLDPE can be pigmented successfully while still providing high IR reflectance properties comparable with that of pure LLDPE.

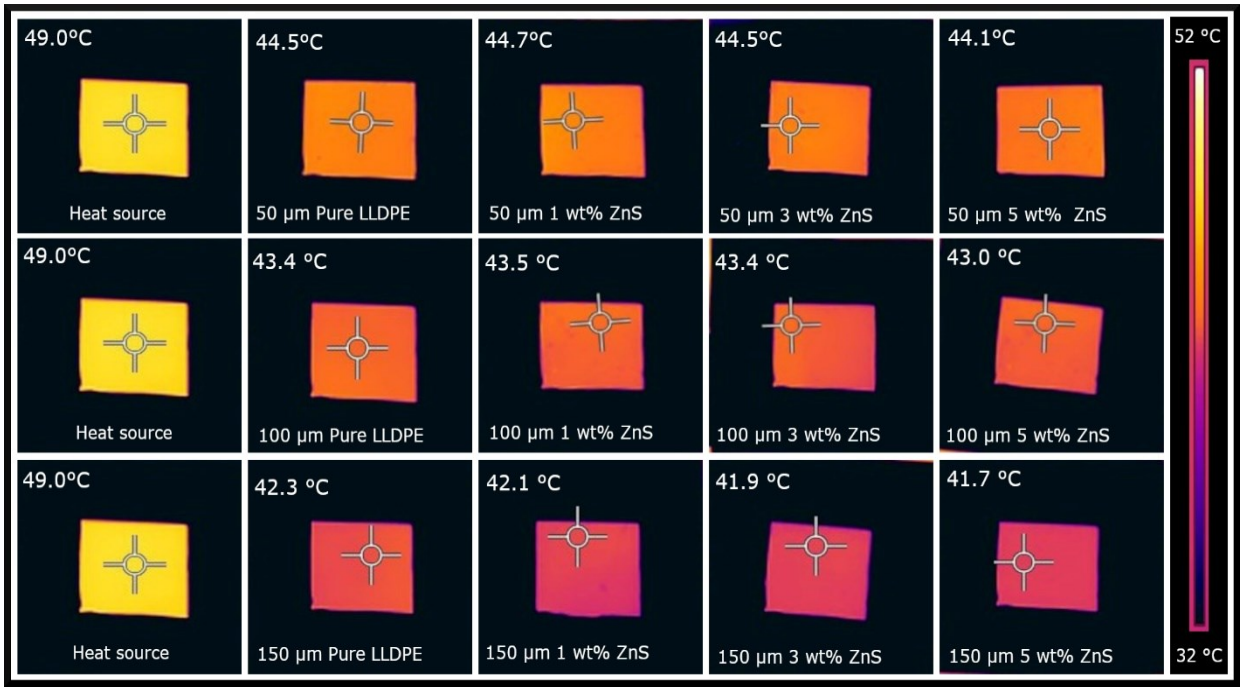

Figure 25: ZnS IR reflectance. 1st column: Heat source, 2nd column (50,100,150um thickness downwards): pure LLDPE, 3rd column: 1 wt% ZnS, 4th column: 3 wt% ZnS, and 5th column: 5 wt% ZnS

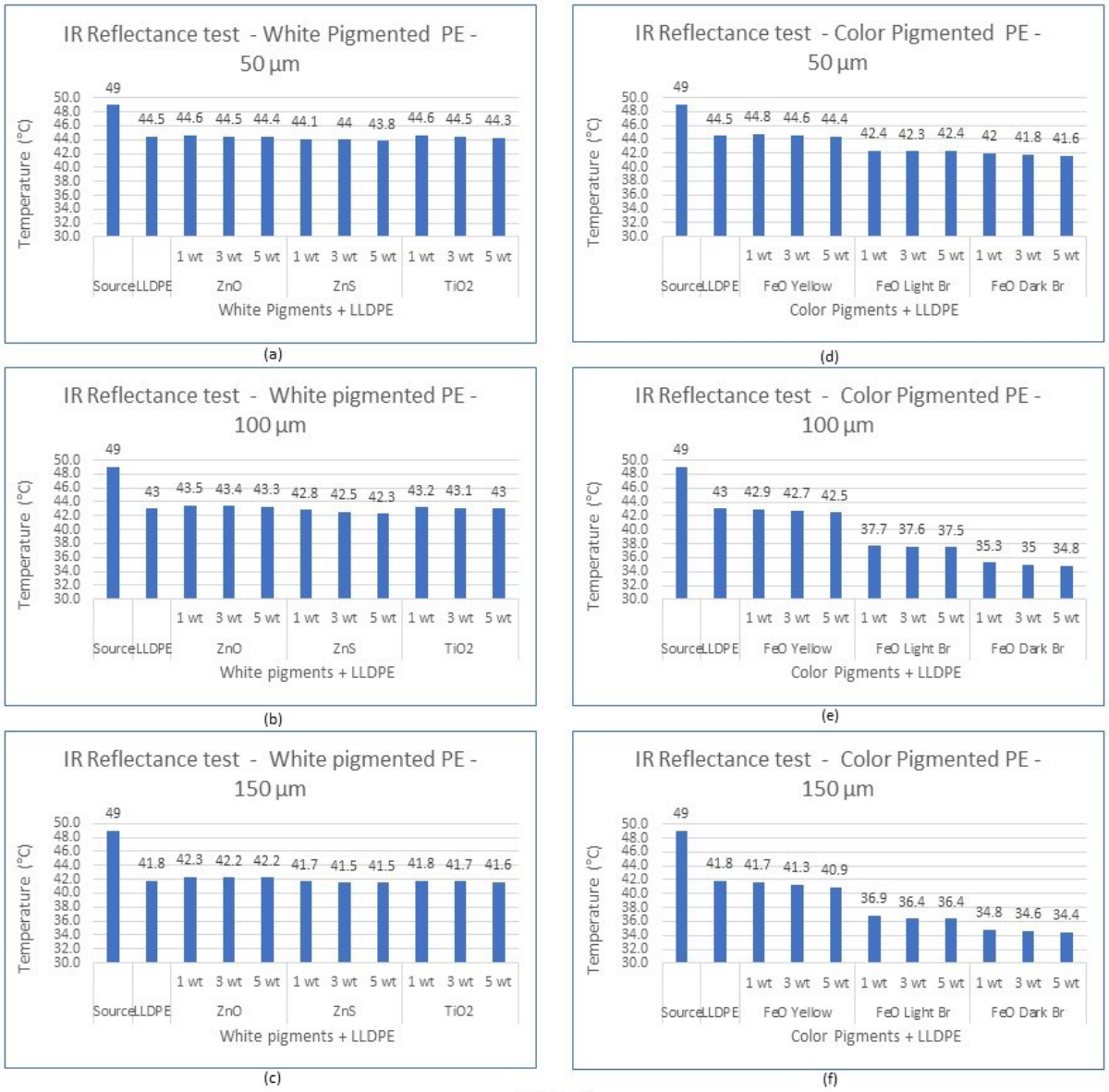

Figure - 2

Figure 26: IR reflectance: a) White pigments (ZnO, ZnS, TiO_2) at 50 µm, b) white pigments at 100 µm, c) white pigments at 150 µm, d) colored pigments (FeO yellow, light brown, dark brown) at 50 µm, e) colored pigments at 100 µm, and f) colored pigments at 150 µm.

2.3.4.3 Emittance

Sample sheets of pure and pigmented LLDPE blends were placed directly onto the heat source

until temperature was stable and IR readings were recorded. It was observed that all the samples exhibited the same temperature as the heat source i.e 49° C. This means LLDPE and pigmented blends all emit the heat source temperature at roughly the same value irrespective of the thickness of the sheets or concertation levels of the pigments as shown below.

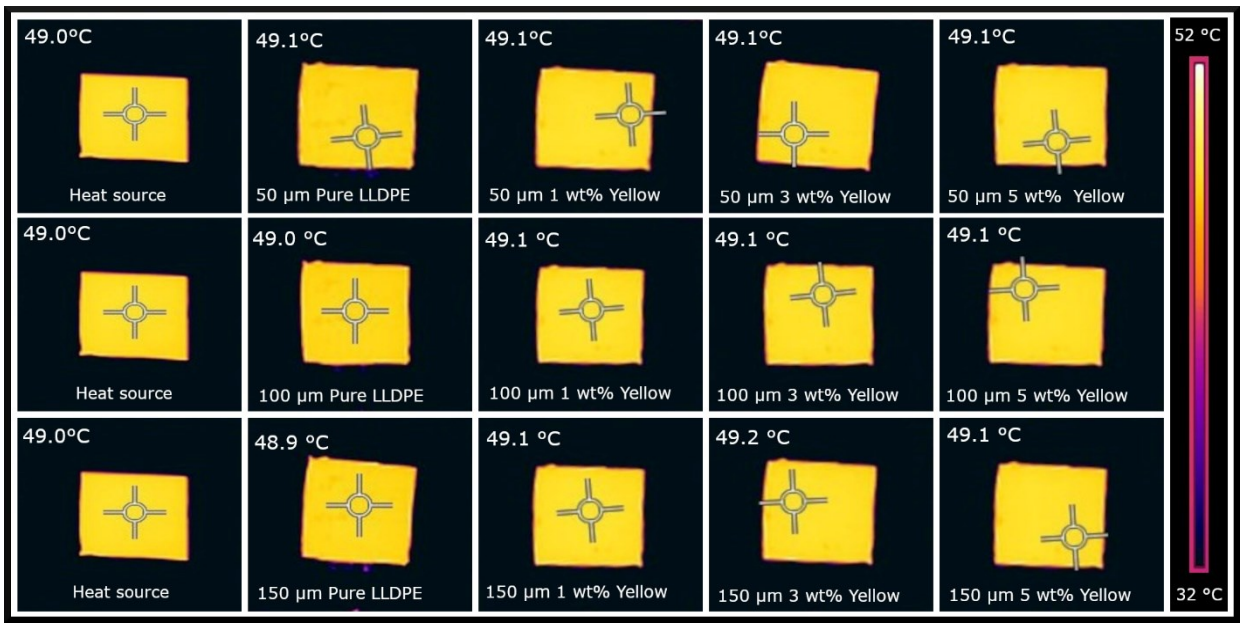

Figure 27: FeO yellow IR emissivity test. 1st column: Heat source, 2nd column (50,100,150um thickness downwards): pure LLDPE, 3rd column: 1 wt% yellow, 4th column: 3 wt% yellow, and 5th column: 5 wt% yellow

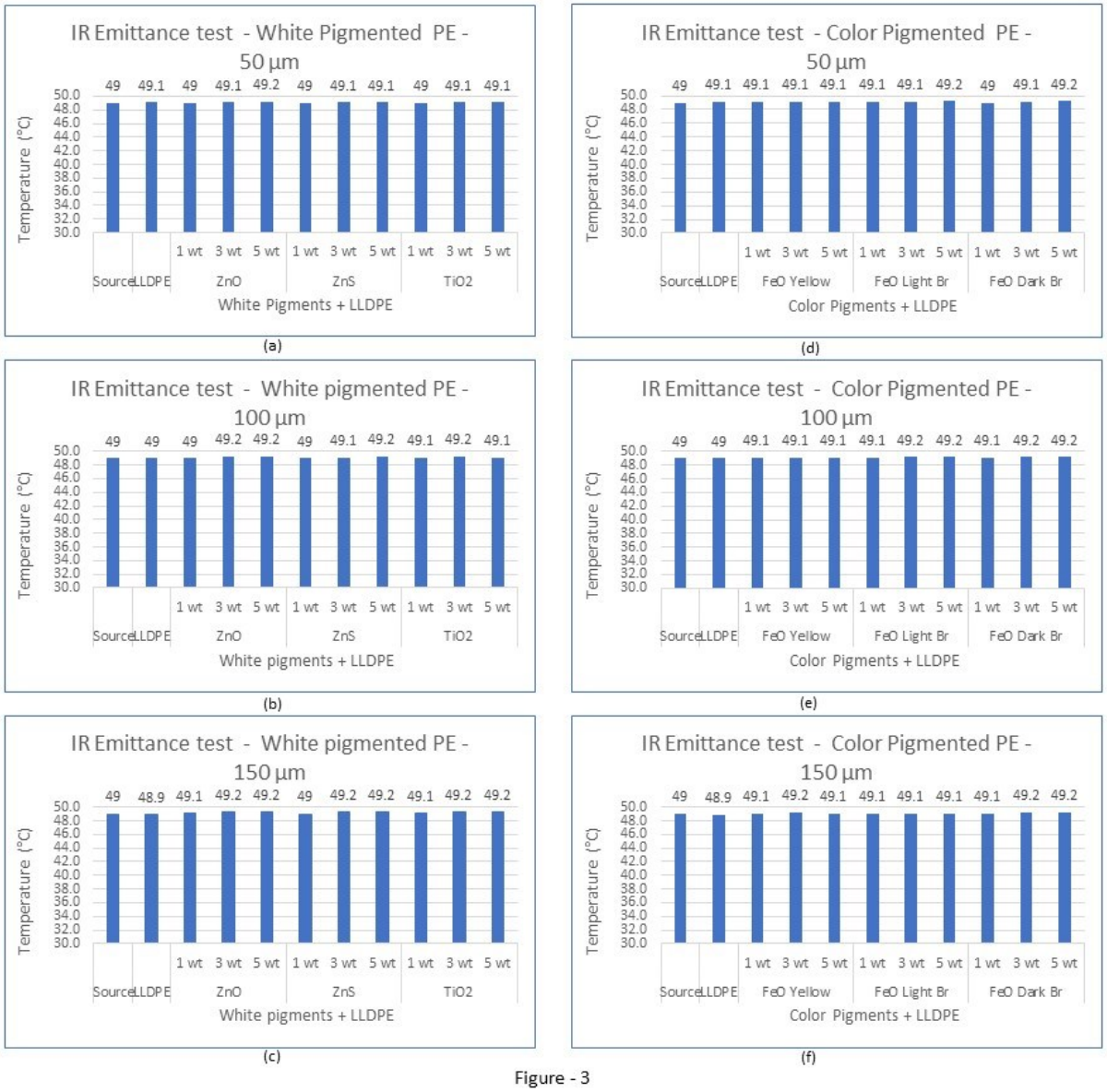

Figure - 3

Figure 28: IR emissivity test: a) White pigments (ZnO, ZnS, TiO_2) at 50 µm, b) white pigments at 100 µm, c) white pigments at 150 µm, d) colored pigments (FeO yellow, light brown, dark brown) at 50 µm, e) colored pigments at 100 µm, and f) colored pigments at 150 µm.

2.4 Conclusion

In conclusion, we have demonstrated a simple method to pigment LLDPE with master

batches of diverse pigments using polymer wax. The pigmented LLDPE has been extruded using commercially available wellzoom desktop extruder and converted into micronized sheets of 50 µm, 100 µm, 150 µm thickness. FTIR analysis has confirmed that IR spectrum of pigmented LLDPE blends do not have absorbance peaks for 7-12 µm wavelength range and therefore do not affect the IR properties at that range. UV-VIS analysis presented the intensity of visible opacity for pigmented LLDPE blends was higher than pure LLDPE. It showed that it is possible to pigment LLDPE to attain visible opacity and acquire different colorations for camouflage and other applications. Mechanical characterization tests confirmed that addition of different concentrations of pigments in LLDPE did not significantly affect the overall mechanical properties of LLDPE. Finally, it was determined that IR transparency, reflectance and emittance properties of pigmented LLDPE blends are very close to those of pure LLDPE. ZnO, ZnS showed an almost similar IR transparency as pure LLDPE followed by TiO_2 and yellow, light brown and dark brown pigments. It was observed that IR properties decline with an increase in concentration of pigments and thickness of sheets. Therefore, we can say this with confidence that LLDPE sheets can be pigmented and converted into visibly opaque yet still highly IR transparent. Thus, we have achieved successful pigmentation of LLDPE without affecting its mechanical and IR properties. The pigmented LLDPE sheets which are visibly opaque, have visually appealing and camouflage colors can be highly desirable in diverse applications especially in radiative cooling and heating and visible and IR camouflage applications for buildings and wearable textiles.

2.5 Future work

2.5.1 Micro structuring of PE – conversion from highly IR transparent to highly IR scattering

In future work, other grades of PE such as HDPE, LDPE and UHMWPE can be

investigated, pigmented and characterized to test their visible and IR camouflage properties. Another forward direction of study is tuning the IR transparency of PE or be able to change the IR properties of PE from highly IR transparent to highly IR scattering. The IR tuning of PE has numerous applications in thermal insulation, camouflage, radiant heating and IR shielding. I have performed qualitative tests on this topic and the results have been very promising. The process used is called micro-structuring of PE. The LLDPE sheets have been micro-structured by sandwiching the sheets between two micro-structured copper cloths. This sandwich structure was then heat pressed at temperatures closer to melting temperature of PE under heat press and left for one minute. After which, the PE sheets were taken out and viewed under microscope which confirmed that copper cloth's microstructures was transferred onto the PE sheets as shown in Figure 29.

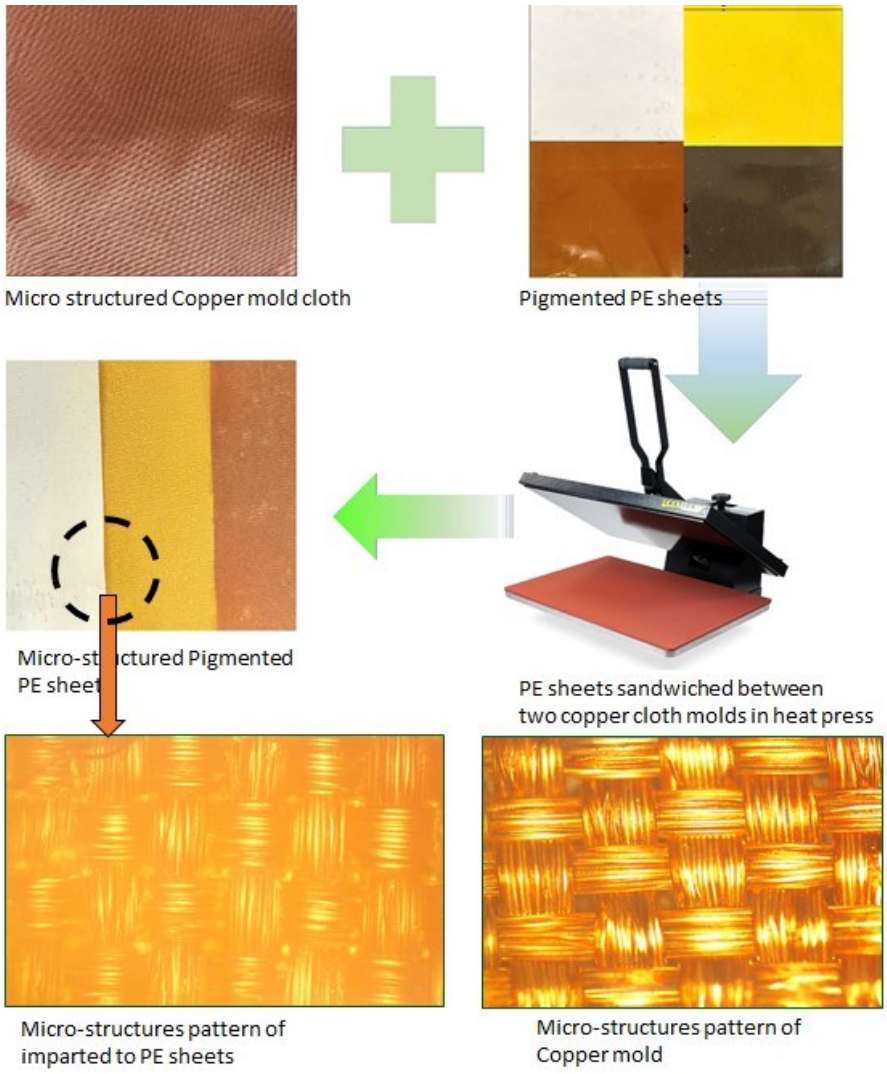

Figure 29: Schematic diagram setup for micro-structuring of pigmented PE sheets

The micro-structured PE sheets were tested under IR and the results are shown in Figure 30. The first column shows the university of Alberta logo made of metalized polyester where some part of it has polymer and other has metal facing. This logo when placed on top of the heat source and viewed under IR camera shows low emitting and high emitting IR surfaces as visible in column two. The high emitting plastic surface shows a reddish color while the low emitting and highly reflective metal surface appears cold and shows a bluish color. In third step, the non-structured PE sheets were placed in front of the university of Alberta logo at a distance of 2 mm one by one and

viewed under IR. As visible in column four, the university of Alberta logo is clearly visible under non-structured PE sheets which is completely expected because PE sheets are highly IR transparent and all the features of the university of Alberta logo are completely visible. In last step, the micro structured PE sheets were placed in front of the university of Alberta logo and viewed under IR. As visible in column five, the university of Alberta logo is completely hidden. This is because micro-structured PE sheets are scattering the IR light rather than being transparent. This is achieved through micro structuring of PE with the size of the microstructures be in the range of the wavelength of the IR light. This range corresponds to the infrared wavelengths typically used in applications, such as 1 to 10 micrometers (mid-infrared region). By having microstructures on this size scale, the incident IR light interacts with the structures, resulting in scattering. Doing so, we can tune the IR properties of PE from highly IR transparent or scattering as per our requirements and applications.

Figure 30: Results of micro-structuring of pigmented PE sheets- conversion of PE from highly IR transparent to highly IR scattering

Applications of micro structured PE films with high IR scattering range from improving

heat management in passive radiative passive heating applications to IR shielding and camouflage. By scattering IR radiation, these materials can reduce heat transfer, minimize thermal radiation losses, and enhance thermal insulation. Other potential applications include building materials, thermal packaging, and energy-efficient windows. The structured PE films with controlled IR scattering can also very useful in IR camouflage applications in instances where it is desired to scatter IR to obstruct thermal imaging and surveillance. Upon further investigation, selective scattering or absorbing specific IR wavelengths can be achieved, which can be used to scatter selective range or extent of IR and transmit the rest as per our requirements and applications.

Chapter 3

Addressing Warpage Challenges in HDPE 3D Printing: Optimized Parameters, Print Bed Selection, and Incorporation of LLDPE for Improved Printability

3.1 Introduction

Advanced digital manufacturing technologies are quickly approaching mainstream adoption as an excellent tool to manufacture complex structures with maximum flexibility, freedom of design and mass customization [179]. Among these, additive manufacturing (AM) has gained immense popularity for its ability to convert computer designed virtual models into real, functional 3D objects using digital slicing by adding materials layer-by-layer to produce end products in much less time and with much less material waste [22], [54], [180]–[182]. Even though impressive advances have been made in application of additive manufacturing toward a diverse variety of materials such metal, ceramic, and concrete , plastics are the most widely adopted materials used for 3D printing at the present day [59], [183]–[187]. The most widely known AM techniques are fused filament fabrication (FFF) or known under its trademark name fused deposition modeling (FDM), Stereolithography (SLA), Digital light processing (DLP) and Selective laser sintering (SLS). Most prominent among these is fused filament fabrication (FFF) due to its lower cost in which an object is built by depositing a melted thermoplastic polymer filament layer-by-layer using a heated nozzle. The melted material is extruded onto a platform called a print bed and the nozzle or print head travels in the X-Y directions to form a two-dimensional layer of the object. Before the next layer, the print bed lowers or the hear rises in the Z direction repeating the extrusion process fusing the subsequent layers together to generate the 3D object.[188], [189]

FFF printing was invented by Scott Crump at Stratasys Inc. in 1989 [190] and is gaining massive popularity in all the fields such as academia, manufacturing, medicine, aerospace etc. Its relatively inexpensive but rugged printer hardware, easy to use user interface and robust design has made it an excellent resource for rapid prototyping [180]. Since each layer is fused on top the previous layer, volume contraction and polymer crystallization of the polymers during solidification is very

challenging to deal with in FFF. Therefore, the most common materials used in FFF are acrylonitrile-butadiene-styrene copolymers (ABS), polylactic acid (PLA) and poly (ethylene terephthalate) copolymer (PET-G), polyamides and polyetheretherketone (PEEK). which are either amorphous or semi-crystalline with lower crystallization in nature [59], [191]–[194]. This means that the range of polymers that are routinely printed with FFF is relatively small. Even though, polyolefin materials like polypropylene (PP) and polyethylene (PE) make up around 50% of plastics usage worldwide, relatively little is known about 3D printing of polyolefin thermoplastics which are very hard to print with due to their crystalline nature [125]. Although some manufacturers have recently started to sell commercial filaments under the marketing name of PP and PE, they mostly consist of lower melting point, less crystalline, and more flexible ethylene-propylene copolymers which have different mechanical properties [54]. The manufacturers also issue a warning that they have not perfected a reliable way to print with this material and advise novices to stay away from HDPE and work with ABS and PLA instead [22]–[25]. Among polyolefins, high density polyethylene (HDPE) is the most challenging to print with FFF due to its higher crystalline nature, low surface energy, massive volume shrinkage upon cooling, and its poor adhesion to anything but hot HDPE. Warpage occurs when the intended shape of the final 3D printed object is distorted or bent during 3D printing process when deposited filament cools inducing stresses in the material that cause distortion out of the printing plane in its effort to relieve those stresses. As a result, the adhesion of the PE polymer with the print is severely poor and the adhesion between adjacent PE layers is also very weak resulting in layer delamination and warpage problems [26]–[29].

To reduce warpage and improve adhesion for FFF of PE, literature suggests the following (i) preparing and testing composites of PE by adding fillers, (ii) improving the print parameters such

as print temperature, extrusion rate, cooling rate, build plate composition etc. Spoerk and Sapkota have published a series of articles in which they have investigated many propylene/ethylene copolymers and composites in FFF printing [196], [197], [203]–[206]. It was shown that spherical fillers like glass or perlite microspheres or reinforced carbon fibers reduce shrinkage in the PP/PE copolymers and increase their mechanical strength. Carneiro et al. investigated thermal distortion in FFF printing of composite PP polymers by improving different printing parameters and presented improvement in printability of PP [46]. Decker et al. explored FFF printing of a maximum of up to 25 wt% HDPE in HDPE/ABS blends and reported poor filament extrusion and mechanical properties [207]. In another study, FFF printing results of 50 Vol% HDPE as shell material and PC/ABS blend as core material showed poor dimensional accuracy due to presence of HDPE [208]. Hees and co-workers used styrene-ethylene/butylene-styrene (SEBS) block copolymer as print bed for FFF printing of HDPE and reported SEBS as a good print bed alternative for HDPE printing by offering easy removal low warpage [54]. Chinga-Carrasco et al. have reported FFF printing of HDPE composites reinforced with compatibilized thermo-mechanical pulp (TMP) fibers and maleic anhydride functionalized polyethylene (MAPE) [209], [209]. Although, these bio composites exhibited better adhesion and extrusion, printing pure HDPE failed due to warpage, shrinkage and poor adhesion problems. Gudadhe et. al used 10 wt% LLDPE, 0.5 wt% dimethyl benzylidene (DMDBS) and 99.5 wt% waste-recycled HDPE blend with polyvinyl acetate-based glue as print bed for FFF printing [180]. They reported reduction in warpage when printed with the blend as compared to neat HDPE however the warpage was only measured at 90° angle and no research was done to monitor warpage at more sharper angles of print objects. Much interest is also shown in finding the feasibility of filament extrusion from recycled HDPE waste and investigating its use in 3D printing to turn HDPE waste into value-

added 3D printed parts. In this regard, Chong and others have reported filament extrusion of waste HDPE but have failed to solve warpage and adhesion problems in its 3D printing [201], [210]–[212]. In spite of the problems encountered with 3D printing of HDPE especially and PE, PP polymers in general, they remain materials of great interest for researchers due to their abundance availability and easier recyclability. This puts them as clear leaders for future recyclable materials used for FFF printing according to life cycle assessments [213]. As listed in the introduction, several researchers have claimed that adding fillers such glass, amorphous fibers to HDPE [180], [196], [205], [209] improves printability of HDPE and helps reduce part shrinkage.

In this work, we aim to solve the warpage problem of HDPE 3D printing by investigating the effect of addition of different concentrations of LLDPE. During FFF printing, the filament is heated and deposited layer by layer. As the printed part cools down, it undergoes thermal contraction. Sharp angles can restrict the natural contraction of the material, leading to increased stresses at those points and more warpage in the final printed part. In this research, we also aim to analyze and quantify warpage at sharper angles of the test object to identify warpage impact at sharper angles of 90°, 60° and 30°. Warpage will be measured for each HDPE-LLDPE blend and compared with pure HDPE. The mechanical properties of the blends will also be determined.

3.2 Materials and methodology

3.2.1 Materials

High density polyethylene (HDPE, MKCR2072; melt index 2.2 g/10 min (190 °C/2.16 Kg)), and linear low-density polyethylene (LLDPE, MKCH0863; melt index 1.0 g/10 min (190 °C/2.16 Kg)), were purchased from Sigma-Aldrich. Creality CR-200B Carborundum Tempered Glass Printing bed and PEI coated steel magnetic print bed were purchased from Creality3dparts.com. Ultra-high Molecular Weight Polyethylene film (product number: 85655K11, thickness 4 mil) was

purchased from McMaster-Carr. UHMWPE tape (3 mil) was purchased from findtapes.com and double-faced clear polyester carrier film FLX000546 (0.5 mil) was obtained from Flexcon.

HDPE, HDPE-LLDPE blend filaments were extruded for 3D printing from HDPE and LLDPE pellets using a Wellzoom B desktop single screw extruder equipped with the extrusion rate capacity of 10”-26”/min, and a temperature of 180-190 ℃ [173]. The extruded polymer strands were pulled off under a gravity fed pulling system, cooled at room temperature and then wound up on a spool [174]. The parameters used are listed in Table 7.

3.2.2 Fabrication of HDPE-LLDPE blends

We compounded 2, 5, 10 and 20 wt% LLDPE to make four blends. The pellets of LLDPE and HDPE were weighed in specified wt% levels, mixed together and put in the hopper of the wellzoom desktop extruder. The concentration details of the HDPE-LLDPE blends are listed in Table 6.

Table 6: Blend concentration levels of LLDPE, HDPE

	HDPE (wt%)	LLDPE (wt%)
Pure HDPE	100	0
2 wt% LLDPE-HDPE	98	2
5 wt% LLDPE-HDPE	95	5
10 wt% LLDPE-HDPE	90	10
20 wt% LLDPE-HDPE	80	20

3.2.3 Filament fabrication

In order to achieve a uniform material extrusion at the nozzle of the Ender 5 plus 3D printer, it is important to have uniform diameter of the filament being fed during printing. Commercially

developed filaments come in variety of sizes and a popular diameter size is 1.75 mm [214]. Preliminary tests showed that the Ender 5 plus 3D printer with 0.8 mm nozzle worked well with 1.75 mm diameter commercial filaments and was less prone to clogging the event of any contamination of the materials. In order to achieve these desired dimensions, pellets of HDPE or the blend of the HDPE-LLDPE pellets was extruded through a Wellzoom B desktop single screw extruder with the parameters listed in Table 7.The extruded filaments were collected through a gravity fed mechanism at a height of three feet which exhibited a uniform thickness. In order to achieve good mixing of the HDPE and LLDPE, pellets were thoroughly pre-mixed before being fed into the extruder. The final extruded filaments exhibited dimension of 1.75 mm (± 0.06 mm) recorded after ten measurements. The schematic of filament extrusion process is shown in Figure *31*.

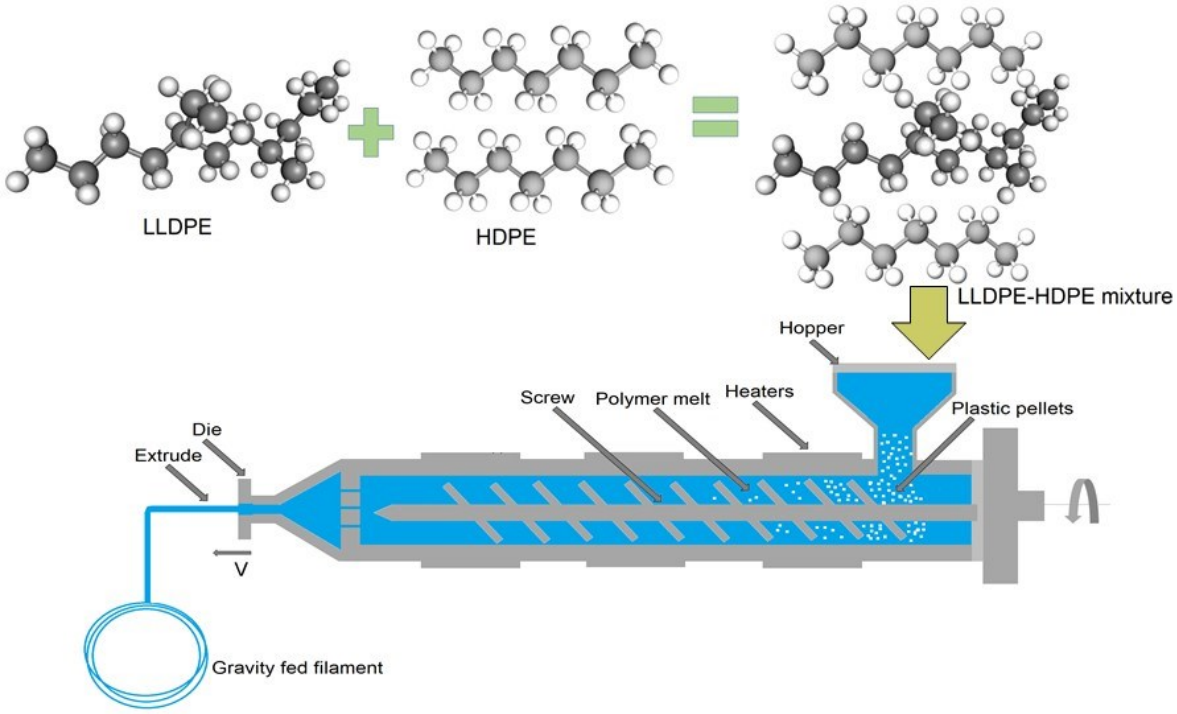

Figure 31: Filament extrusion schematic of HDPE-LLDPE blends

Table 7: Extrusion parameters for HDPE, HDPE-LLDPE blend filament fabrication

Process Parameter	Value
Extrusion Temperature (HDPE)	190 °C
Extrusion Temperature (HDPE-LLDPE blend)	180 °C
Speed of rotation	4 RPM
Ambient temperature	22 °C
Extrusion rate	15’’/min

3.2.4 3D printing process parameters

Fused filament fabrication (FFF) was performed on a Creality Ender 5 plus 3D printer. Ultimaker Cura5.2.1 was used to slice the 3D model and generate the G-Code files for the print specimen. There were also some manual modifications made to the G-Code to further improve printing parameters during the FFF printing. A round nozzle with diameter of 0.8 mm was used for printing. The print parameters used are listed in Table 8.

Table 8: Printing parameters for HDPE, LLDPE-HDPE blends

Print parameters	Standard (Non-improved)	Improved parameters
Nozzle size	0.8 mm	0.8 mm
Nozzle temperature	230 – 240 °C	230 – 240 °C
Nozzle temperature - layers 1,2	230 – 240 °C	210 °C
Bed temperature	50 °C	60 °C
Print speed	25 – 100 mm/s	25 - 100 mm/s

Print speed – layers 1,2	25 – 100 mm/s	20 mm/s
Line width	0.8 mm	0.8 mm
Layer Height	0.6 mm	0.6 mm
No. of walls	3	2
Filling/ infill density	20%	20%
Material flow	100 – 107% gradually	100 – 107% gradually
Filling pattern	cubic	cubic

A range of print parameters were tested to find the optimal values that offered best results for FFF printing of all the blends in terms of minimum warpage, good adhesion, easier detachment and superior dimensional accuracy. In this regard, different printing temperatures *Tprint* (200°C, 210°C, 220°C, 230°C, 240°C) were tested keeping other parameters constant (infill density: 20%, infill pattern: cubic, print speed: 25 mm/s, print bed temperature, *Tbed*: 60 °C). A *Tprint* = 200°C allowed for acceptable adhesion but detachment was very easy and that contributed to high warpage. *Tprint* = 210°C, 220°C offered best adhesion to the print bed with least warpage but the print quality on higher layers was not good. *Tprint* = 230°C, 240°C offered excellent print quality and surface finish but offered very strong adhesion to the build plate that made it challenging to peel off the print specimen from print bed with normal hand force, especially at the center of the object. In some cases, the adhesion was so strong that it caused layer detachment between upper layers of the print object causing layer delamination. To solve this problem, manual changes were made to the *G-Code* to print the first two layers at *Tprint* = 210°C and the rest of the print object was printed at *Tprint* = 230°C with cooling at 50% for first two layers and 100% for the rest. Doing so provided best overall results for FFF printing of all the blends with strong adhesion, easier

detachment and excellent print quality. A visual representation of these tests is shown in Figure 32.

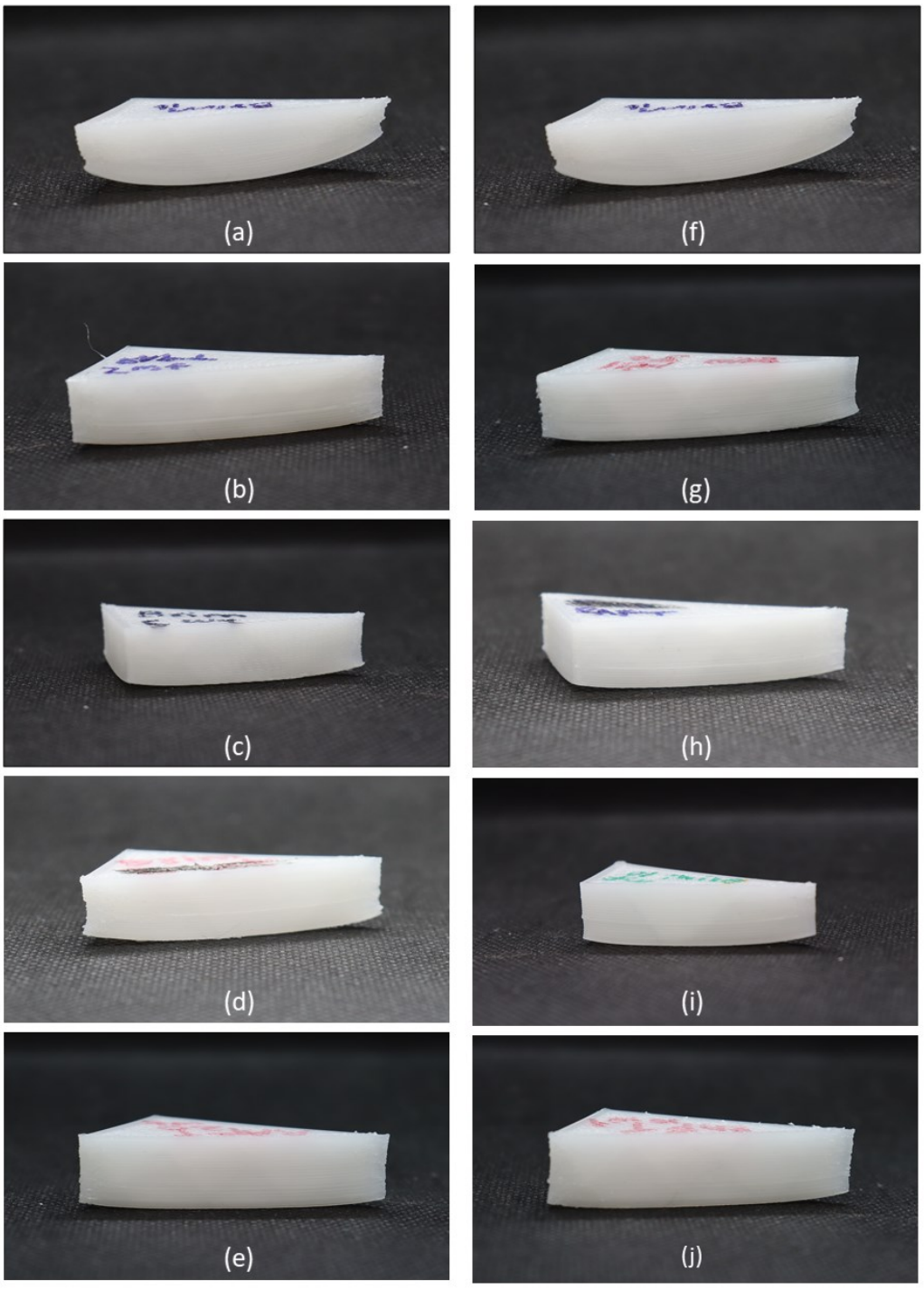

Figure 32:Images of FFF Printing of test specimen with brim (left) and raft (right). (a,f) pure HDPE without optimized printing parameters. (b,g) 2 wt% LLDPE-HDPE blend, (c,h) 5 wt% LLDPE-HDPE blend (d,i) 10 wt% LLDPE-HDPE blend (e,h) 20 wt% LLDPE-HDPE blend [with optimized parameters]

Once printing parameters were finalized, FFF printing was conducted using two build types (brim and raft) As warpage is maximum at the bottom layers of the print object, having brim layers that enclose the print object absorb some of the induced stress due to shrinkage which helps in minimizing the warpage. A brim of 5 perimeters was printed around the print specimen as after 5 lines, there was no change noted in warpage or adhesion. Similarly, the print specimens were printed on a raft. So, in total, print specimens of pure HDPE, and 2, 5, 10, and 20 wt% LLDPE blends were printed on brim and raft with optimized parameters. Three specimens for each blend as well as for pure HDPE were printed with a dimensional accuracy of ± 0.2 mm. Printing on a brim and a raft reduced offered adhesion support to the first few layers of printing to the build plate.

3.2.5 Warpage measurement

Warpage of the printed specimen was quantified and the extent of warpage (W) was measured by imaging the printed specimen using a high-resolution Epson-workforce ES-400 II scanner (800 dpi) with the specimen laid on its sides. The images were analyzed by digitizing their profiles using ImageJ software. The extent of warpage (W) at the edges was measured with reference to the bottom plane of the printed specimen at the center. There is no standard artifact for analyzing warpage values of the print specimens for additive manufacturing. Although National Institute of Standards and Technology (NIST) has suggested a standardized test specimen it is typically used for evaluating performance of FFF hardware only [215], [216]. Since objects with sharp corners exhibit more severe warpage, we selected a triangular specimen for our studies. The test specimen, we chose for FFF printing, has the following dimensions - (Angles: 30°, 60°, 90°, (base: 1 inch, perpendicular: 1.73-inch, hypotenuse: 2 inches, with respect to angle 60°), height: 12.50 mm). By observation, more warpage occurs on the edges of the specimen and minimum or no warpage is

observed in the center. The maximum thickness of the object around the center is already measured and noted using a caliper. The maximum value of the difference between the top and bottom coordinates of the test specimen profiles is the extent of warpage occurred at each corner and is denoted as *W*. All the warpage measurements are recorded in mm.

3.2.6 Mechanical characterization

Tensile strength, Young's modulus and elongation at break were determined using Instron 5960 series according to ASTM D 638-IV standard with a load of 10 KN. ASTM D 638-IV test specimens were designed in SolidWorks. The files were saved as stl. format, exported to Cura 5.2.1 sliced and were printed with 100% infill density at an angle of 45° and cubic infill pattern shown in Figure 33. The samples were clamped in the Instron 5960 machine and were elongated at a load speed of 5 mm/min until break. The mechanical load capacity of LLDPE-HDPE blends was investigated to determine what negative impacts on modulus and strength would occur with the addition of the LLDPE. In this regard, Young's modulus, tensile strength and elongation at break were calculated for each blend and compared with the mechanical characterization values of pure HDPE.

Figure 33:ASTM D638-IV - 3D printed Tensile test specimen: 100% infill density

This was done to minimize the anisotropic mechanical behavior effect which cannot be entirely excluded during FFF printing of objects.

3.3 Results and discussion

3.3.1 Fabrication of HDPE and HDPE-LLDPE blend filaments

The filament extruded using the wellzoom desktop extruder was of uniform thickness. The diameter was measured at different parts of the filament and was found to be consistent at 1.75mm which is suitable for FFF printing. Furthermore, there were no visible impurities or imperfections in the filament which could impact the 3D printing of print object.

3.3.2 Evaluation of build plate

Proper adhesion of HDPE onto the print bed during the entire printing process which can take several hours is another perquisite for successful 3D printing of HDPE by means of FFF. The build plate/print bed should offer two qualities for optimal performance. (i) It should offer high adhesion to the print object during printing, and (ii) the print object at the end of the printing process should be able to readily and easily detach from the print bed without damage to the part or the plate. Since HDPE is a very difficult material to bond with any other material but HDPE, this makes it exceptionally challenging to find a suitable build plate material for this purpose. Here, we tested variety of materials such as glass, Polyethyleneimine (PEI) coated steel, HDPE, UHMWPE sheet with double sided tape, and UHMWPE tape as build plate materials. The test object was a tensile specimen according to ASTM D 638-IV which was printed using a 0.8 mm nozzle and a filling degree of 100% and a cubic filling pattern at an angle of ± 45° to the longitudinal axis. The results of the adhesion and detaching tests are summarized in Table 9. The build plate materials commonly applied in FFF such as carborundum tempered glass did not adhere to HDPE at all at any nozzle/print temperatures. Similarly, no adhesion was observed on PEI coating at any *Tprint*. On the other hand, permanent bonding was observed on HDPE sheet at $Tprint \geq 215$ °C and at $Tbed = 60$ °C. Lastly, UHMWPE sheet with double sided tape and UHMWPE tape were tested which showed by far the best adhesion when printing in the temperature range of $Tprint = 200 - 240$ °C and at $Tbed = 60$ °C. Based on these results, we choose UHMWPE tape as build plate material. As

is apparent from Figure 34 and Figure *35*, UHMWPE sheet as not only showed excellent adhesion to the print object during the complete 3D printing process, it was easily pulled off from the final part by hand without causing any damage to the print object.

Table 9: Evaluation of build plate material

Build plate material/type	Results
Carborundum Tempered glass	No adhesion
PEI-coated steel build plate	No adhesion
HDPE sheet	Permanent bonding at *Tprint* ≥ 215 °C and *Tbed* =60 °C; difficult detaching; detaching impossible at *Tprint* ≥ 230 °C
UHMWPE film (adhered to the print bed with double sided tape)	Good adhesion at *Tprint* = 200 – 240 °C and *Tbed* =60 °C; easily detachable; difficult detaching at *Tprint* ≥ 230 °C
UHMWPE tape	Good adhesion at *Tprint* = 200 – 240 °C and *Tbed* =60 °C; easily detachable; difficult detaching at *Tprint* ≥ 230 °C

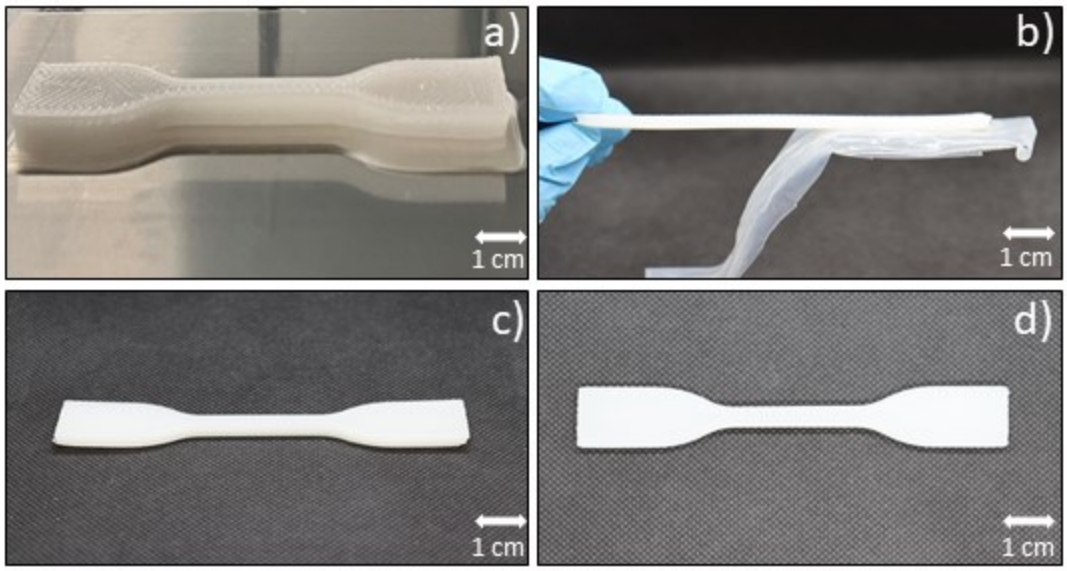

Figure 34: a) Printing of ASTM D638-IV test specimen, b) partial detachment from build plate, c) complete detachment from build plate by peeling it off with hand, d) ASTM D638 -IV test specimen reading for testing

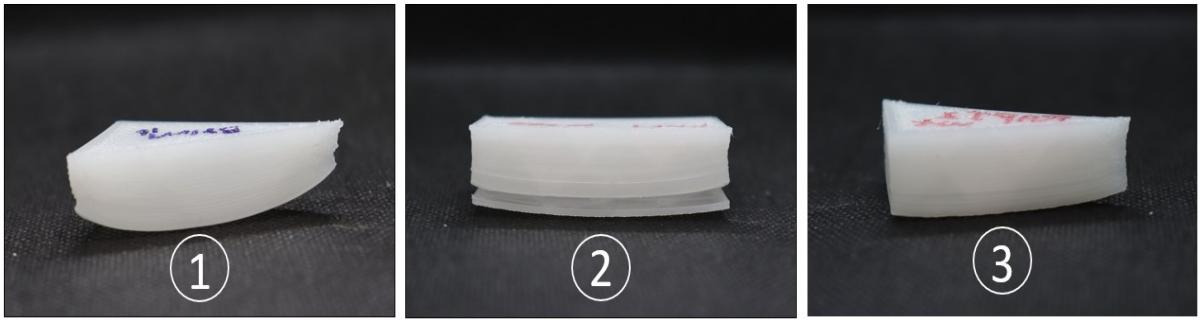

Figure 35: (1) FFF printing of pure HDPE exhibiting max warpage at Tprint = 200°C. (2) FFF printing of of pure HDPE exhibiting layer delamination at Tprint = 240°C. (3) FFF printing of pure HDPE exhibiting best overall result at Tprint = 210°C for first two layers

3.3.3 Mechanical characterization

For mechanical characterization, six samples were tested for each blend. The mechanical characterization results are summarized in Table 10 and are displayed in Figure 38. The force vs displacement curve is shown in Figure *36*.

The force vs. displacement curve is a fundamental characterization tool for understanding the mechanical behavior of materials. The force vs. displacement behavior of Pure HDPE and its blends through tensile testing is listed below. This analysis sheds light on HDPE's mechanical properties. The findings provide valuable insights into the material's suitability for various engineering applications. As can be seen in the graph, the blends follow a very close trend with pure HDPE in terms of their force vs displacement curve, which is in accordance with our experimental expectations.

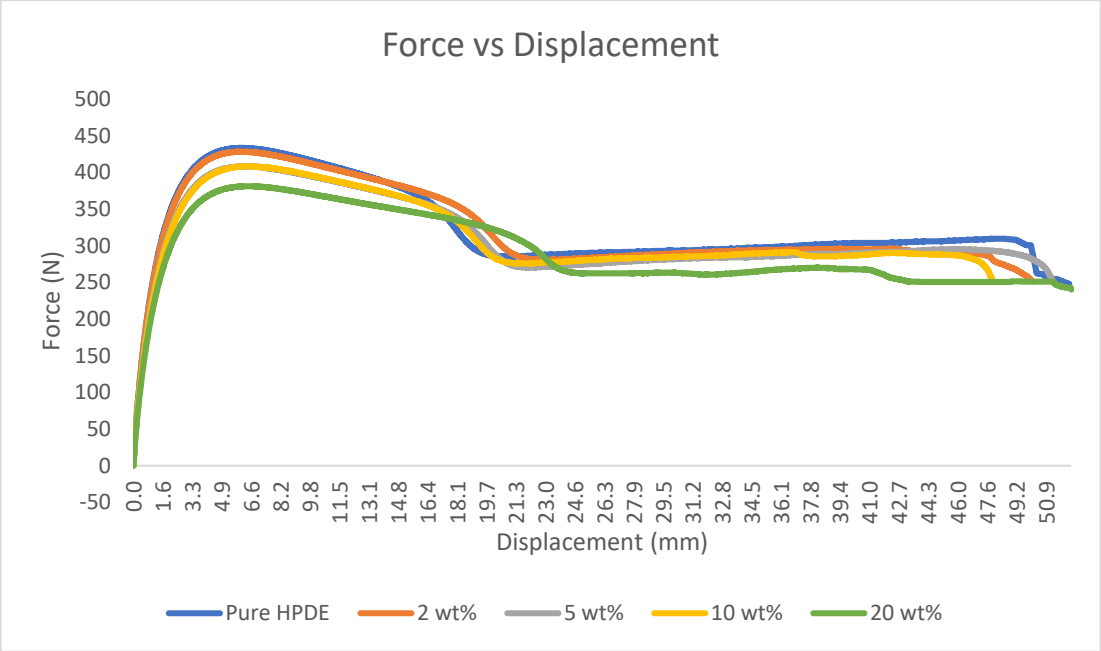

Figure 36: Force vs Displacement curve: HDPE-LLDPE blends

The stress strain curve is showed in Figure 37. The results indicate that pure HDPE exhibit the highest modulus of 453 MPa with 20% LLDPE-HDPE blend exhibiting the least value at 316 MPa. The 2, 5 and 10 wt% lie in between the two. The Young's modulus of 10 wt% and 20 wt% is 21% and 30% less than pure HDPE respectively. Young's modulus gradually decreases with increase of LLDPE concentrations due to an overall decrease in crystallinity and stiffness of the blend. Pure HDPE has a value of tensile strength of 18 MPa followed by 2, 5, 10 and then 20 wt%. The tensile

strength values for 2, 5 and 10 wt% are in the range of 17 MPa with 20 wt% at approximately 16 MPa. This shows that blending HDPE with LLDPE concentrations reduces its tensile strength by a very small margin. Elongation at break is approximately same for all the blends which means it is minimally impacted by addition of small concentrations of LLDPE. The overall trend is a minimal reduction in mechanical properties of the 3D printed objects with increase in concertation of LLDPE grade. Therefore, we can use HDPE-LLDPE blends (up to a concentration level of 20wt% LLDPE) in place of pure HDPE for 3D printing without impacting the parts mechanical properties.

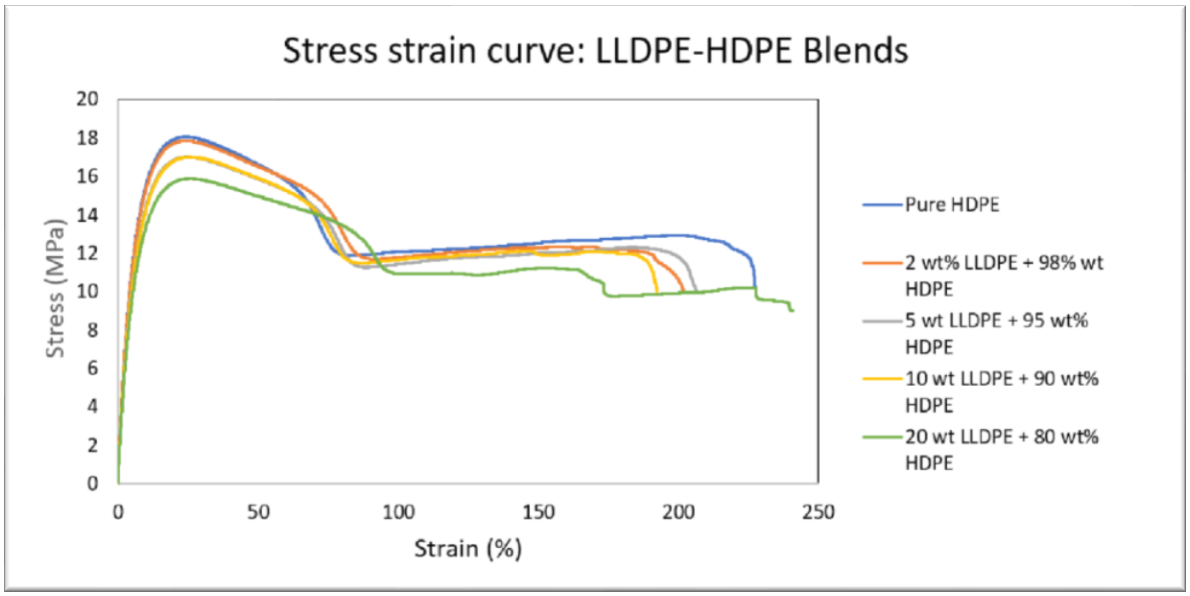

Figure 37: Stress strain curve - LLDPE: HDPE blends

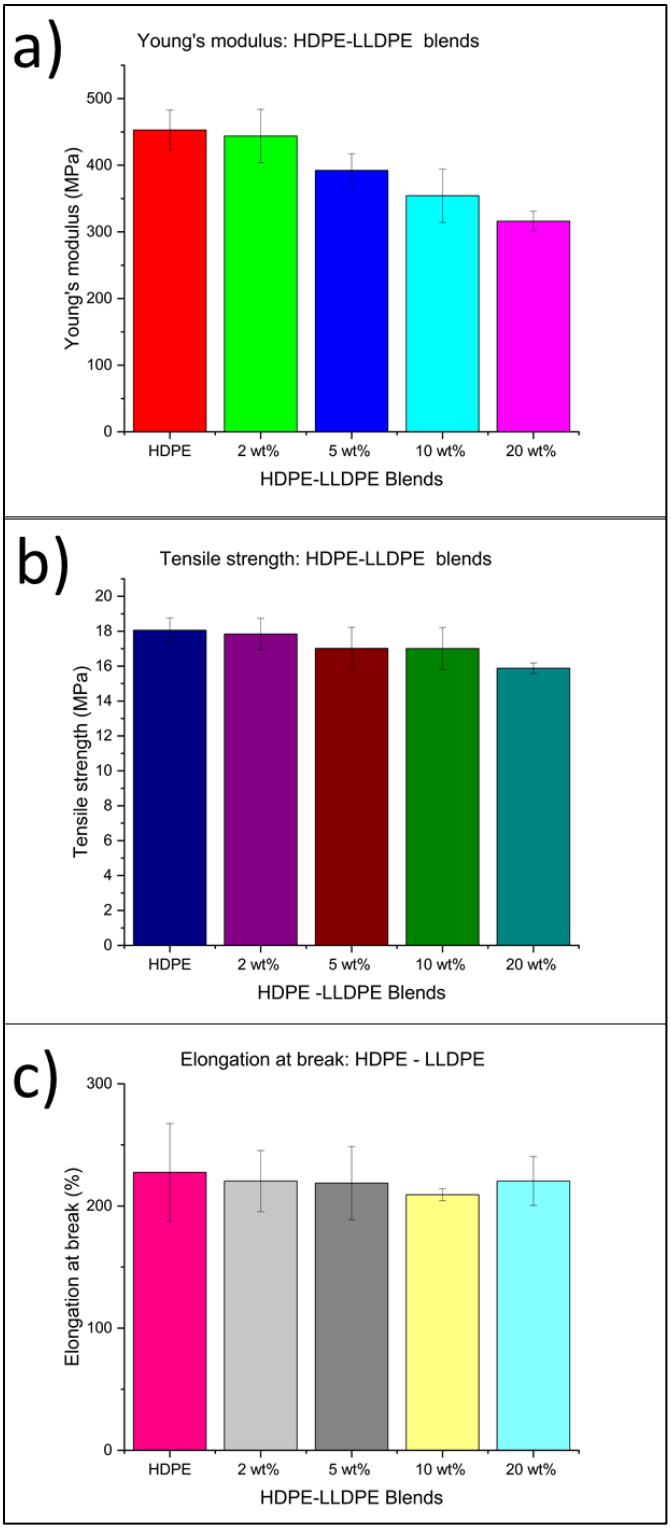

Figure 38:Mechanical properties (in terms of Young's Modulus, tensile strength, elongation at break) of pure HDPE, LLDPE-HDPE blends

Table 10: Mechanical properties (in terms of Young's Modulus, tensile strength, elongation at break) of pure HDPE, LLDPE-HDPE blends

Blends	Young's modulus (MPa)	Tensile strength (MPa)	ε_{max} (%)
Pure HDPE	452.97 ± 30	18.06 ± 0.7	227.54 ± 40
2 wt% LLDPE-HDPE	443.97 ± 40	17.84 ± 0.9	220.42 ± 25
5 wt% LLDPE-HDPE	392.39 ± 25	17.02 ± 1.2	218.69 ± 30
10 wt% LLDPE-HDPE	354.32 ± 40	17.01 ± 1.2	209.26 ± 5
20 wt% LLDPE-HDPE	316.12 ± 15	15.88 ± 0.3	220.46 ± 20

3.3.4 Warpage measurement

The 90°-30° side and 90°-60° side profiles of the test specimen with optimized parameters are printed with brim and raft respectively, are presented in Figure 39 and Figure 40, respectively. It is worth noting that HDPE when printed without optimized parameters exhibits worse warpage values of 6.2 mm, 4.45 mm, and 1.73 mm at 30°, 60°, and 90° angles respectively. 30° angle being the sharpest angle exhibits maximum warpage followed by 60° and 90° angles. This trend is followed in all the blends. Then print parameters are optimized and a brim is incorporated for 3D printing of pure HDPE and HDPE-LLDPE blends. After incorporation of brim, we observed an overall reduction trend in the warpage of all the print objects. Pure HDPE exhibits warpage values of 2.9 mm, 1.8 mm, and 1.60 mm at 30°, 60°, and 90° angles respectively. This corresponds to approximately 56.0%, 59.5% and 7.5% reduction in warpage at 30°, 60°, and 90° angles respectively when compared with pure HDPE printed with non-optimized parameters. This is followed by 2, 5, 10 and 20 wt% with 20 wt% exhibiting the maximum reduction in warpage. 20

wt% shows an approximate 79%, 75% and 59.5% reduction in warpage at 30°, 60°, and 90° angles, respectively. This significant reduction in warpage is attributed to addition of LLDPE which lowers overall crystallinity of the blend leading to less induced stresses upon cooling during printing. 10 wt% is not far behind 20 wt% with a reduction of approximately 78%, 72% and 48% at 30°, 60°, and 90° angles respectively.

With incorporation of a raft, no significant reduction in warpage is observed for pure HDPE. However, a significant reduction was observed for the HDPE-LLDPE blends. 2 and 5 wt% blends exhibited an approximate 75%, 70% and 45% reduction in warpage at30°, 60°, and 90° angles respectively. 10 wt% HDPE-LLDPE blend presented an approximate reduction of 81%, 80% and 75% in warpage at 30°, 60°, and 90° angles respectively whereas 20 wt% HDPE-LLDPE blend offered an approximate 86%, 86% and 80% reduction in warpage for 30°, 60°, and 90° angles respectively. Therefore, with the addition of LLDPE in HDPE, we can see an overall reduction of more than 80% in the warpage. As mechanical strength decreases for higher LLDPE concentration blends therefore, we can conclude that 10 wt% HDPE-LLDPE blend offers the most optimal result with optimal reduction in warpage and optimal retention of mechanical properties. Another interesting trend was observed which presents that addition of LLDPE had more impact on warpage reduction at sharper angles such as 30° and 60° as compared to as 90°. For instance, 10 wt% blend when printed with brim exhibits a reduction of 78% and 72% at 30° and 60° angles respectively while a 50% reduction at 90°angle. While this trend is not significantly impacting and is not translated across all blends, it is still worth noting. The complete list of warpage values (in mm) and warpage reduction (in %) for each blend are listed in Table 11 and Table 12 respectively. In conclusion, the warpage problem during FFF printing of HDPE can be partially solved through addition of LLDPE in small concentrations, particularly at 10 wt% with most optimal values,

without compromising on the mechanical properties of the 3D printed parts. This strategy has been successfully employed to print a Canadian maple leaf with LLDPE-HDPE blends which exhibits excellent 3D printing qualities as shown in Figure 41.

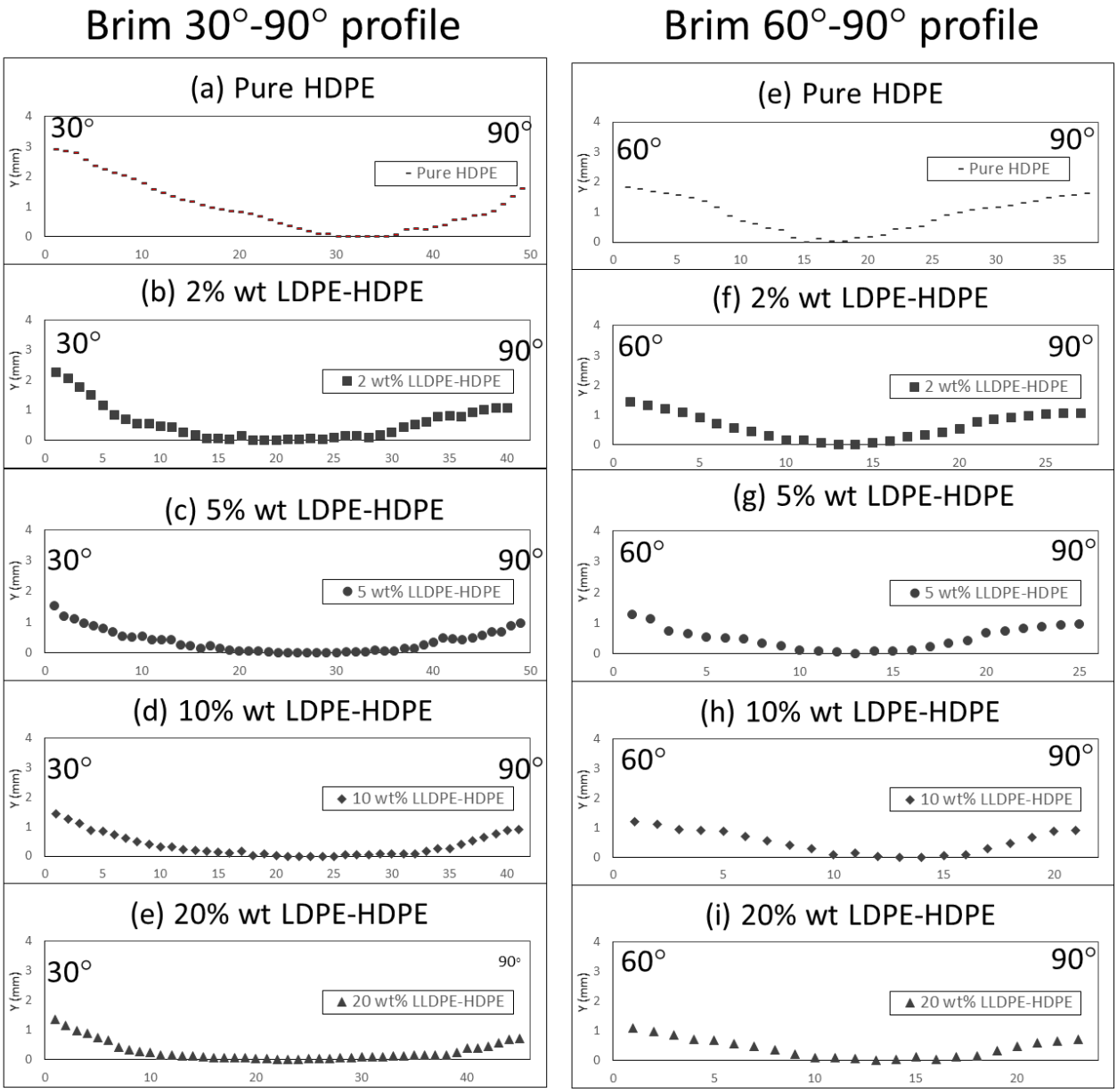

Figure 39: Warpage profiles of 90°-30° side (left) and 90°-60° side (right) of the test specimen for FFF printing with brim. (a) Pure HDPE (b) 2 wt% LLDPE-HDPE blend, (c) 5 wt% LLDPE-HDPE blend (d) 10 wt% LLDPE-HDPE blend (e) 20 wt% LLDPE-HDPE blend

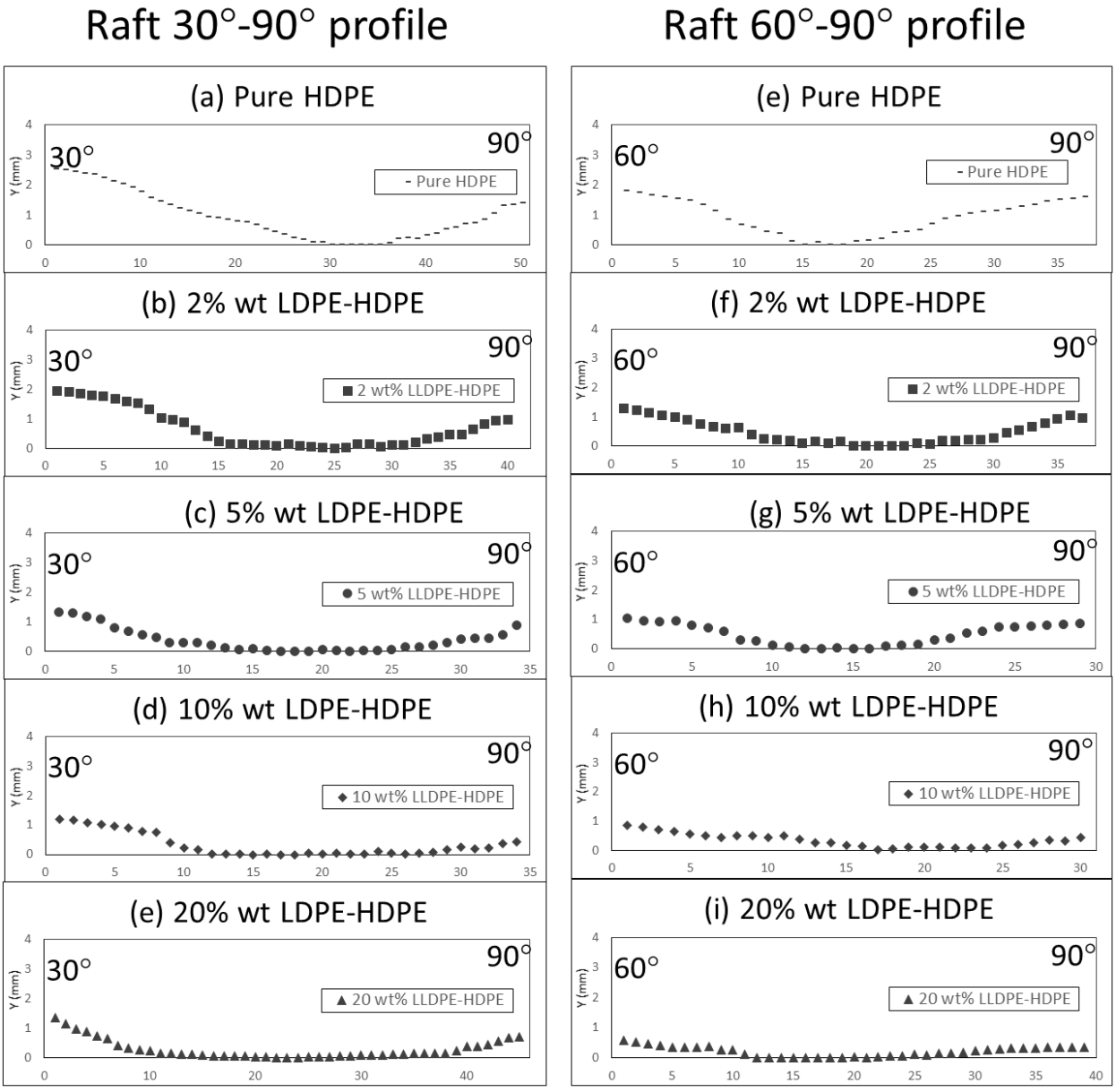

Figure 40: Warpage profiles of 90°-30° side (left) and 90°-60° side (right) of the test specimen for FFF printing with raft. (a) Pure HDPE (b) 2 wt% LLDPE-HDPE blend, (c) 5 wt% LLDPE-HDPE blend (d) 10 wt% LLDPE-HDPE blend (e) 20 wt% LLDPE-HDPE blend.

Table 11: Warpage values at angles 90°, 60° and 30° for printing of HDPE, LLDPE-HDPE blends

Blends	Warpage (mm)					
	Brim			Raft		
	90°	60°	30°	90°	60°	30°
Pure HDPE (without optimized parameters)	1.73	4.45	6.62			
Pure HDPE	1.60	1.8	2.9	1.40	1.62	2.53
2 wt% LLDPE-HDPE	1.07	1.4	2.25	0.97	1.30	1.93
5 wt% LLDPE-HDPE	0.97	1.29	1.55	0.88	1.03	1.34
10 wt% LLDPE-HDPE	0.9	1.21	1.42	0.43	0.85	1.21
20 wt% LLDPE-HDPE	0.7	1.1	1.35	0.35	0.58	0.92

Table 12: Warpage reduction in (%) with respect to pure HDPE printed without optimized parameters

Blends	Warpage reduction (%)					
	Brim			Raft		
	90°	60°	30°	90°	60°	30°
Pure HDPE	7.52	59.55	56.12	19.00	63.50	61.70
2 wt% LLDPE-HDPE	38.15	71.01	66.0	43.93	70.75	70.85
5 wt% LLDPE-HDPE	43.94	71.1	76.58	49.13	76.85	79.76
10 wt% LLDPE-HDPE	47.97	72.81	78.54	75.14	80.85	81.72
20 wt% LLDPE-HDPE	59.50	75.28	79.60	79.77	86.96	86.10

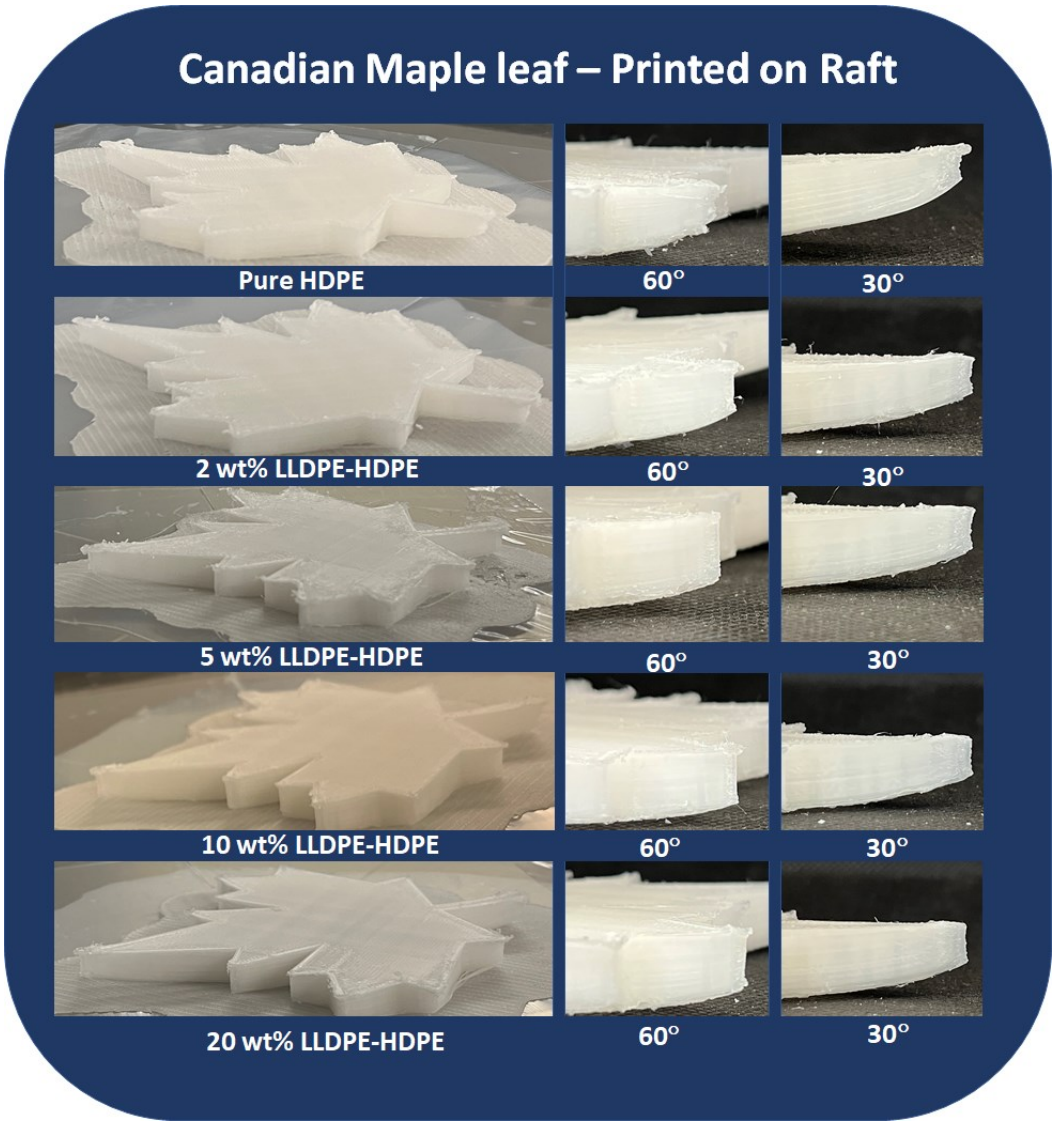

Figure 41: Canadian Maple leaf printed with blends of HDPE.

3.4 Conclusion

In conclusion, HDPE is very challenging to print due to its warpage and shrinkage problem upon cooling during printing. Warpage is even worse at sharper angles of the print object. We demonstrate warpage problem of HDPE printing can be solved by improving print parameters, using UHMWPE tape as build material, and through addition of LLDPE in small concentration with HDPE. By using optimal print process parameters and printing with brim and raft as support and addition of 10 wt% of LLDPE in pure HDPE making a 10 wt% LLDPE-HDPE blend, we can

significantly reduce the warpage. This solution can provide an approximate 80% reduction in warpage when compared with pure HDPE especially at sharper angles. Mechanical characterization tests show that addition of 10 wt% LLDPE results in very minimal, almost negligible, change in mechanical strength of the final print object as compared to that of pure HDPE. This means HDPE warpage and shrinkage problem can be solved using this technique without making a compromise on the higher mechanical properties of HDPE during FFF printing. This approach expands the range of materials for 3D printing by including semi-crystalline polyolefins, which are typically very challenging to print, but are very common in industrial plastic products. Our strategy of mixing HDPE with LLDPE, filament extrusion and FFF printing can be readily implemented on commercially available extruders and printers without the need for any hardware changes such as heated chambers. It can very easily be scaled up due to the simplicity of the technique and operations involved.

Chapter 4

Concluding Remarks and Future Direction of Research

4.1 Conclusion and closing remarks

In this thesis research, we addressed key challenges associated with two grades of polyethylene (PE): LLDPE and HDPE. Each grade of PE offers diverse applications in various industries, the military, and civilian sectors. Moreover, grades of PE form a significant fraction of the world scale production of plastics and are of high interest due to their low cost, good chemical resistance and abundant availability. Our research focused on overcoming specific limitations of these materials to enhance their performance and expand their potential applications.

In the **first part** of this research work, chapter two was dedicated to addressing the issue of LLDPE's semi-transparency while maintaining its high infrared (IR) transparency. To achieve this, we employed pigmentation techniques with different pigments to render LLDPE visibly opaque without compromising its IR transparency. We conducted a comprehensive analysis, including FTIR analysis, UV-VIS analysis, mechanical testing, and IR analysis under a FLIR E75 camera. The results confirmed that the pigmented LLDPE maintained its exceptional IR transparency while becoming visibly opaque. This breakthrough opens up new opportunities for using LLDPE in radiative passive heating and cooling applications, IR and visible camouflage applications, IR shielding, and other diverse fields. For pigmentation, we demonstrated a simpler method for pigmenting LLDPE using polymer wax and master batches of different pigments. LLDPE was pigmented with six different pigments: three white pigments (ZnS, ZnO, TiO_2) and three colored pigments (FeO yellow, light brown and dark brown). It was shown that the resulting pigmented LLDPE maintains its mechanical and IR properties and is suitable for diverse applications, including radiative cooling for buildings and wearable textiles. ZnO and ZnS showed the highest IR transparency and reflectance rates which were same as those of pure LLDPE. With ZnO exhibiting the most visible opacity and highest IR transparency, it is definitely the best overall

pigment that can offer high visible opacity and reflectance and highest IR transparency, reflectance and emission properties in white pigments whereas FeO yellow showed best results in colored pigments. It was noted that lower thickness of PE sheets are more IR transparent than higher thickness overall which confirms that IR transparency decreases with increase in thickness. Moreover, it was also presented that IR transparency also decreases with increase in concentration of the pigments. Therefore, up to 5 wt% addition of pigments can offer excellent visible opacity and high IR transparency. Overall, It was presented that PE can virtually be pigmented in any color for visible camouflage and attractiveness for passive radiative heating and cooling applications.

In the **second part** of this research work, chapter three focused on addressing the challenges associated with HDPE in the context of 3D printing. HDPE exhibited severe warpage, particularly at sharper angles during FFF (Fused Filament Fabrication) 3D printing. To overcome this issue, we employed a systematic approach. Firstly, we optimized printing parameters and investigated different types of print beds and then we introduced a solution by incorporating 10 wt% of LLDPE into HDPE. This addition reduced crystallinity and subsequently decreased stresses within the printed object during 3D printing, thereby mitigating warpage issues in the final 3D printed parts. Here in, LLDPE was blended with HDPE in concentrations of 2, 5, 10 and 20 wt%. Warpage was measured for each blend at three different angles: 90°, 60° and 30°, of the print specimen. Mechanical characterization tests: tensile strength, Young's modulus and elongation at break were performed. 10 wt% LLDPE-HDPE blend was the overall winner and provided best solution by exhibiting excellent warpage reduction at all the angles whereas maintaining its mechanical properties comparable to that of pure HDPE. UHMWPE was used as print bed as it offered excellent adhesion and removal for the print objects. The overall gains in printing performance with negligible impact on mechanical performance makes blends of HDPE-LLDPE a viable solution to overcome polyolefin FFF printing challenges. This approach expanded

the range of materials for 3D printing, making semi-crystalline polyolefins easier to print.

To sum up, this research contributes significantly to the understanding and improvement of PE materials. By pigmenting LLDPE to achieve both visual opacity and high IR transparency, we have expanded the potential applications of LLDPE. Furthermore, our findings regarding HDPE and its warpage issues during 3D printing provide practical solutions to enhance the printability and quality of HDPE objects. These advancements have significant implications for various industries, such as additive manufacturing, packaging, construction, and beyond. The outcomes of this research open up exciting possibilities for the utilization of PE materials in a wide range of industrial, military, and civilian applications, making them more versatile and valuable resources in various fields.

4.2 Possible future directions

Based on the accomplished works, the following future directions of research are identified:

i. Investigating the IR transparency, reflectance and emission properties of HDPE and LLDPE-HDPE blends. If they show high IR transparency and other similar desirable IR properties, then this step will allow us to produce sheets which are more durable and stronger for use in buildings and other applications while making use of their IR properties.

ii. Structuring and patterning the LLDPE and other grades of PE to tune their visible and IR properties. A preliminary research has been done in this direction and the results have been promising. This can allow us to use structured/patterned pigmented PE sheets to be tunable to scatter visible and IR light when and where needed. Doing so, we will be able to control the intensity of visible and IR transparency and opaqueness of PE sheets enhancing their applications even more. To achieve this, other experimental techniques like surface texturing, nanoparticle incorporation, or blending with other materials could be explored to achieve the desired scattering effect.

References

[1] "Polyolefin - an overview | ScienceDirect Topics." https://www.sciencedirect.com/topics/engineering/polyolefin (accessed Jun. 29, 2023).

[2] W. Kaminsky, "Trends in Polyolefin Chemistry," *Macromolecular Chemistry and Physics*, vol. 209, no. 5, pp. 459–466, 2008, doi: 10.1002/macp.200700575.

[3] A. Shamiri *et al.*, "The Influence of Ziegler-Natta and Metallocene Catalysts on Polyolefin Structure, Properties, and Processing Ability," *Materials*, vol. 7, no. 7, Art. no. 7, Jul. 2014, doi: 10.3390/ma7075069.

[4] "Introduction to Polyolefins," in *Polyolefin Reaction Engineering*, John Wiley & Sons, Ltd, 2012, pp. 1–13. doi: 10.1002/9783527646944.ch1.

[5] "Polymerization Catalysis and Mechanism," in *Polyolefin Reaction Engineering*, John Wiley & Sons, Ltd, 2012, pp. 53–86. doi: 10.1002/9783527646944.ch3.

[6] M. D. F. ltd, "Polyolefins Market | Size, Share, Growth | 2023-2028," *Market Data Forecast*. http://www.marketdataforecast.com/ (accessed Apr. 08, 2023).

[7] "Global Polyolefin Market Size, Share & Growth Report, 2030." https://www.grandviewresearch.com/industry-analysis/polyolefin-market (accessed Apr. 08, 2023).

[8] N. Verma, P. Awasthi, A. Gupta, and S. S. Banerjee, "Fused Deposition Modeling of Polyolefins: Challenges and Opportunities," *Macro Materials & Eng*, vol. 308, no. 1, p. 2200421, Jan. 2023, doi: 10.1002/mame.202200421.

[9] D. W. Sauter, M. Taoufik, and C. Boisson, "Polyolefins, a Success Story," *Polymers*, vol. 9, no. 6, Art. no. 6, Jun. 2017, doi: 10.3390/polym9060185.

[10] H. Islam, Md. E. Hoque, and M. H. Hasan, "Chapter 7 - Biodegradability of polyolefins: Processes and procedures," in *Biodegradability of Conventional Plastics*, A. Sarkar, B. Sharma, and S. Shekhar, Eds., Elsevier, 2023, pp. 121–154. doi: 10.1016/B978-0-323-89858-4.00002-6.

[11] X. Xu, F. Wang, and J. Mao, "Achieving a high positive temperature coefficient effect at low temperature through combining spherical HDPE/SBR with MCMB," *Materials Science and Engineering: B*, vol. 288, p. 116177, Feb. 2023, doi: 10.1016/j.mseb.2022.116177.

[12] S. L. Aggarwal and G. P. Tilley, "Determination of crystallinity in polyethylene by X-ray diffractometer," *Journal of Polymer Science*, vol. 18, no. 87, pp. 17–26, 1955, doi: 10.1002/pol.1955.120188702.

[13] M. De Sarkar *et al.*, "Development of high melt strength polypropylene and its application in thermoplastic elastomeric composition," *Journal of Elastomers & Plastics*, vol. 54, no. 3, pp. 429–456, Apr. 2022, doi: 10.1177/00952443211051010.

[14] J. Karger-Kocsis, *Polypropylene Structure, blends and Composites: Volume 3 Composites*. Springer Science & Business Media, 2012.

[15] J. Karger-Kocsis and T. Bárány, Eds., *Polypropylene Handbook: Morphology, Blends and Composites*. Cham: Springer International Publishing, 2019. doi: 10.1007/978-3-030-12903-3.

[16] T. Campbell, C. Williams, O. Ivanova, and B. Garrett, "Could 3D Printing Change the World?: Technologies, Potential, and Implications of Additive Manufacturing," Atlantic Council, 2011. Accessed: Apr. 08, 2023. [Online]. Available:

https://www.jstor.org/stable/resrep03564
[17] J. R. C. Dizon, A. H. Espera, Q. Chen, and R. C. Advincula, "Mechanical characterization of 3D-printed polymers," *Additive Manufacturing*, vol. 20, pp. 44–67, Mar. 2018, doi: 10.1016/j.addma.2017.12.002.
[18] "Innovations in 3D printing: a 3D overview from optics to organs | British Journal of Ophthalmology." https://bjo.bmj.com/content/98/2/159 (accessed Apr. 08, 2023).
[19] J. V. Crivello and E. Reichmanis, "Photopolymer Materials and Processes for Advanced Technologies," *Chem. Mater.*, vol. 26, no. 1, pp. 533–548, Jan. 2014, doi: 10.1021/cm402262g.
[20] C. Schubert, M. C. van Langeveld, and L. A. Donoso, "Innovations in 3D printing: a 3D overview from optics to organs," *British Journal of Ophthalmology*, vol. 98, no. 2, pp. 159–161, Feb. 2014, doi: 10.1136/bjophthalmol-2013-304446.
[21] N. Shahrubudin, T. C. Lee, and R. Ramlan, "An Overview on 3D Printing Technology: Technological, Materials, and Applications," *Procedia Manufacturing*, vol. 35, pp. 1286–1296, Jan. 2019, doi: 10.1016/j.promfg.2019.06.089.
[22] T. D. Ngo, A. Kashani, G. Imbalzano, K. T. Q. Nguyen, and D. Hui, "Additive manufacturing (3D printing): A review of materials, methods, applications and challenges," *Composites Part B: Engineering*, vol. 143, pp. 172–196, Jun. 2018, doi: 10.1016/j.compositesb.2018.02.012.
[23] J.-Y. Lee, J. An, and C. K. Chua, "Fundamentals and applications of 3D printing for novel materials," *Applied Materials Today*, vol. 7, pp. 120–133, Jun. 2017, doi: 10.1016/j.apmt.2017.02.004.
[24] D. K. Yadav, R. Srivastava, and S. Dev, "Design & fabrication of ABS part by FDM for automobile application," *Materials Today: Proceedings*, vol. 26, pp. 2089–2093, Jan. 2020, doi: 10.1016/j.matpr.2020.02.451.
[25] A. Dawood, B. M. Marti, V. Sauret-Jackson, and A. Darwood, "3D printing in dentistry," *Br Dent J*, vol. 219, no. 11, Art. no. 11, Dec. 2015, doi: 10.1038/sj.bdj.2015.914.
[26] C. L. Ventola, "Medical Applications for 3D Printing: Current and Projected Uses," *P T*, vol. 39, no. 10, pp. 704–711, Oct. 2014.
[27] S. El-Sayegh, L. Romdhane, and S. Manjikian, "A critical review of 3D printing in construction: benefits, challenges, and risks," *Archiv.Civ.Mech.Eng*, vol. 20, no. 2, p. 34, Mar. 2020, doi: 10.1007/s43452-020-00038-w.
[28] A. Paolini, S. Kollmannsberger, and E. Rank, "Additive manufacturing in construction: A review on processes, applications, and digital planning methods," *Additive Manufacturing*, vol. 30, p. 100894, Dec. 2019, doi: 10.1016/j.addma.2019.100894.
[29] Q. Yan *et al.*, "A Review of 3D Printing Technology for Medical Applications," *Engineering*, vol. 4, no. 5, pp. 729–742, Oct. 2018, doi: 10.1016/j.eng.2018.07.021.
[30] Y. W. D. Tay, B. Panda, S. C. Paul, N. A. Noor Mohamed, M. J. Tan, and K. F. Leong, "3D printing trends in building and construction industry: a review," *Virtual and Physical Prototyping*, vol. 12, no. 3, pp. 261–276, Jul. 2017, doi: 10.1080/17452759.2017.1326724.
[31] I. Hager, A. Golonka, and R. Putanowicz, "3D Printing of Buildings and Building Components as the Future of Sustainable Construction?," *Procedia Engineering*, vol. 151, pp. 292–299, Jan. 2016, doi: 10.1016/j.proeng.2016.07.357.
[32] M. Sakin and Y. C. Kiroglu, "3D Printing of Buildings: Construction of the Sustainable Houses of the Future by BIM," *Energy Procedia*, vol. 134, pp. 702–711, Oct. 2017, doi: 10.1016/j.egypro.2017.09.562.
[33] G. Chen, Y. Xu, P. Chi Lip Kwok, and L. Kang, "Pharmaceutical Applications of 3D

Printing," *Additive Manufacturing*, vol. 34, p. 101209, Aug. 2020, doi: 10.1016/j.addma.2020.101209.
[34] E. Macdonald *et al.*, "3D Printing for the Rapid Prototyping of Structural Electronics," *IEEE Access*, vol. 2, pp. 234–242, Dec. 2014, doi: 10.1109/ACCESS.2014.2311810.
[35] A. García-Collado, J. M. Blanco, M. K. Gupta, and R. Dorado-Vicente, "Advances in polymers based Multi-Material Additive-Manufacturing Techniques: State-of-art review on properties and applications," *Additive Manufacturing*, vol. 50, p. 102577, Feb. 2022, doi: 10.1016/j.addma.2021.102577.
[36] J. P. Kruth, X. Wang, T. Laoui, and L. Froyen, "Lasers and materials in selective laser sintering," *Assembly Automation*, vol. 23, no. 4, pp. 357–371, Jan. 2003, doi: 10.1108/01445150310698652.
[37] J. Z. Manapat, Q. Chen, P. Ye, and R. C. Advincula, "3D Printing of Polymer Nanocomposites via Stereolithography," *Macromolecular Materials and Engineering*, vol. 302, no. 9, p. 1600553, 2017, doi: 10.1002/mame.201600553.
[38] C. J. Thrasher, J. J. Schwartz, and A. J. Boydston, "Modular Elastomer Photoresins for Digital Light Processing Additive Manufacturing," *ACS Appl. Mater. Interfaces*, vol. 9, no. 45, pp. 39708–39716, Nov. 2017, doi: 10.1021/acsami.7b13909.
[39] D. Manfredi *et al.*, "Direct Metal Laser Sintering: an additive manufacturing technology ready to produce lightweight structural parts for robotic applications," no. 10.
[40] I. Zein, D. W. Hutmacher, K. C. Tan, and S. H. Teoh, "Fused deposition modeling of novel scaffold architectures for tissue engineering applications," *Biomaterials*, vol. 23, no. 4, pp. 1169–1185, Feb. 2002, doi: 10.1016/S0142-9612(01)00232-0.
[41] L. E. Murr, S. M. Gaytan, E. Martinez, F. Medina, and R. B. Wicker, "Next Generation Orthopaedic Implants by Additive Manufacturing Using Electron Beam Melting," *International Journal of Biomaterials*, vol. 2012, pp. 1–14, 2012, doi: 10.1155/2012/245727.
[42] I. J. Solomon, P. Sevvel, and J. Gunasekaran, "A review on the various processing parameters in FDM," *Materials Today: Proceedings*, vol. 37, pp. 509–514, Jan. 2021, doi: 10.1016/j.matpr.2020.05.484.
[43] A. D. Mazurchevici, D. Nedelcu, and R. Popa, "Additive manufacturing of composite materials by FDM technology: A review," *IJEMS Vol.27(2) [April 2020]*, Apr. 2020, Accessed: Apr. 08, 2023. [Online]. Available: http://nopr.niscpr.res.in/handle/123456789/54873
[44] P. Awasthi and S. S. Banerjee, "Fused deposition modeling of thermoplastic elastomeric materials: Challenges and opportunities," *Additive Manufacturing*, vol. 46, p. 102177, Oct. 2021, doi: 10.1016/j.addma.2021.102177.
[45] O. A. Mohamed, S. H. Masood, and J. L. Bhowmik, "Optimization of fused deposition modeling process parameters: a review of current research and future prospects," *Adv. Manuf.*, vol. 3, no. 1, pp. 42–53, Mar. 2015, doi: 10.1007/s40436-014-0097-7.
[46] O. S. Carneiro, A. F. Silva, and R. Gomes, "Fused deposition modeling with polypropylene," *Materials & Design*, vol. 83, pp. 768–776, Oct. 2015, doi: 10.1016/j.matdes.2015.06.053.
[47] N. Verma, P. Awasthi, P. M. Pandey, and S. S. Banerjee, "Development of material extrusion 3D printing compatible tailorable thermoplastic elastomeric materials from acrylonitrile butadiene styrene and styrene-(ethylene-butylene)-styrene block copolymer blends," *Journal of Applied Polymer Science*, vol. 139, no. 42, p. e53039, 2022, doi: 10.1002/app.53039.
[48] S. Ahn, M. Montero, D. Odell, S. Roundy, and P. K. Wright, "Anisotropic material properties of fused deposition modeling ABS," *Rapid Prototyping Journal*, vol. 8, no. 4, pp. 248–257,

Jan. 2002, doi: 10.1108/13552540210441166.
[49] J. Torres, J. Cotelo, J. Karl, and A. P. Gordon, "Mechanical Property Optimization of FDM PLA in Shear with Multiple Objectives," *JOM*, vol. 67, no. 5, pp. 1183–1193, May 2015, doi: 10.1007/s11837-015-1367-y.
[50] L. Fang, Y. Yan, O. Agarwal, J. E. Seppala, K. J. Hemker, and S. H. Kang, "Processing-structure-property relationships of bisphenol-A-polycarbonate samples prepared by fused filament fabrication," *Additive Manufacturing*, vol. 35, p. 101285, Oct. 2020, doi: 10.1016/j.addma.2020.101285.
[51] Z. C. Kennedy *et al.*, "Mica filled polyetherketoneketones for material extrusion 3D printing," *Additive Manufacturing*, vol. 49, p. 102492, Jan. 2022, doi: 10.1016/j.addma.2021.102492.
[52] C. R. Lindsey, D. R. Paul, and J. W. Barlow, "Mechanical properties of HDPE–PS–SEBS blends," *Journal of Applied Polymer Science*, vol. 26, no. 1, pp. 1–8, 1981, doi: 10.1002/app.1981.070260101.
[53] "Global HDPE market value 2020," *Statista*. https://www.statista.com/statistics/950506/market-value-hdpe-worldwide/ (accessed Apr. 08, 2023).
[54] C. G. Schirmeister, T. Hees, E. H. Licht, and R. Mülhaupt, "3D printing of high density polyethylene by fused filament fabrication," *Additive Manufacturing*, vol. 28, pp. 152–159, Aug. 2019, doi: 10.1016/j.addma.2019.05.003.
[55] V. Mazzanti, L. Malagutti, and F. Mollica, "FDM 3D Printing of Polymers Containing Natural Fillers: A Review of their Mechanical Properties," *Polymers*, vol. 11, no. 7, Art. no. 7, Jul. 2019, doi: 10.3390/polym11071094.
[56] S. Wickramasinghe, T. Do, and P. Tran, "FDM-Based 3D Printing of Polymer and Associated Composite: A Review on Mechanical Properties, Defects and Treatments," *Polymers*, vol. 12, no. 7, Art. no. 7, Jul. 2020, doi: 10.3390/polym12071529.
[57] Z. Liu, Y. Wang, B. Wu, C. Cui, Y. Guo, and C. Yan, "A critical review of fused deposition modeling 3D printing technology in manufacturing polylactic acid parts," *Int J Adv Manuf Technol*, vol. 102, no. 9, pp. 2877–2889, Jun. 2019, doi: 10.1007/s00170-019-03332-x.
[58] P. K. Penumakala, J. Santo, and A. Thomas, "A critical review on the fused deposition modeling of thermoplastic polymer composites," *Composites Part B: Engineering*, vol. 201, p. 108336, Nov. 2020, doi: 10.1016/j.compositesb.2020.108336.
[59] S. C. Ligon, R. Liska, J. Stampfl, M. Gurr, and R. Mülhaupt, "Polymers for 3D Printing and Customized Additive Manufacturing," *Chem. Rev.*, vol. 117, no. 15, pp. 10212–10290, Aug. 2017, doi: 10.1021/acs.chemrev.7b00074.
[60] A. M. Peterson, "Review of acrylonitrile butadiene styrene in fused filament fabrication: A plastics engineering-focused perspective," *Additive Manufacturing*, vol. 27, pp. 363–371, May 2019, doi: 10.1016/j.addma.2019.03.030.
[61] S. Nikazar, E. Nikzinat, A. Sepahi, R. Rashedi, M. Saati, and M. Najafi, "Impact of Prepolymerization Monomer on Polymerization of LLDPE," 2021.
[62] P. S. M. Cardoso, M. M. Ueki, J. D. V. Barbosa, F. C. Garcia Filho, B. S. Lazarus, and J. B. Azevedo, "The Effect of Dialkyl Peroxide Crosslinking on the Properties of LLDPE and UHMWPE," *Polymers*, vol. 13, no. 18, Art. no. 18, Jan. 2021, doi: 10.3390/polym13183062.
[63] L. Göpperl, D. C. Pernusch, J. F. Schwarz, and C. Paulik, "Customizing the comonomer incorporation distribution in Ziegler–Natta-based LLDPE: Harnessing the influences of the titanation temperature during catalyst synthesis and of polymerization process parameters,"

The Canadian Journal of Chemical Engineering, vol. n/a, no. n/a, doi: 10.1002/cjce.24896.
[64] V. Sangeetha, D. Gopinath, R. Prithivirajan, V. Girish Chandran, and R. Manoj Kumar, "Investigating the mechanical, thermal and melt flow index properties of HNTs – LLDPE nano composites for the applications of rotational moulding," *Polymer Testing*, vol. 89, p. 106595, Sep. 2020, doi: 10.1016/j.polymertesting.2020.106595.
[65] M. Bekhit, S. H. El-Sabbagh, R. M. Mohamed, G. S. El-Sayyad, and R. Sokary, "Mechanical, Thermal and Antimicrobial Properties of LLDPE/EVA/MMT/Ag Nanocomposites Films Synthesized by Gamma Irradiation," *J Inorg Organomet Polym*, vol. 32, no. 2, pp. 631–645, Feb. 2022, doi: 10.1007/s10904-021-02137-4.
[66] X. Li, Q. Guo, F. Yang, X. Sun, W. Li, and Z. Yao, "Electrical Properties of LLDPE/LLDPE-g-PS Blends with Carboxylic Acid Functional Groups for Cable Insulation Applications," *ACS Appl. Polym. Mater.*, vol. 2, no. 8, pp. 3450–3457, Aug. 2020, doi: 10.1021/acsapm.0c00506.
[67] E. Leguebe, V. Huart, N. Krajka, J. Pellot, M. le Baillif, and D. Erre, "Effect of relaxation time, recovery time and extension speed during characterization of LLDPE wrap film properties," *Packaging Technology and Science*, vol. 35, no. 12, pp. 913–921, 2022, doi: 10.1002/pts.2688.
[68] A. Abd Elbary, M. Tammam, and N. Aljuraide, "Swelling and electrical properties of LLDPE reinforced by SWCNTs nanocomposites for radiation and sensors applications," *Journal of Thermoplastic Composite Materials*, vol. 35, no. 3, pp. 416–446, Mar. 2022, doi: 10.1177/0892705719879209.
[69] J. Li, E. Gunister, and I. Barsoum, "Effect of graphene oxide as a filler material on the mechanical properties of LLDPE nanocomposites," *Journal of Composite Materials*, vol. 53, no. 19, pp. 2761–2773, Aug. 2019, doi: 10.1177/0021998319839215.
[70] H. Zhang *et al.*, "Evaluating melt foamability of LLDPE/LDPE blends with high LLDPE content by bubble coalescence mechanism," *Polymer*, vol. 213, p. 123209, Jan. 2021, doi: 10.1016/j.polymer.2020.123209.
[71] A. Anžlovar, A. Krajnc, and E. Žagar, "Silane modified cellulose nanocrystals and nanocomposites with LLDPE prepared by melt processing," *Cellulose*, vol. 27, no. 10, pp. 5785–5800, Jul. 2020, doi: 10.1007/s10570-020-03181-y.
[72] N. Gupta and P. L. Ramkumar, "Effect of coir content on mechanical and thermal properties of LLDPE/coir blend processed by rotational molding," *Sādhanā*, vol. 46, no. 1, p. 40, Feb. 2021, doi: 10.1007/s12046-021-01566-8.
[73] PL. Ramkumar, Y. Panchal, D. Panchal, and N. Gupta, "Characterization of LLDPE/coir blend using FTIR technique," *Materials Today: Proceedings*, vol. 28, pp. 1450–1454, Jan. 2020, doi: 10.1016/j.matpr.2020.04.819.
[74] T. Panrong, T. Karbowiak, and N. Harnkarnsujarit, "Effects of acetylated and octenyl-succinated starch on properties and release of green tea compounded starch/LLDPE blend films," *Journal of Food Engineering*, vol. 284, p. 110057, Nov. 2020, doi: 10.1016/j.jfoodeng.2020.110057.
[75] T. Chatkitanan and N. Harnkarnsujarit, "Development of nitrite compounded starch-based films to improve color and quality of vacuum-packaged pork," *Food Packaging and Shelf Life*, vol. 25, p. 100521, Sep. 2020, doi: 10.1016/j.fpsl.2020.100521.
[76] S. M. Noor, N. A. Muhamad, K. A. Abdul Halim, S. A. Ghani, B. Darussalam, and M. K. Mohd Jamil, "Effect of Al2O3 Nanofillers on Polarization and Depolarization Current (PDC) of New LLDPE/HDPE Compounding for HVDC Application," in *2022 IEEE International*

Conference on Power and Energy (PECon), Dec. 2022, pp. 230–233. doi: 10.1109/PECon54459.2022.9987706.
[77] A. D. Porfyris *et al.*, "Enhancing the UV/heat stability of LLDPE irrigation pipes via different stabilizer formulations," *SPE Polymers*, vol. 2, no. 4, pp. 336–350, 2021, doi: 10.1002/pls2.10055.
[78] M. Heinz, C. Callsen, W. Stöcklein, V. Altstädt, and H. Ruckdäschel, "Halogen-free flame-retardant cable compounds: Influence of magnesium-di-hydroxide filler and coupling agent on EVA/LLDPE blend system morphology," *Polymer Engineering & Science*, vol. 62, no. 2, pp. 461–471, 2022, doi: 10.1002/pen.25858.
[79] H. Luo, M. Yang, J. Guo, W. Zou, J. Xu, and N. Zhao, "UV-cured coatings for highly efficient passive all-day radiative cooling," In Review, preprint, Feb. 2022. doi: 10.21203/rs.3.rs-1280366/v1.
[80] M. Alberghini *et al.*, "Sustainable polyethylene fabrics with engineered moisture transport for passive cooling," *Nat Sustain*, vol. 4, no. 8, Art. no. 8, Aug. 2021, doi: 10.1038/s41893-021-00688-5.
[81] H. Luo, M. Yang, J. Guo, W. Zou, J. Xu, and N. Zhao, "Hierarchical Porous Polymer Coatings Based on UV-Curing for Highly Efficient Passive All-Day Radiative Cooling," *ACS Appl. Polym. Mater.*, vol. 4, no. 8, pp. 5746–5755, Aug. 2022, doi: 10.1021/acsapm.2c00694.
[82] T. Al-Gunaid *et al.*, "Phase change materials designed from Tetra Pak waste and paraffin wax as unique thermal energy storage systems," *Journal of Energy Storage*, vol. 64, p. 107173, Aug. 2023, doi: 10.1016/j.est.2023.107173.
[83] E. Di Mauro, X. Li, C. Pellerin, F. Cicoira, and C. Santato, "Smart Packaging in the Sustainability Challenge: Eumelanin as a UV-Absorption Enhancer of Polymers," *IEEE Transactions on Nanotechnology*, vol. 18, pp. 1160–1165, 2019, doi: 10.1109/TNANO.2019.2941370.
[84] D. Krieg, O. Sergeieva, S. Jungkind, M. Rennert, and M. Nase, "Influence of E-beam irradiation on compounds from linear low density polyethylene and thermoplastic vulcanized rubber consisting of a polypropylene and ethylene propylene diene monomer rubber phase," *Journal of Applied Polymer Science*, vol. 140, no. 17, p. e53765, 2023, doi: 10.1002/app.53765.
[85] T. F. da Silva, G. P. M. de Souza, G. F. de M. Morgado, E. Quinteiro, A. P. F. Albers, and F. R. Passador, "Effect of Different Surface Modifications of Brazilian Attapulgite (ATP) on the Mechanical and Thermal Properties of LLDPE/ATP Nanocomposites," *Macromolecular Symposia*, vol. 406, no. 1, p. 2200012, 2022, doi: 10.1002/masy.202200012.
[86] M. Marín-Genescà, J. García-Amorós, R. Mujal-Rosas, L. Massagués, and X. Colom, "Study and Characterization of the Dielectric Behavior of Low Linear Density Polyethylene Composites Mixed with Ground Tire Rubber Particles," *Polymers*, vol. 12, no. 5, Art. no. 5, May 2020, doi: 10.3390/polym12051075.
[87] N. Bumbudsanpharoke, P. Wongphan, K. Promhuad, P. Leelaphiwat, and N. Harnkarnsujarit, "Morphology and permeability of bio-based poly(butylene adipate-co-terephthalate) (PBAT), poly(butylene succinate) (PBS) and linear low-density polyethylene (LLDPE) blend films control shelf-life of packaged bread," *Food Control*, vol. 132, p. 108541, Feb. 2022, doi: 10.1016/j.foodcont.2021.108541.
[88] "Low Density Poly-Ethylene - an overview | ScienceDirect Topics." https://www.sciencedirect.com/topics/engineering/low-density-poly-ethylene (accessed Apr. 08, 2023).

[89] R. González-Mota, J. Soto-Bernal, I. Rosales-Candelas, and J. T. Vega-Dúran, "Absorbance and color change of LLDPE samples exposed to natural weathering in Aguascalientes City, Mexico - art. no. 64221D," *Proceedings of SPIE - The International Society for Optical Engineering*, vol. 6422, Jun. 2007, doi: 10.1117/12.742348.
[90] W. Rungswang *et al.*, "Structure–Property–Process Relationship for Blown Films of Bimodal HDPE and Its LLDPE Blend," *Macromolecular Materials and Engineering*, vol. 304, no. 9, p. 1900325, 2019, doi: 10.1002/mame.201900325.
[91] N. Basiron, S. Sreekantan, L. Jit Kang, H. Md Akil, and R. B. S. M.N. Mydin, "Coupled Oxides/LLDPE Composites for Textile Effluent Treatment: Effect of Neem and PVA Stabilization," *Polymers*, vol. 12, no. 2, Art. no. 2, Feb. 2020, doi: 10.3390/polym12020394.
[92] F. Muniz-Miranda *et al.*, "Aggregation Effects on Pigment Coatings: Pigment Red 179 as a Case Study," *ACS Omega*, vol. 4, no. 23, pp. 20315–20323, Dec. 2019, doi: 10.1021/acsomega.9b02819.
[93] R. Lowrie, J. Henry, M. DeAngelo, C. Cavalier, and D. Seiler, "THE EFFECT OF FLUORINATED THERMOPLASTIC PROCESSING AIDS IN FILM PROCESSING OF RECYCLED POLYETHYLENE RESINS".
[94] C. J. Cabello-Alvarado, Z. V. Quiñones-Jurado, V. J. Cruz-Delgado, and C. A. Avila-Orta, "Pigmentation and Degradative Activity of TiO2 on Polyethylene Films Using Masterbatches Fabricated Using Variable-Frequency Ultrasound-Assisted Melt-Extrusion," *Materials*, vol. 13, no. 17, Art. no. 17, Jan. 2020, doi: 10.3390/ma13173855.
[95] L. M. Degenstein, D. Sameoto, J. D. Hogan, A. Asad, and P. I. Dolez, "Smart Textiles for Visible and IR Camouflage Application: State-of-the-Art and Microfabrication Path Forward," *Micromachines*, vol. 12, no. 7, Art. no. 7, Jul. 2021, doi: 10.3390/mi12070773.
[96] S. M. Burkinshaw, G. Hallas, and A. D. Towns, "Infrared camouflage," *Review of Progress in Coloration and Related Topics*, vol. 26, no. 1, pp. 47–53, 1996, doi: 10.1111/j.1478-4408.1996.tb00109.x.
[97] H. Pisavadia, A. Asad, D. Sameoto, P. Dolez, and J. D. Hogan, "Design of micro- and macro-scale polymeric metamaterial solutions for passive and active thermal camouflaging applications," *Nano Select*, vol. 4, no. 4, pp. 263–270, 2023, doi: 10.1002/nano.202200212.
[98] E. Wilusz, *Military Textiles*. Elsevier, 2008.
[99] Y.-N. Song, M.-Q. Lei, L.-F. Deng, J. Lei, and Z.-M. Li, "Hybrid Metamaterial Textiles for Passive Personal Cooling Indoors and Outdoors," *ACS Appl. Polym. Mater.*, vol. 2, no. 11, pp. 4379–4386, Nov. 2020, doi: 10.1021/acsapm.0c00234.
[100] K. R. Hart, R. M. Dunn, and E. D. Wetzel, "Tough, Additively Manufactured Structures Fabricated with Dual-Thermoplastic Filaments," *Advanced Engineering Materials*, vol. 22, no. 4, p. 1901184, 2020, doi: 10.1002/adem.201901184.
[101] "Adaptive optoelectronic camouflage systems with designs inspired by cephalopod skins | PNAS." https://www.pnas.org/doi/abs/10.1073/pnas.1410494111 (accessed Jun. 20, 2023).
[102] "Microfluidic fabrication of microparticles for biomedical applications - Chemical Society Reviews (RSC Publishing) DOI:10.1039/C7CS00263G." https://pubs.rsc.org/en/content/articlehtml/2018/cs/c7cs00263g?casa_token=7ZpXU3Seb8IAAAAA:ClBLn2OzMCWfW9Xj0Sd1hJWhWcEGGx3CBKUxHn3Lrv9hhXPd1h1YCvnCv9nYr-RXjm6AlR7kF7qENEqQ (accessed Jun. 20, 2023).
[103] "Assembly of Advanced Materials into 3D Functional Structures by Methods Inspired by Origami and Kirigami: A Review - Ning - 2018 - Advanced Materials Interfaces - Wiley Online Library."

https://onlinelibrary.wiley.com/doi/abs/10.1002/admi.201800284?casa_token=2HtuUCrsQ9sAAAAA:fMTrBj6JWKZLsn7HzkSlrVGKbRS22Pl63go75XTt-iJNCaXgz7Ej1hZ3LWzNkZWZ14duE3VOPcprS0Ou (accessed Jun. 29, 2023).
[104] G. S. Ranganath, "Black-body radiation," *Reson*, vol. 13, no. 2, pp. 115–133, Feb. 2008, doi: 10.1007/s12045-008-0028-7.
[105] J. A. S. de Lima and J. Santos, "Generalized Stefan-Boltzmann law," *Int J Theor Phys*, vol. 34, no. 1, pp. 127–134, Jan. 1995, doi: 10.1007/BF00670992.
[106] M. Engelman and M.-A. Jamnia, "Grey-body surface radiation coupled with conduction and convection for general geometries," *International Journal for Numerical Methods in Fluids*, vol. 13, no. 8, pp. 1029–1053, 1991, doi: 10.1002/fld.1650130806.
[107] J. R. Simonson, "The laws of black—and grey — body radiation," in *Engineering Heat Transfer*, J. R. Simonson, Ed., London: Macmillan Education UK, 1975, pp. 200–225. doi: 10.1007/978-1-349-15605-4_14.
[108] J.-W. Lin, M.-H. Lu, and Y.-H. Lin, "A Thermal Camera Based Continuous Body Temperature Measurement System," presented at the Proceedings of the IEEE/CVF International Conference on Computer Vision Workshops, 2019, pp. 0–0. Accessed: Sep. 11, 2023. [Online]. Available: https://openaccess.thecvf.com/content_ICCVW_2019/html/CVPM/Lin_A_Thermal_Camera_Based_Continuous_Body_Temperature_Measurement_System_ICCVW_2019_paper.html
[109] J. Zhang, J. Yu, L. Y. Jiang, and P. Liu, "Analysis of the Composition of Infrared Stealth Coating and the Influence Factors of its Emissivity," *Advanced Materials Research*, vol. 926–930, pp. 56–59, 2014, doi: 10.4028/www.scientific.net/AMR.926-930.56.
[110] T. Charinpanitkul, K. Ruenjaikaen, P. Sunsap, A. Wijitamornlert, and K.-S. Kim, "Optical Transmission of Greenhouse Film Prepared from Composite of Polyethylene and Microsilica," vol. 13, Nov. 2007.
[111] "High-temperature infrared camouflage with efficient thermal management | Light: Science & Applications." https://www.nature.com/articles/s41377-020-0300-5 (accessed Sep. 11, 2023).
[112] S. Chandra, D. Franklin, J. Cozart, A. Safaei, and D. Chanda, "Adaptive Multispectral Infrared Camouflage," *ACS Photonics*, vol. 5, no. 11, pp. 4513–4519, Nov. 2018, doi: 10.1021/acsphotonics.8b00972.
[113] "Buildings – Analysis - IEA." https://www.iea.org/reports/buildings (accessed Jun. 20, 2023).
[114] "Heating and Cooling," *Energy.gov*. https://www.energy.gov/energysaver/heating-and-cooling (accessed Jun. 20, 2023).
[115] "Heating and Cooling," *MIT Climate Portal*. https://climate.mit.edu/explainers/heating-and-cooling (accessed Jun. 20, 2023).
[116] "Heat – Renewables 2019 – Analysis," *IEA*. https://www.iea.org/reports/renewables-2019/heat (accessed Jun. 20, 2023).
[117] S. C. Government of Canada, "Census of Population," Jan. 15, 2001. https://www12.statcan.gc.ca/census-recensement/index-eng.cfm (accessed Jun. 20, 2023).
[118] E. and C. C. Canada, "Greenhouse gas emissions," Jan. 09, 2007. https://www.canada.ca/en/environment-climate-change/services/environmental-indicators/greenhouse-gas-emissions.html (accessed Jun. 20, 2023).
[119] "Energy statistics." https://www.statcan.gc.ca/en/subjects-start/energy (accessed Jun. 20,

2023).
[120] T. M. J. Nilsson, G. A. Niklasson, and C. G. Granqvist, “A solar reflecting material for radiative cooling applications: ZnS pigmented polyethylene,” *Solar Energy Materials and Solar Cells*, vol. 28, no. 2, pp. 175–193, Nov. 1992, doi: 10.1016/0927-0248(92)90010-M.
[121] K. D. Dobson, G. Hodes, and Y. Mastai, “Thin semiconductor films for radiative cooling applications,” *Solar Energy Materials and Solar Cells*, vol. 80, no. 3, pp. 283–296, Nov. 2003, doi: 10.1016/j.solmat.2003.06.007.
[122] “KryoZesto |.” https://kryozesto.com/ (accessed Jul. 13, 2023).
[123] “Top 3D Printing Applications Across Industries | MakerBot.” https://www.makerbot.com/stories/design/top-5-3d-printing-applications/ (accessed Jun. 29, 2023).
[124] “Industrial Applications of 3D Printing: The Ultimate Guide - AMFG.” https://amfg.ai/industrial-applications-of-3d-printing-the-ultimate-guide/ (accessed Jun. 29, 2023).
[125] “HDPE Filament: 3D Printing Basics | All3DP.” https://all3dp.com/2/hdpe-3d-printing-material-all-you-need-to-know/ (accessed Apr. 10, 2023).
[126] S. C. Xue, M. C. J. Large, G. W. Barton, R. I. Tanner, L. Poladian, and R. Lwin, “Role of Material Properties and Drawing Conditions in the Fabrication of Microstructured Optical Fibers,” *J. Lightwave Technol., JLT*, vol. 24, no. 2, p. 853, Feb. 2006.
[127] H. M. Reeve, A. M. Mescher, and A. F. Emery, “Investigation of Steady-State Drawing Force and Heat Transfer in Polymer Optical Fiber Manufacturing,” *Journal of Heat Transfer*, vol. 126, no. 2, pp. 236–243, May 2004, doi: 10.1115/1.1677420.
[128] “The mathematical modelling of capillary drawing for holey fibre manufacture | SpringerLink.” https://link.springer.com/article/10.1023/A:1020328606157 (accessed Jun. 20, 2023).
[129] G.-B. Jin, M.-J. Wang, D.-Y. Zhao, H.-Q. Tian, and Y.-F. Jin, “Design and experiments of extrusion die for polypropylene five-lumen micro tube,” *Journal of Materials Processing Technology*, vol. 214, no. 1, pp. 50–59, Jan. 2014, doi: 10.1016/j.jmatprotec.2013.07.016.
[130] H. Tian, D. Zhao, M. Wang, G. Jin, and Y. Jin, “Study on extrudate swell of polypropylene in double-lumen micro profile extrusion,” *Journal of Materials Processing Technology*, vol. 225, pp. 357–368, Nov. 2015, doi: 10.1016/j.jmatprotec.2015.06.015.
[131] G. Lestoquoy, N. Chocat, Z. Wang, J. D. Joannopoulos, and Y. Fink, “Fabrication and characterization of thermally drawn fiber capacitors,” *Applied Physics Letters*, vol. 102, no. 15, p. 152908, Apr. 2013, doi: 10.1063/1.4802783.
[132] “Piezoelectric Fibers for Conformal Acoustics - Chocat - 2012 - Advanced Materials - Wiley Online Library.” https://onlinelibrary.wiley.com/doi/abs/10.1002/adma.201201355?casa_token=VkUsSk9gNnIAAAAA:HmvmH-DzzgTPCYfFZjtJDB1ke46t6U5y4gk3crTNbAXlbfL-AwUXrx2cLLY-DMhabzDcUHpUlaWrgera (accessed Jun. 20, 2023).
[133] A. F. Abouraddy *et al.*, “Towards multimaterial multifunctional fibres that see, hear, sense and communicate,” *Nature Mater*, vol. 6, no. 5, Art. no. 5, May 2007, doi: 10.1038/nmat1889.
[134] “The Market Overview of Linear Low-Density Polyethylene and its Rising Demand.” https://www.procurementresource.com/blog/the-increasing-demand-for-linear-low-density-polyethylene (accessed Apr. 08, 2023).
[135] “All About Linear Low-Density Polyethylene (LLDPE).” https://www.xometry.com/resources/materials/linear-low-density-polyethylene-lldpe/

(accessed Apr. 08, 2023).
[136] C. Gabriel and D. Lilge, "Comparison of different methods for the investigation of the short-chain branching distribution of LLDPE," *Polymer*, vol. 42, no. 1, pp. 297–303, Jan. 2001, doi: 10.1016/S0032-3861(00)00314-1.
[137] B. M. Weckhuysen and R. A. Schoonheydt, "Olefin polymerization over supported chromium oxide catalysts," *Catalysis Today*, vol. 51, no. 2, pp. 215–221, Jun. 1999, doi: 10.1016/S0920-5861(99)00046-2.
[138] O. Delgadillo-Velázquez, S. G. Hatzikiriakos, and M. Sentmanat, "Thermorheological properties of LLDPE/LDPE blends," *Rheol Acta*, vol. 47, no. 1, pp. 19–31, Jan. 2008, doi: 10.1007/s00397-007-0193-8.
[139] D. M. Simpson and G. A. Vaughan, "Ethylene Polymers, LLDPE," in *Encyclopedia of Polymer Science and Technology*, John Wiley & Sons, Ltd, 2001. doi: 10.1002/0471440264.pst122.
[140] J. L. Koontz, J. E. Marcy, S. F. O'Keefe, S. E. Duncan, T. E. Long, and R. D. Moffitt, "Polymer processing and characterization of LLDPE films loaded with α-tocopherol, quercetin, and their cyclodextrin inclusion complexes," *Journal of Applied Polymer Science*, vol. 117, no. 4, pp. 2299–2309, 2010, doi: 10.1002/app.32044.
[141] J. M. Gohil and R. R. Choudhury, "Chapter 2 - Introduction to Nanostructured and Nano-enhanced Polymeric Membranes: Preparation, Function, and Application for Water Purification," in *Nanoscale Materials in Water Purification*, S. Thomas, D. Pasquini, S.-Y. Leu, and D. A. Gopakumar, Eds., in Micro and Nano Technologies. Elsevier, 2019, pp. 25–57. doi: 10.1016/B978-0-12-813926-4.00038-0.
[142] B. Y. Zhao, X. W. Yi, R. Y. Li, P. F. Zhu, and K. A. Hu, "Characterization to the weathering extent of LLDPE/LDPE thin film," *Journal of Applied Polymer Science*, vol. 88, no. 1, pp. 12–16, 2003, doi: 10.1002/app.11634.
[143] A. Khumkomgool, T. Saneluksana, and N. Harnkarnsujarit, "Active meat packaging from thermoplastic cassava starch containing sappan and cinnamon herbal extracts via LLDPE blown-film extrusion," *Food Packaging and Shelf Life*, vol. 26, p. 100557, Dec. 2020, doi: 10.1016/j.fpsl.2020.100557.
[144] S. S. K., I. M.p., and R. G.r., "Mahua oil-based polyurethane/chitosan/nano ZnO composite films for biodegradable food packaging applications," *International Journal of Biological Macromolecules*, vol. 124, pp. 163–174, Mar. 2019, doi: 10.1016/j.ijbiomac.2018.11.195.
[145] A. Riaz *et al.*, "Chitosan-based biodegradable active food packaging film containing Chinese chive (Allium tuberosum) root extract for food application," *International Journal of Biological Macromolecules*, vol. 150, pp. 595–604, May 2020, doi: 10.1016/j.ijbiomac.2020.02.078.
[146] M. L. Goñi, N. A. Gañán, M. C. Strumia, and R. E. Martini, "Eugenol-loaded LLDPE films with antioxidant activity by supercritical carbon dioxide impregnation," *The Journal of Supercritical Fluids*, vol. 111, pp. 28–35, May 2016, doi: 10.1016/j.supflu.2016.01.012.
[147] W. N. W. Busu *et al.*, "Enhanced tensile and barrier properties of modified LLDPE with rubbery materials and graphene nanoplatelets for packaging application," *Journal of Applied Polymer Science*, vol. 140, no. 18, p. e53810, 2023, doi: 10.1002/app.53810.
[148] S. Dadbin, M. Noferesti, and M. Frounchi, "Oxygen Barrier LDPE/LLDPE/Organoclay Nano-Composite Films for Food Packaging," *Macromolecular Symposia*, vol. 274, no. 1, pp. 22–27, 2008, doi: 10.1002/masy.200851404.
[149] T. Panrong, T. Karbowiak, and N. Harnkarnsujarit, "Thermoplastic starch and green tea

blends with LLDPE films for active packaging of meat and oil-based products," *Food Packaging and Shelf Life*, vol. 21, p. 100331, Sep. 2019, doi: 10.1016/j.fpsl.2019.100331.
[150] S. A. Seven, Ö. F. Tastan, C. E. Tas, H. Ünal, İ. A. Ince, and Y. Z. Menceloglu, "Insecticide-releasing LLDPE films as greenhouse cover materials," *Materials Today Communications*, vol. 19, pp. 170–176, Jun. 2019, doi: 10.1016/j.mtcomm.2019.01.015.
[151] H. Xu, M. Dun, Z. Zhang, L. Zhang, W. Shan, and W. Wang, "A New Process of Preparing Rice Straw-Reinforced LLDPE Composite," *Polymers*, vol. 14, no. 11, Art. no. 11, Jan. 2022, doi: 10.3390/polym14112243.
[152] S. Yang *et al.*, "Synthesis of a dripping agent based on lauric acid diethanolamide and delaying its migration in LLDPE films," *Polymer-Plastics Technology and Materials*, vol. 59, no. 10, pp. 1100–1108, Jul. 2020, doi: 10.1080/25740881.2020.1719145.
[153] J. Korol, A. Hejna, K. Wypiór, K. Mijalski, and E. Chmielnicka, "Wastes from Agricultural Silage Film Recycling Line as a Potential Polymer Materials," *Polymers*, vol. 13, no. 9, Art. no. 9, Jan. 2021, doi: 10.3390/polym13091383.
[154] C. Subharaj, M. Logesh, A. Abdul Munaf, J. Srinivas, and S. Joe Patrick Gnanaraj, "Sustainable approach on cement mortar incorporating silica fume, LLDPE and sisal fiber," *Materials Today: Proceedings*, vol. 68, pp. 1342–1348, Jan. 2022, doi: 10.1016/j.matpr.2022.06.361.
[155] E. S. Okhotnikova, Y. M. Ganeeva, I. N. Frolov, T. N. Yusupova, and G. R. Fazylzyanova, "Structural characterization and application of bitumen modified by recycled polyethylenes," *Construction and Building Materials*, vol. 316, p. 126118, Jan. 2022, doi: 10.1016/j.conbuildmat.2021.126118.
[156] S. Panda, S. P. Mishra, and M. Mohanty, "Effect of Blended Waste LDPE/LLDPE on Properties of Bitumen for Rural Roads," in *Sustainable Development in Energy and Environment*, V. Sivasubramanian, A. Pugazhendhi, and I. G. Moorthy, Eds., in Springer Proceedings in Energy. Singapore: Springer, 2020, pp. 197–215. doi: 10.1007/978-981-15-4638-9_16.
[157] F. K. Alqahtani, I. S. Abotaleb, and M. ElMenshawy, "Life cycle cost analysis of lightweight green concrete utilizing recycled plastic aggregates," *Journal of Building Engineering*, vol. 40, p. 102670, Aug. 2021, doi: 10.1016/j.jobe.2021.102670.
[158] S. Nizamuddin, M. Jamal, R. Gravina, and F. Giustozzi, "Recycled plastic as bitumen modifier: The role of recycled linear low-density polyethylene in the modification of physical, chemical and rheological properties of bitumen," *Journal of Cleaner Production*, vol. 266, p. 121988, Sep. 2020, doi: 10.1016/j.jclepro.2020.121988.
[159] F. K. Alqahtani, I. S. Abotaleb, and S. Harb, "LEED Assessment of Green Lightweight Concrete Containing Plastic Based Aggregates in Construction," pp. 696–705, Mar. 2022, doi: 10.1061/9780784483978.071.
[160] S. Benimam, M. Bentchikou, F. Debieb, S. Kenai, and M. Guendouz, "Physical and mechanical properties of cement mortar with LLDPE powder and PET fiber wastes," *Advances in concrete construction*, vol. 12, no. 6, pp. 461–467, 2021, doi: 10.12989/acc.2021.12.6.461.
[161] F. K. Alqahtani, I. S. Abotaleb, and S. Harb, "LEED Study of Green Lightweight Aggregates in Construction," *Sustainability*, vol. 13, no. 3, Art. no. 3, Jan. 2021, doi: 10.3390/su13031395.
[162] S.-W. Xiong, P. Zhang, Y. Xia, P.-G. Fu, and J.-G. Gai, "Antimicrobial hexagonal boron nitride nanoplatelet composites for the thermal management of medical electronic devices,"

Materials Chemistry Frontiers, vol. 3, no. 11, pp. 2455–2462, 2019, doi: 10.1039/C9QM00411D.
[163] X. Li *et al.*, "Effects of Pine Needle Extracts on the Degradation of LLDPE," *Polymers*, vol. 15, no. 1, Art. no. 1, Jan. 2023, doi: 10.3390/polym15010032.
[164] J. Widakdo *et al.*, "Evaluation of the Antibacterial Activity of Eco-Friendly Hybrid Composites on the Base of Oyster Shell Powder Modified by Metal Ions and LLDPE," *Polymers*, vol. 14, no. 15, Art. no. 15, Jan. 2022, doi: 10.3390/polym14153001.
[165] N. H. Harun, R. B. S. M. N. Mydin, S. Sreekantan, K. A. Saharudin, N. Basiron, and A. Seeni, "The bactericidal potential of LLDPE with TiO2/ZnO nanocomposites against multidrug resistant pathogens associated with hospital acquired infections," *Journal of Biomaterials Science, Polymer Edition*, vol. 31, no. 14, pp. 1757–1769, Sep. 2020, doi: 10.1080/09205063.2020.1775759.
[166] S. Chavan, V. Gumtapure, and A. P. D, "Numerical and experimental analysis on thermal energy storage of polyethylene/functionalized graphene composite phase change materials," *Journal of Energy Storage*, vol. 27, p. 101045, Feb. 2020, doi: 10.1016/j.est.2019.101045.
[167] Y. Guo, H. Wu, K. Du, G. Huang, and X. Xu, "Experimental study on radiant cooling with double-skin infrared-transparent membranes," *Energy and Buildings*, vol. 278, p. 112654, Jan. 2023, doi: 10.1016/j.enbuild.2022.112654.
[168] X. Guo and J. Feng, "Facilely prepare passive thermal management materials by foaming phase change materials to achieve long-duration thermal insulation performance," *Composites Part B: Engineering*, vol. 245, p. 110203, Oct. 2022, doi: 10.1016/j.compositesb.2022.110203.
[169] E. Huttunen, M. T. Nykänen, and J. Alexandersen, "Material extrusion additive manufacturing and experimental testing of topology-optimised passive heat sinks using a thermally-conductive plastic filament," *Additive Manufacturing*, vol. 59, p. 103123, Nov. 2022, doi: 10.1016/j.addma.2022.103123.
[170] M. Zhang, T. Yan, W. Wang, X. Jia, J. Wang, and J. J. Klemeš, "Energy-saving design and control strategy towards modern sustainable greenhouse: A review," *Renewable and Sustainable Energy Reviews*, vol. 164, p. 112602, Aug. 2022, doi: 10.1016/j.rser.2022.112602.
[171] V. Štěpánová *et al.*, "Adhesion improvement on the inner side of LLDPE/PA tubular film exposed to DCSBD roll-to-roll plasma system from the outer side of the film," *Plasma Processes and Polymers*, vol. n/a, no. n/a, p. e2200226, doi: 10.1002/ppap.202200226.
[172] Y. Peng *et al.*, "Nanoporous polyethylene microfibres for large-scale radiative cooling fabric," *Nat Sustain*, vol. 1, no. 2, pp. 105–112, Feb. 2018, doi: 10.1038/s41893-018-0023-2.
[173] "Wellzoom desktop filament extruder B – Wellzoom." http://wellzoomextruder.com/product/wellzoom-desktop-filament-extruder-b/ (accessed Dec. 15, 2022).
[174] E. Hull, W. Grove, M. Zhang, X. Song, Z. J. Pei, and W. Cong, "Effects of Process Variables on Extrusion of Carbon Fiber Reinforced ABS Filament for Additive Manufacturing," in *Volume 1: Processing*, Charlotte, North Carolina, USA: American Society of Mechanical Engineers, Jun. 2015, p. V001T02A065. doi: 10.1115/MSEC2015-9396.
[175] J. L. Jordan, D. T. Casem, J. M. Bradley, A. K. Dwivedi, E. N. Brown, and C. W. Jordan, "Mechanical Properties of Low Density Polyethylene," *J. dynamic behavior mater.*, vol. 2,

no. 4, pp. 411–420, Dec. 2016, doi: 10.1007/s40870-016-0076-0.
[176] B. Smith, “The Infrared Spectra of Polymers II: Polyethylene,” *Spectroscopy*, vol. 36, no. 9, pp. 24–29, Sep. 2021.
[177] J. Rosen-Kligvasser, R. Y. Suckeveriene, R. Tchoudakov, and M. Narkis, “LLDPE films containing monoester of oleic acid grafted to silica particles as durable antifog additives,” *Polymers for Advanced Technologies*, vol. 28, no. 8, pp. 931–939, 2017, doi: 10.1002/pat.3827.
[178] G. Singh, H. Bhunia, A. Rajor, and V. Choudhary, “Thermal properties and degradation characteristics of polylactide, linear low density polyethylene, and their blends,” *Polym. Bull.*, vol. 66, no. 7, pp. 939–953, Apr. 2011, doi: 10.1007/s00289-010-0367-x.
[179] K. V. Wong and A. Hernandez, “A Review of Additive Manufacturing,” *ISRN Mechanical Engineering*, vol. 2012, pp. 1–10, Aug. 2012, doi: 10.5402/2012/208760.
[180] A. Gudadhe, N. Bachhar, A. Kumar, P. Andrade, and G. Kumaraswamy, “Three-Dimensional Printing with Waste High-Density Polyethylene,” *ACS Appl. Polym. Mater.*, vol. 1, no. 11, pp. 3157–3164, Nov. 2019, doi: 10.1021/acsapm.9b00813.
[181] S. A. M. Tofail, E. P. Koumoulos, A. Bandyopadhyay, S. Bose, L. O’Donoghue, and C. Charitidis, “Additive manufacturing: scientific and technological challenges, market uptake and opportunities,” *Materials Today*, vol. 21, no. 1, pp. 22–37, Jan. 2018, doi: 10.1016/j.mattod.2017.07.001.
[182] W. Gao *et al.*, “The status, challenges, and future of additive manufacturing in engineering,” *Computer-Aided Design*, vol. 69, pp. 65–89, Dec. 2015, doi: 10.1016/j.cad.2015.04.001.
[183] C. S. Davis, K. E. Hillgartner, S. H. Han, and J. E. Seppala, “Mechanical strength of welding zones produced by polymer extrusion additive manufacturing,” *Additive Manufacturing*, vol. 16, pp. 162–166, Aug. 2017, doi: 10.1016/j.addma.2017.06.006.
[184] M. Dehurtevent, L. Robberecht, J.-C. Hornez, A. Thuault, E. Deveaux, and P. Béhin, “Stereolithography: A new method for processing dental ceramics by additive computer-aided manufacturing,” *Dental Materials*, vol. 33, no. 5, pp. 477–485, May 2017, doi: 10.1016/j.dental.2017.01.018.
[185] P. M., “Additive Manufacturing of Tungsten Carbide Hardmetal Parts by Selective Laser Melting (SLM), Selective Laser Sintering (SLS) and Binder Jet 3D Printing (BJ3DP) Techniques,” *Lasers Manuf. Mater. Process.*, vol. 7, no. 3, pp. 338–371, Sep. 2020, doi: 10.1007/s40516-020-00124-0.
[186] Y. Lakhdar, C. Tuck, J. Binner, A. Terry, and R. Goodridge, “Additive manufacturing of advanced ceramic materials,” *Progress in Materials Science*, vol. 116, p. 100736, Feb. 2021, doi: 10.1016/j.pmatsci.2020.100736.
[187] F. Ning, W. Cong, Y. Hu, and H. Wang, “Additive manufacturing of carbon fiber-reinforced plastic composites using fused deposition modeling: Effects of process parameters on tensile properties,” *Journal of Composite Materials*, vol. 51, no. 4, pp. 451–462, Feb. 2017, doi: 10.1177/0021998316646169.
[188] G. Kollamaram, D. M. Croker, G. M. Walker, A. Goyanes, A. W. Basit, and S. Gaisford, “Low temperature fused deposition modeling (FDM) 3D printing of thermolabile drugs,” *International Journal of Pharmaceutics*, vol. 545, no. 1, pp. 144–152, Jul. 2018, doi: 10.1016/j.ijpharm.2018.04.055.
[189] S. Singh, G. Singh, C. Prakash, and S. Ramakrishna, “Current status and future directions of fused filament fabrication,” *Journal of Manufacturing Processes*, vol. 55, pp. 288–306,

Jul. 2020, doi: 10.1016/j.jmapro.2020.04.049.
[190] S. S. Crump, "Apparatus and method for creating three-dimensional objects," US5121329A, Jun. 09, 1992 Accessed: Feb. 26, 2023. [Online]. Available: https://patents.google.com/patent/US5121329/en
[191] X. Wang, M. Jiang, Z. Zhou, J. Gou, and D. Hui, "3D printing of polymer matrix composites: A review and prospective," *Composites Part B: Engineering*, vol. 110, pp. 442–458, Feb. 2017, doi: 10.1016/j.compositesb.2016.11.034.
[192] S. H. Masood and W. Q. Song, "Development of new metal/polymer materials for rapid tooling using Fused deposition modelling," *Materials & Design*, vol. 25, no. 7, pp. 587–594, Oct. 2004, doi: 10.1016/j.matdes.2004.02.009.
[193] M. Domingo-Espin, J. M. Puigoriol-Forcada, A.-A. Garcia-Granada, J. Llumà, S. Borros, and G. Reyes, "Mechanical property characterization and simulation of fused deposition modeling Polycarbonate parts," *Materials & Design*, vol. 83, pp. 670–677, Oct. 2015, doi: 10.1016/j.matdes.2015.06.074.
[194] M. Vaezi and S. Yang, "Extrusion-based additive manufacturing of PEEK for biomedical applications," *Virtual and Physical Prototyping*, vol. 10, no. 3, pp. 123–135, Jul. 2015, doi: 10.1080/17452759.2015.1097053.
[195] "Ultimaker PP and PE commercial filaments," Feb. 26, 2023. https://ultimaker.com/materials/pp
[196] M. Spoerk *et al.*, "Polypropylene Filled With Glass Spheres in Extrusion-Based Additive Manufacturing: Effect of Filler Size and Printing Chamber Temperature," *Macromolecular Materials and Engineering*, vol. 303, no. 7, p. 1800179, 2018, doi: 10.1002/mame.201800179.
[197] M. Spoerk, J. Sapkota, G. Weingrill, T. Fischinger, F. Arbeiter, and C. Holzer, "Shrinkage and Warpage Optimization of Expanded-Perlite-Filled Polypropylene Composites in Extrusion-Based Additive Manufacturing," *Macromolecular Materials and Engineering*, vol. 302, no. 10, p. 1700143, 2017, doi: 10.1002/mame.201700143.
[198] "HDPE Filament - Natural - 1.75mm - 1KG," Feb. 26, 2023. https://filaments.ca/products/hdpe-filament-natural-1-75mm?variant=%2042590589320
[199] J. Fischer, *Handbook of Molded Part Shrinkage and Warpage*. William Andrew, 2012.
[200] M. Stürzel, S. Mihan, and R. Mülhaupt, "From Multisite Polymerization Catalysis to Sustainable Materials and All-Polyolefin Composites," *Chem. Rev.*, vol. 116, no. 3, pp. 1398–1433, Feb. 2016, doi: 10.1021/acs.chemrev.5b00310.
[201] S. Chong, G.-T. Pan, M. Khalid, T. C.-K. Yang, S.-T. Hung, and C.-M. Huang, "Physical Characterization and Pre-assessment of Recycled High-Density Polyethylene as 3D Printing Material," *J Polym Environ*, vol. 25, no. 2, pp. 136–145, Jun. 2017, doi: 10.1007/s10924-016-0793-4.
[202] S. H. Jung, S. H. Park, D. H. Lee, and S. D. Kim, "Surface modification of HDPE powders by oxygen plasma in a circulating fluidized bed reactor," *Polymer Bulletin*, vol. 47, no. 2, pp. 199–205, Oct. 2001, doi: 10.1007/s002890170012.
[203] B. Kaynak, M. Spoerk, A. Shirole, W. Ziegler, and J. Sapkota, "Polypropylene/Cellulose Composites for Material Extrusion Additive Manufacturing," *Macromolecular Materials and Engineering*, vol. 303, no. 5, p. 1800037, 2018, doi: 10.1002/mame.201800037.
[204] M. Spoerk *et al.*, "Optimisation of the Adhesion of Polypropylene-Based Materials during Extrusion-Based Additive Manufacturing," *Polymers*, vol. 10, no. 5, Art. no. 5, May 2018, doi: 10.3390/polym10050490.

[205] M. Spoerk, C. Savandaiah, F. Arbeiter, J. Sapkota, and C. Holzer, "Optimization of mechanical properties of glass-spheres-filled polypropylene composites for extrusion-based additive manufacturing," *Polymer Composites*, vol. 40, no. 2, pp. 638–651, 2019, doi: 10.1002/pc.24701.

[206] M. Spoerk *et al.*, "Anisotropic properties of oriented short carbon fibre filled polypropylene parts fabricated by extrusion-based additive manufacturing," *Composites Part A: Applied Science and Manufacturing*, vol. 113, pp. 95–104, Oct. 2018, doi: 10.1016/j.compositesa.2018.06.018.

[207] N. Decker and A. Yee, "Assessing the use of binary blends of acrylonitrile butadiene styrene and post-consumer high density polyethylene in fused filament fabrication," *International Journal of Additive and Subtractive Materials Manufacturing*, vol. 1, no. 2, pp. 161–171, Jan. 2017, doi: 10.1504/IJASMM.2017.088203.

[208] F. Peng *et al.*, "3D Printing with Core–Shell Filaments Containing High or Low Density Polyethylene Shells," *ACS Appl. Polym. Mater.*, vol. 1, no. 2, pp. 275–285, Feb. 2019, doi: 10.1021/acsapm.8b00186.

[209] D. Filgueira, S. Holmen, J. K. Melbø, D. Moldes, A. T. Echtermeyer, and G. Chinga-Carrasco, "3D Printable Filaments Made of Biobased Polyethylene Biocomposites," *Polymers*, vol. 10, no. 3, Art. no. 3, Mar. 2018, doi: 10.3390/polym10030314.

[210] T. Hees, F. Zhong, M. Stürzel, and R. Mülhaupt, "Tailoring Hydrocarbon Polymers and All-Hydrocarbon Composites for Circular Economy," *Macromolecular Rapid Communications*, vol. 40, no. 1, p. 1800608, 2019, doi: 10.1002/marc.201800608.

[211] C. Baechler, M. DeVuono, and J. M. Pearce, "Distributed recycling of waste polymer into RepRap feedstock," *Rapid Prototyping Journal*, vol. 19, no. 2, pp. 118–125, Jan. 2013, doi: 10.1108/13552541311302978.

[212] M. A. Kreiger, M. L. Mulder, A. G. Glover, and J. M. Pearce, "Life cycle analysis of distributed recycling of post-consumer high density polyethylene for 3-D printing filament," *Journal of Cleaner Production*, vol. 70, pp. 90–96, May 2014, doi: 10.1016/j.jclepro.2014.02.009.

[213] M. D. Tabone, J. J. Cregg, E. J. Beckman, and A. E. Landis, "Sustainability Metrics: Life Cycle Assessment and Green Design in Polymers," *Environ. Sci. Technol.*, vol. 44, no. 21, pp. 8264–8269, Nov. 2010, doi: 10.1021/es101640n.

[214] "3d Printing Filament Hdpe Polyethylene Printer Material High Densitytoughness Heat Cold Resistance Rigidity Mechanical Strength - 3d Printing Materials - AliExpress." https://www.aliexpress.com/item/1005002428377862.html?pdp_npi=2%40dis%21CAD%21C%24%2080.46%21C%24%2060.35%21%21%21%21%21%4021030111168114322119 24499ef618%21120000020665254418%21btf&_t=pvid:72aab47a-7e5a-4a5a-8ca4-db8be616c83e&afTraceInfo=1005002428377862__pc__pcBridgePPC__xxxxxx__1681143221&spm=a2g0o.ppclist.product.mainProduct (accessed Apr. 10, 2023).

[215] S. Moylan, J. Slotwinski, A. Cooke, K. Jurrens, and M. A. Donmez, "PROPOSAL FOR A STANDARDIZED TEST ARTIFACT FOR ADDITIVE MANUFACTURING MACHINES AND PROCESSES".

[216] "NIST Additive Manufacturing Test Artifact," Jun. 02, 2021. https://www.nist.gov/topics/additive-manufacturing/resources/additive-manufacturing-test-artifact (accessed Feb. 27, 2023).